

UNCLASSIFIED

AD NUMBER	
AD092663	
CLASSIFICATION CHANGES	
TO:	unclassified
FROM:	confidential
LIMITATION CHANGES	
TO:	Approved for public release, distribution unlimited
FROM:	Distribution authorized to U.S. Gov't. agencies and their contractors; Administrative/Operational Use; 04 APR 1956. Other requests shall be referred to National Aeronautics and Space Administration, Washington, DC.
AUTHORITY	
NACA Reclassification List no. 124 dtd 10 Feb 1968; NASA TR Server Website	

THIS PAGE IS UNCLASSIFIED

CONFIDENTIAL

AD 92663

Armed Services Technical Information Agency

Reproduced by

DOCUMENT SERVICE CENTER

KNOTT BUILDING, DAYTON, 2, OHIO

This document is the property of the United States Government. It is furnished for the duration of the contract and shall be returned when no longer required, or upon recall by ASTIA to the following address: Armed Services Technical Information Agency, Document Service Center, Knott Building, Dayton 2, Ohio.

NOTICE: WHEN GOVERNMENT OR OTHER DRAWINGS, SPECIFICATIONS OR OTHER DATA ARE USED FOR ANY PURPOSE OTHER THAN IN CONNECTION WITH A DEFINITELY RELATED GOVERNMENT PROCUREMENT OPERATION, THE U. S. GOVERNMENT THEREBY INCURS NO RESPONSIBILITY, NOR ANY OBLIGATION WHATSOEVER; AND THE FACT THAT THE GOVERNMENT MAY HAVE FORMULATED, FURNISHED, OR IN ANY WAY SUPPLIED THE SAID DRAWINGS, SPECIFICATIONS, OR OTHER DATA IS NOT TO BE REGARDED BY IMPLICATION OR OTHERWISE AS IN ANY MANNER LICENSING THE HOLDER OR ANY OTHER PERSON OR CORPORATION, OR CONVEYING ANY RIGHTS OR PERMISSION TO MANUFACTURE, USE OR SELL ANY PATENTED INVENTION THAT MAY IN ANY WAY BE RELATED THERETO.

CONFIDENTIAL

**NOTICE: THIS DOCUMENT CONTAINS INFORMATION AFFECTING THE
NATIONAL DEFENSE OF THE UNITED STATES WITHIN THE MEANING
OF THE ESPIONAGE LAWS, TITLE 18, U.S.C., SECTIONS 793 and 794.
THE TRANSMISSION OR THE REVELATION OF ITS CONTENTS IN
ANY MANNER TO AN UNAUTHORIZED PERSON IS PROHIBITED BY LAW.**

CONFIDENTIAL

Copy
RM L56A06a

NACA RM L56A06a

92663

ASTIA FILE COPY



RESEARCH MEMORANDUM

AN EXPERIMENTAL STUDY AT HIGH SUBSONIC SPEEDS OF
SEVERAL TAIL CONFIGURATIONS ON A MODEL
WITH AN UNSWEPT WING

By William C. Sleeman, Jr.

Langley Aeronautical Laboratory
Langley Field, Va.

FC

CLASSIFIED DOCUMENT

This material contains information affecting the National Defense of the United States within the meaning of the espionage laws, Title 18, U.S.C., Secs. 793 and 794, the transmission or revelation of which in any manner to an unauthorized person is prohibited by law.

**NATIONAL ADVISORY COMMITTEE
FOR AERONAUTICS**

WASHINGTON

April 4, 1956

CONFIDENTIAL

APR 12 1956

56A

13175

NATIONAL ADVISORY COMMITTEE FOR AERONAUTICS

RESEARCH MEMORANDUM

AN EXPERIMENTAL STUDY AT HIGH SUBSONIC SPEEDS OF
SEVERAL TAIL CONFIGURATIONS ON A MODEL

WITH AN UNSWEPT WING

By William C. Sleeman, Jr.

SUMMARY

An investigation has been conducted in the Langley high-speed 7- by 10-foot tunnel of the static longitudinal and lateral stability characteristics of a model having an unswept wing and several different tail arrangements. A systematic series of Y-tails was tested in which the height of the vertical stub supporting a 40° V-tail was varied and in which the dihedral angle was varied $\pm 10^\circ$ at an intermediate stub height. In addition to these tails, a cruciform tail having both X- and +-orientations was tested, and a more conventional T-tail was investigated as a basis for comparison. All of the tails were unswept and of rectangular plan form. The wing used in this investigation had an unswept half-chord line and was of aspect ratio 3 and taper ratio 0.5. The test Mach number range extended from 0.60 to 0.94 and the angle of attack extended to 22° at the lowest test Mach number.

The overall results for the series of Y-tails were generally influenced by dihedral and vertical stub span in a manner to be expected from the geometrical differences in the tails. Rather large effects of orientation of the cruciform tail were indicated for both longitudinal and directional stability. Although none of the configurations tested provided ideal tail contributions to stability, some directional stability advantages of Y-tails at high angles of attack were indicated.

A tail-interference effect on directional stability of the T-tail configuration was indicated by the loss of end-plate effect of the horizontal tail at low angles of attack and high Mach numbers. In addition to the loss of end-plate effect, a large adverse effect of negative stabilizer incidence on directional stability near 0° angle of attack was found for both the T-tail and V-tail at the higher Mach numbers. Flight difficulty from this source would be unlikely, except possibly during some transient maneuvers for which the airplane may be momentarily out of trim.

CONFIDENTIAL

INTRODUCTION

Flight experience and wind-tunnel tests for a number of current airplane configurations have indicated the existence of various stability difficulties, and work on alleviating these problems has, for a large part, been directed toward achieving modifications to an existing basic arrangement which would eliminate or delay the onset of these difficulties. The present experimental study, while not concerned with a specific problem, was undertaken to explore the possibilities of avoiding some of the stability problems by use of tail arrangements other than those currently considered conventional. The possibility appears, that a V-tail (refs. 1 and 2) or a modified V-tail could improve the directional stability characteristics of airplanes at high angles of attack by location of the vertical stabilizing surfaces away from the fuselage. Supporting a V-tail on a vertical stub, thus forming a Y-tail would appear to be a means for obtaining additional directional stability and eliminating the need for the V-tail controls to provide directional as well as longitudinal control by placing the rudder in the vertical stub.

Static longitudinal and lateral stability characteristics were determined on a model having a number of tail configurations for Mach numbers from 0.60 to 0.94 and for an angle-of-attack range up to 22° at the lowest test Mach number. The wing used in the present tests was of aspect ratio 3, taper ratio 0.5, and had an unswept half-chord line; all of the tails had rectangular unswept plan forms. The test results were for a series of Y-tails in which the height of the vertical stub was varied down to that for a V-tail. The effect of dihedral angle was studied for the Y-tail at an intermediate stub height. Results were also obtained with a +-tail, an X-tail, and a more conventional T-tail, as well as tail off. Inasmuch as this experimental study was exploratory rather than specific, some of the configurations tested may not be considered practical from the standpoint of direct design application.

SYMBOLS

The results of this investigation are referred to the stability system of axes which is shown in figure 1 together with an indication of positive directions of forces, moments, and displacements of the model. Moment coefficients are given about the reference center shown in figure 2 (located on the fuselage center line at a longitudinal position corresponding to the 25-percent wing mean aerodynamic chord).

C_L lift coefficient, $\frac{Lift}{qS}$

CONFIDENTIAL

**NOTICE: THIS DOCUMENT CONTAINS INFORMATION AFFECTING THE
NATIONAL DEFENSE OF THE UNITED STATES WITHIN THE MEANING
OF THE ESPIONAGE LAWS, TITLE 18, U.S.C., SECTIONS 793 and 794.
THE TRANSMISSION OR THE REVELATION OF ITS CONTENTS IN
ANY MANNER TO AN UNAUTHORIZED PERSON IS PROHIBITED BY LAW.**

C_D	drag coefficient, $\frac{\text{Drag}}{qS}$
C_m	pitching-moment coefficient, $\frac{\text{Pitching moment}}{qS\bar{c}}$
C_l	rolling-moment coefficient, $\frac{\text{Rolling moment}}{qSb}$
C_n	yawing-moment coefficient, $\frac{\text{Yawing moment}}{qSb}$
C_y	lateral-force coefficient, $\frac{\text{Lateral force}}{qS}$
q	dynamic pressure, $\frac{\rho V^2}{2}$, lb/sq ft
V	velocity, ft/sec
ρ	air density, slugs/cu ft
M	Mach number
S	wing area, sq ft
b	wing span, ft
\bar{c}	wing mean aerodynamic chord, ft
α	angle of attack of fuselage center line, deg
β	angle of sideslip, deg
Γ	dihedral angle of tail, deg
i_t	stabilizer incidence measured in plane of symmetry, deg

Subscripts:

β	partial derivative of a coefficient with respect to sideslip, for example $C_{l_\beta} = \frac{\partial C_l}{\partial \beta}$
t	denotes increment due to addition of tail surfaces

MODEL DESCRIPTION

The wing-fuselage arrangement used in this investigation for all of the tail configurations is shown in figure 2. Details of the fuselage geometry can be found in reference 3. The steel wing of the model had an aspect ratio of 3, taper ratio 0.5, and unswept half-chord line (6.34° of quarter-chord sweep) and had NACA 65A004 airfoil sections parallel to the free-stream direction.

Tail 1 is shown on the model in figure 2 and indicates the longitudinal location of all the other tails. A sketch showing a rear view of the test tails on the fuselage is given as figure 3. All of the tails had a chord of 1.80 inches and NACA 65A006 airfoil sections. The tails were constructed of steel and were soldered to interchangeable fuselage blocks as shown in figure 4.

In the present study of unconventional tail arrangements, a T-tail configuration (tail 1 shown in figs. 2 and 3) was selected to represent a basic arrangement for comparative purposes. The geometry of tail 2 was selected to obtain a comparison of longitudinal stability characteristics of a T-tail and a Y-tail occupying roughly the same region inasmuch as the midpanel spans of these two tails coincided. The possibility was apparent that the losses in directional stability at high angles of attack encountered on many conventional tail arrangements could be alleviated by use of a Y-tail for which the stabilizing surfaces were located away from the fuselage. It was also expected that tail 2 could provide some longitudinal stability benefits over tail 1 in that an abrupt pitch-up tendency possible with the T-tail might be softened considerably or even eliminated. The favorable effect of the Y-tail on longitudinal characteristics would be expected first from the consideration that the tail with dihedral would enter the wing wake or regions of high downwash more gradually than a horizontal tail, and, secondly, the downwash effects on longitudinal stability would be decreased by the favorable sidewash effect on the V-tail portion as discussed in reference 2.

The dihedral angle of 40° used with tail 2 was considered the basic angle and the vertical stub span of tail 2 was reduced to give tail 3. This tail was selected, on the basis of estimated characteristics, as an arrangement giving a more reasonable combination of longitudinal and directional stability contribution. The dihedral angle for tail 3 was varied $\pm 10^\circ$ to obtain tail 4 and tail 5 in order to assess effects of this variable for a Y-tail having a moderate stub span. It is evident in figure 3 that the tail panel area increased with increasing dihedral angle inasmuch as the horizontal span of the tails was held constant. Further information on effects of stub span at the basic dihedral angle were obtained by reducing the stub to slightly less than the fuselage radius to obtain tail 6, the V-tail.

In addition to the series of Y-tails, an X-tail (tail 7) and a +-tail (tail 8) were tested. These two tails were of identical geometry and location with the exception of their orientation about the body center line. The size of these tails was selected to give close to the same directional stability contribution as the basic T-tail.

TESTS AND RESULTS

Test Conditions

Tests were conducted in the Langley high-speed 7- by 10-foot tunnel for a Mach number range from 0.60 to 0.94 and an angle-of-attack range from -2° to 22° at the lowest test Mach number. All the configurations were tested at sideslip angles of 0° and $\pm 4^{\circ}$ through the angle-of-attack range on the sting support shown in figure 5. The T-tail and X-tail configurations were also tested through a sideslip-angle range of -4° to 12° at a low and high angle of attack. Failure of a solder joint and consequent destruction of the T-tail prevented completion of all of the sideslip tests with this tail.

The average test Reynolds number based on the wing mean aerodynamic chord varied from approximately 1.00×10^6 to 1.25×10^6 for the lowest and highest test Mach numbers, respectively.

Corrections

No jet-boundary or blockage corrections have been applied to the data inasmuch as the model size was very small relative to the size of the tunnel test section. Corrections to the angles of attack and sideslip angles due to deflection of the strain-gage balance and support system under load have been applied. Corrections to the drag coefficients have been applied such that the base-pressure conditions correspond to free-stream static pressure.

Some remarks concerning the accuracy of the drag results of this investigation are warranted because the minimum drag coefficients did not always appear reasonable. The accuracy level of the drag coefficients is believed to be low because the balance chord-force gages were not sensitive enough to measure accurately the minimum drag values on the present model and the maximum values of chord force measured were only about 10 percent of the design balance capacity. Drag results are presented, therefore, only for the tail-off configuration to provide an indication of the drag due to lift. The accuracy of the lateral-force derivatives also is somewhat low inasmuch as the maximum value of lateral force attained in the tests was only about 15 percent of the design

loading capacity for this component. The experimental yawing moments on the model were closer to the design loading condition for the strain-gage balance and the yawing-moment derivative would therefore be expected to be a more accurate indication of tail effects on lateral characteristics than the lateral-force derivative $C_{Y\beta}$.

Presentation of Results

The basic aerodynamic characteristics for the wing-body configuration and for its combination with the various tail configurations are presented in figures 6 to 15. Aerodynamic characteristics through the sideslip range for the T-tail and X-tail are included in figures 8 and 15. Lateral stability derivatives obtained from tests at $\pm 4^\circ$ sideslip for the various model configurations are presented in figures 16 to 20 and include effects of stabilizer incidence for the T-tail and V-tail. Some of the pertinent tail-configuration effects are summarized in figures 21 to 24 and a comparison of lateral derivatives with respect to the body axes and stability axes is given in figure 25.

DISCUSSION

Wing-Body Characteristics

Test results for the complete model exhibit some significant stability effects which are for the most part attributable to the wing-body behavior rather than to the tail contribution. These wing-body effects, of course, must be considered for a more general evaluation of the tail configurations studied.

The tail-off pitching-moment characteristics presented in figure 6 indicate a large rearward shift in aerodynamic-center location in going from low to moderately high values of lift coefficient. In the higher lift-coefficient range (above approximately 15° angle of attack), a large reduction in stability occurred. These pitching-moment characteristics generally persist in all of the tail-on test data and therefore the large longitudinal stability changes over the angle-of-attack range shown in the complete-model results may be attributed to a large extent to the basic tail-off characteristics.

Directional stability results for the wing-body configuration (fig. 17) also exhibit characteristics worthy of attention at angles of attack above 15° . For angles of attack below about 10° , the unstable moments of the wing-body configuration varied only slightly with increasing angle of attack. At higher angles, however, the wing-body configuration became directionally stable. This occurrence of positive

directional stability at high angles of attack has been encountered experimentally on other wing-body configurations and appears to be due to the stabilizing contribution of the unswept wing as indicated in reference 4.

In view of the aforementioned wing-body characteristics, which would tend to make the complete-model results less directly indicative of tail characteristics, the tail contributions to pitching moments and lateral stability derivatives are summarized in figures 21 and 22 for Mach numbers of 0.60 and 0.94.

Effects of Stabilizer Incidence on Lateral Characteristics

The importance of selecting a proper stabilizer incidence with regard to the longitudinal characteristics was recognized in the design of the test tail configurations. In order to reduce the chance of interpreting positive tail stall as pitch-up, and to have the model in longitudinal trim at a moderately high angle of attack, the tails (with the exception of tails 7 and 8) were constructed with a fixed setting of -6° .

The use of a moderate negative stabilizer setting afforded some definite advantages in interpreting pitching-moment data in the higher lift range; however, some unexpected lateral stability characteristics were encountered at Mach number of 0.80 and above, at low lift where the model was not in longitudinal trim. The lateral stability derivatives presented in figures 16 and 17 show a large loss in directional stability for the -6° stabilizer setting at low angles of attack as the Mach number increased from 0.60 and in some cases the occurrence of directional instability at 0° angle of attack was indicated for both the T-tail (fig. 16) and the V-tail (fig. 17). This large directional stability loss at 0° angle of attack of course appeared unusual and both the T-tail and V-tail were modified to obtain a neutral setting which would be more appropriate from the standpoint of longitudinal trim at low lift than the -6° setting. Lateral stability characteristics with the neutral stabilizer setting are also given in figures 16 and 17 and show no outstanding effects of stabilizer setting through the angle-of-attack range for the lowest Mach number ($M = 0.60$). For the higher Mach numbers and at low angles of attack, the directional stability of the model with the neutral stabilizer was much higher and appeared more reasonable than that obtained with the -6° setting. Directional stability characteristics for angles of attack above approximately 10° were not appreciably affected by stabilizer setting with the exception of the T-tail at $M = 0.94$ (fig. 16). It might be of interest to observe that with both the T-tail and V-tail at high Mach numbers, the increment of

CONFIDENTIAL

C_{n_p} in going from 0° to 6° angle of attack for the negative stabilizer setting was approximately the same as the increment in going from a stabilizer setting of -6° to 0° at $\alpha = 0^\circ$. This would appear to indicate that the losses in C_{n_p} at low angles of attack were associated primarily with the horizontal-tail angle of attack.

The adverse effect of negative stabilizer setting on directional stability shown in figures 16 and 17 is believed to be due to flow breakdown resulting from shock formation. These Mach number effects on the vertical tail in the presence of the horizontal tail will be discussed more fully in the following section on T-tail characteristics. The adverse effects of negative stabilizer setting for the V-tail are believed to be due to the adverse juncture at the acute angle formed by the tail and the converging fuselage afterbody.

Test results for the Y-tails (figs. 18 and 19) which had -6° incidence showed directional characteristics at low angles of attack and high Mach numbers similar to those of the T-tail. Although data were not obtained with a neutral setting for the Y-tails, it is believed that the effects of stabilizer setting shown for the T-tail may be indicative of effects to be expected for the Y-tails. Inasmuch as the lateral stability derivatives for all the tails with -6° incidence probably were affected by incidence at the higher test Mach numbers, subsequent comparison of estimates with experimental results will be confined to the lowest test Mach number. The tail contribution to both longitudinal and lateral characteristics is presented, however, for the lowest and highest test Mach numbers in order to illustrate the Mach number interference effect.

T-Tail Characteristics

Pitching-moment characteristics for the complete model with the T-tail given in figure 7 indicate the abrupt pitch-up tendency with the neutral stabilizer setting was delayed to a slightly higher angle of attack when the negative setting was used. This may have been due to either the onset of tail stalling for the neutral setting or a decrease in stabilizer effectiveness resulting from the tail entering the wake at high angles of attack. The contribution of the T-tail to pitching moments is compared with the other tails in figure 21 for the lowest and highest test Mach numbers (0.60 and 0.94).

Aerodynamic characteristics over a range of sideslip angle from -4° to 12° are presented in figure 8 for the T-tail configuration at nominal angles of attack of 0° , 10° , and 15° . These test results were obtained with the stabilizer set at -6° incidence and show the occurrence of directional instability at $M = 0.90$ which was indicated in the derivatives of figure 16 for a range of sideslip angle of $\pm 4^\circ$. The directional

CONFIDENTIAL

stability of the model with the T-tail was generally less at sideslip angles approaching the maximum test angles than at moderate sideslip angles. Pitching-moment characteristics with the T-tail for $\alpha = 0^\circ$ presented in figure 8 shows the fairly large variation in pitching moment with increasing sideslip expected for a T-tail configuration (ref. 5); however, the pitching-moment variation was much less at the highest angle of attack than at 0° angle of attack.

Lateral stability derivatives for the T-tail configuration are presented in figure 16 and the tail contribution at Mach numbers of 0.60 and 0.94 is given in figure 22. The results of figure 22 show that the vertical-tail contribution to $C_{n\beta}$ was increased about 30 percent at 0.60 Mach number by addition of the horizontal tail for angles of attack up to approximately 12° . Above this angle of attack, the effect of the horizontal tail decreased to the vanishing point at $\alpha = 22^\circ$. At the highest test Mach number, the end-plate effect of the horizontal tail at 0° angle of attack was unfavorable even with an incidence of 0° (fig. 22(b)). This loss of end-plate effect can be seen from the basic data of figure 16 to increase progressively with Mach number above $M = 0.80$. Reasons for this unfavorable effect of the horizontal tail at the higher Mach numbers have not been definitely established; however, it is believed to be due to the same type of interference as that encountered previously for the effects of stabilizer setting. A possible explanation of this horizontal-tail interference encountered at 0° angle of attack and stabilizer setting may be the simple addition of velocities due to thickness of the intersecting airfoils causing shock formation and flow breakdown. Of course, the effects of a down load on the horizontal tail would add to the thickness effects to cause the interference to increase with negative increments in either model angle of attack or stabilizer incidence. There is evidence that this flow breakdown at 0° angle of attack and stabilizer incidence can be alleviated by stagger of the horizontal and vertical surfaces or by incorporation of sweepback in the tail surfaces. The possibility exists that the fuselage afterbody shape contributed to the flow breakdown; therefore modifications to the afterbody might also be expected to improve the tail contribution.

A rather unusual aspect of the end-plate effect was noted for the T-tail at the higher test Mach numbers, and for discussion of these results reference is made to the basic stability derivatives presented in figure 16. Attention is called to the variation of directional stability with angle of attack at the different Mach numbers for the neutral stabilizer setting. These results show a large increase in the variation of $C_{n\beta}$ with angle of attack as the Mach number increased; however, the peak value of $C_{n\beta}$ (occurring slightly below 10° for Mach numbers from 0.80 to 0.94) remained approximately the same, whereas the values of $C_{n\beta}$ at low angles of attack decreased appreciably with Mach number. The data

also indicate that further decreases in directional stability would be expected for increasing negative angles of attack. This large variation in directional stability with angle of attack, characterized by significant losses at low angles of attack, is believed to be further manifestation of the horizontal-tail interference discussed in relation to end-plate effects and stabilizer incidence. Additional test results relative to this problem were obtained (unpublished data for a model three times the size of the present model) which substantiated the interference effects encountered in the present study. These data were obtained on a model having a delta-plan-form horizontal tail mounted at the tip of a swept vertical tail and results were obtained for a fairly large negative as well as positive angle-of-attack range. These results were in agreement with the trends in the variation of directional stability with angle of attack at negative angles shown for the present test results. These data indicate furthermore the desirability of exploring directional stability characteristics in the negative as well as positive angle-of-attack range in wind-tunnel studies inasmuch as large negative angles have been reached inadvertently on a number of current high-speed airplanes which experienced large lateral-longitudinal coupled motions (for example, ref. 6).

Y-Tail Characteristics

The longitudinal and particularly the directional stability characteristics of the model were generally affected by dihedral and tail height in a manner to be expected from the obvious geometrical differences in the tails (figs. 21 and 22). The pitching-moment contribution of the Y-tails was not appreciably different from that of the T-tail at $M = 0.60$ (fig. 21(a)) and all of the Y-tails as well as the T-tail showed a pitch-up tendency of the tail contribution in the angle-of-attack range from 18° to 20° . Pitching-moment contributions of the Y-tails at $M = 0.94$ were more favorable than for the T-tail in that the destabilizing break shown for the T-tail (fig. 21(b); $i_t = -6^\circ$) above $\alpha = 2^\circ$ was greatly reduced with tail 2 and tail 4. Somewhat smaller stabilizing gains in tail contribution were realized with tail 3 and tail 5 which had lower effective tail heights.

Very large differences in directional stability, of course, accompanied changes in dihedral and stub span (fig. 22) and appreciable changes in the tail contribution with angle of attack occurred for the Y-tails. The large differences in tail contribution shown in figure 22(a) at 0° angle of attack for the different configurations is due, for the most part, to differences in tail area rather than to tail location. The results of figure 22(a) have therefore been normalized at 0° angle of attack to indicate more clearly the comparative effects of tail configuration throughout the angle-of-attack range. These results are presented in figure 23 as a ratio of the tail contribution to $C_{n\beta}$ divided by the

value of the tail contribution at 0° angle of attack. The directional stability contribution at the highest test angle of attack (fig. 23) was greater than 50 percent of the value at 0° angle of attack for the Y- and V-tails (excepting tail 2), whereas the stability contribution for the T-, X-, and +-tails was less than half of the stability at 0° . The Y-tails, furthermore, generally showed much less stability decrease with angle of attack above $\alpha = 20^\circ$ than the T-tail, X-tail or +-tail.

+- and X-Tails

The +-tail and X-tail were of identical geometry with the exception of their orientation on the body center line and the effects of orientation were found to be quite large on both the longitudinal and lateral characteristics. Pitching-moment results, for example (figs. 14 and 21), indicate that considerably less low-lift stability was obtained with the +-tail than with the X-tail and at the highest test Mach number the presence of the +-tail was actually destabilizing near zero lift (fig. 21(b)). In the high angle-of-attack range at the lower test Mach numbers (fig. 21(a)), however, somewhat more stability was obtained with the +-tail than with the X-tail, and both of these tails had more favorable pitching-moment characteristics than either the Y-tails or T-tails at high angles of attack.

Directional stability characteristics at the two lowest test Mach numbers with the X-tail and +-tail (fig. 20) were approximately the same for angles of attack up to about 15° . Above 15° the overall stability with the X-tail deteriorated rapidly with increasing angle of attack (fig. 20) and the contribution of the X-tail was destabilizing at angles of attack above 21° and 24° for $M = 0.60$ and 0.80 , respectively (figs. 17 and 20). Directional stability of the complete model with the +-tail was almost invariant with angle of attack (fig. 20) at the lowest Mach number tested; however, the tail contribution shown in figure 22 for both the X-tail and +-tail decreased appreciably at high angles of attack at $M = 0.60$. No large differences in directional stability for the +- and X-tail were evident at the highest test Mach numbers (fig. 22(b)) where the angle-of-attack range was limited.

The variation of tail contribution to directional stability with angle of attack for the X-tail and +-tail at the lowest test Mach number (figs. 22(a) and 23) showed the same general trends and values as the T-tail. At Mach number 0.94 , the contribution of the X-tail and +-tails was almost invariant with angle of attack at low angles; whereas the T-tail showed the aforementioned large variation with angle of attack near 0° .

Estimated Tail Contribution

Estimates of the tail contribution to stability have been made only for the lateral stability derivatives inasmuch as the degree to which these derivatives were affected by tail configuration was much greater than for the longitudinal stability. Experimental and estimated results showing the variation of tail contribution to lateral derivatives with dihedral and stub height are presented in figure 24. The results of figure 24 were confined to the lowest test Mach number and 0° angle of attack because of the aforementioned effects of Mach number and stabilizer setting.

Estimates of the V-tail contribution to the lateral derivatives were obtained by using the relationships of V-tail theory given in reference 1 and using values of lift slopes obtained from the relationships given in appendix A of reference 7. In the estimation of the contribution of the tail to yawing moments and rolling moments, the resultant force on the V-portion of the tail was assumed to act at the quarter chord and mid-span for each panel. The contribution of the vertical stub was estimated from the theoretical approach of reference 8 and the end-plate effect of the V-portion on the stub of the Y-tail was obtained from the theory given in reference 8 for a horizontal tail located at the tip of a vertical tail.

Estimates of the contribution of the V-tail presented on the right-hand side of figure 24 are in fairly good agreement with experiment and, likewise, the estimated variation of $C_{n\beta_t}$ with dihedral angle shown on the left-hand side of figure 24 is in good agreement with the experimental variation. These comparisons indicate that simple V-tail theory would be expected to afford reliable means for estimating the V-tail contribution for the range of tails used in this investigation. The estimated contribution of the Y-tails, however, shows an increasing discrepancy with experiment with increasing stub height. The discrepancy between estimates and experiment could be because of either the underestimation of end-plate effects of the fuselage and V-portion of the tail or to inaccuracies in the estimated sidewash effects. Inasmuch as sidewash effects would be expected to be minimized for the condition at 0° angle of attack selected, it would appear that mutual interference effects of the fuselage, stub and V-portion of the tail were probably underestimated. Possible effects not accounted for in the estimates are the end-plate effect of the fuselage on the V-tail and the loading induced on the fuselage by the V-tail; however, these effects would probably diminish with increasing stub height. Also, it would be expected that in sideslip, the stub would induce additional loading on the V-portion of the tail and likewise the V-portion would induce a loading on the stub in addition to the type of end-plate effect contributed by a horizontal tail. The extent to which these effects for the Y-tails caused the experimental results to differ from the estimates

CONFIDENTIAL

is not known; however, estimates of the angularity induced on the stub by the V-portion in sideslip indicated that this effect was probably quite small.

Characteristics Referred to Body-Axis System

The lateral stability derivatives C_{l_β} and C_{n_β} are presented in figure 25 for all of the tail configurations to indicate the differences in these derivatives when referred to the body-axis system instead of the stability-axis system. The comparison presented in figure 25 shows that the directional stability derivatives for all configurations was appreciably reduced in going from the stability-axis system to the body axis as the angle of attack was increased from 0° . The effective dihedral parameter C_{l_β} was increased when referred to the body-axis system for the tail-on configurations.

CONCLUSIONS

An experimental investigation at high subsonic speeds of several unswept-tail arrangements on a model having a low-aspect-ratio unswept wing indicated the following conclusions:

1. Although an optimum arrangement having a constant tail contribution to stability throughout the angle-of-attack range was not closely approached in the present study, some directional stability advantages of Y-tails at high angles of attack were indicated without any outstanding stability disadvantages being evident compared to the T-tail.

2. Pitching-moment characteristics of the T-tail and the series of Y-tails tested were not greatly different, and the directional stability characteristics with the Y-tails were generally affected by dihedral and vertical stub span in a manner to be expected from the geometrical differences in the tails.

3. Rather large effects of orientation of a cruciform tail were indicated on both longitudinal and directional stability. The contribution to longitudinal stability for the cruciform tail oriented as an X-tail was greater than the +-tail arrangement in the low lift range. Directional stability characteristics with the X-tail were markedly inferior to the +-tail at high angles of attack for Mach numbers of 0.60 and 0.80.

4. A large tail-interference effect on directional stability of the T-tail configuration was indicated by the loss of end-plate effect of the horizontal tail at low angles of attack and high Mach numbers. This

CONFIDENTIAL

interference effect at high speeds was also characterized by a large variation of directional stability with angle of attack, accompanied by significant stability losses in the low angle-of-attack range.

5. A large effect of stabilizer incidence on the directional stability at low angles of attack was found at high Mach numbers for the T-tail and V-tail. The directional stability for these conditions decreased from a reasonably high positive value to a negative value in going from 0° to -6° stabilizer incidence. This adverse effect of negative stabilizer incidence would be important for an out-of-trim condition such as may occur in some transient maneuvers. At angles of attack above 6° there was little consistent effect of stabilizer setting on directional stability.

6. Estimates of the V-tail contribution to directional characteristics using available V-tail theory were in good agreement with experimental results at the lowest test Mach number for the V-tail and the Y-tails. Estimates of the vertical-stub contribution for the Y-tails were lower than experiment at a Mach number of 0.60 particularly for the greatest stub span tested.

Langley Aeronautical Laboratory,
National Advisory Committee for Aeronautics,
Langley Field, Va., December 23, 1955.

REFERENCES

1. Purser, Paul E., and Campbell, John P.: Experimental Verification of a Simplified Vee-Tail Theory and Analysis of Available Data on Complete Models with Vee Tails. NACA Rep. 823, 1945. (Supersedes NACA ACR L5A03.)
2. Polhamus, Edward C., and Moss, Robert J.: Wind-Tunnel Investigation of the Stability and Control Characteristics of a Complete Model Equipped With a Vee Tail. NACA TN 1478, 1947.
3. Few, Albert G., Jr., and King, Thomas J., Jr.: Some Effects of Tail Height and Wing Plan Form on the Static Longitudinal Stability Characteristics of a Small-Scale Model at High Subsonic Speeds. NACA RM L54G12, 1954.
4. Kuhn, Richard E., and Fournier, Paul G.: Wind-Tunnel Investigation of the Static Lateral Stability Characteristics of Wing-Fuselage Combinations at High Subsonic Speeds - Sweep Series. NACA RM L52G11a, 1952.
5. Polhamus, Edward C.: Some Factors Affecting the Variation of Pitching Moment With Sideslip of Aircraft Configurations. NACA RM L55E20b, 1955.
6. NACA High-Speed Flight Station: Flight Experience with Two High-Speed Airplanes Having Violent Lateral-Longitudinal Coupling in Aileron Rolls. NACA RM H55A13, 1955.
7. Polhamus, Edward C., and Sleeman, William C., Jr.: The Rolling Moment Due to Sideslip of Swept Wings at Subsonic and Transonic Speeds. NACA RM L54L01, 1955.
8. Weber, J., and Hawk, A. C.: Theoretical Load Distributions on Fin-Body-Tailplane Arrangements in a Sidewind. Rep. no. Aero. 2518, British R.A.E., Aug. 1954.

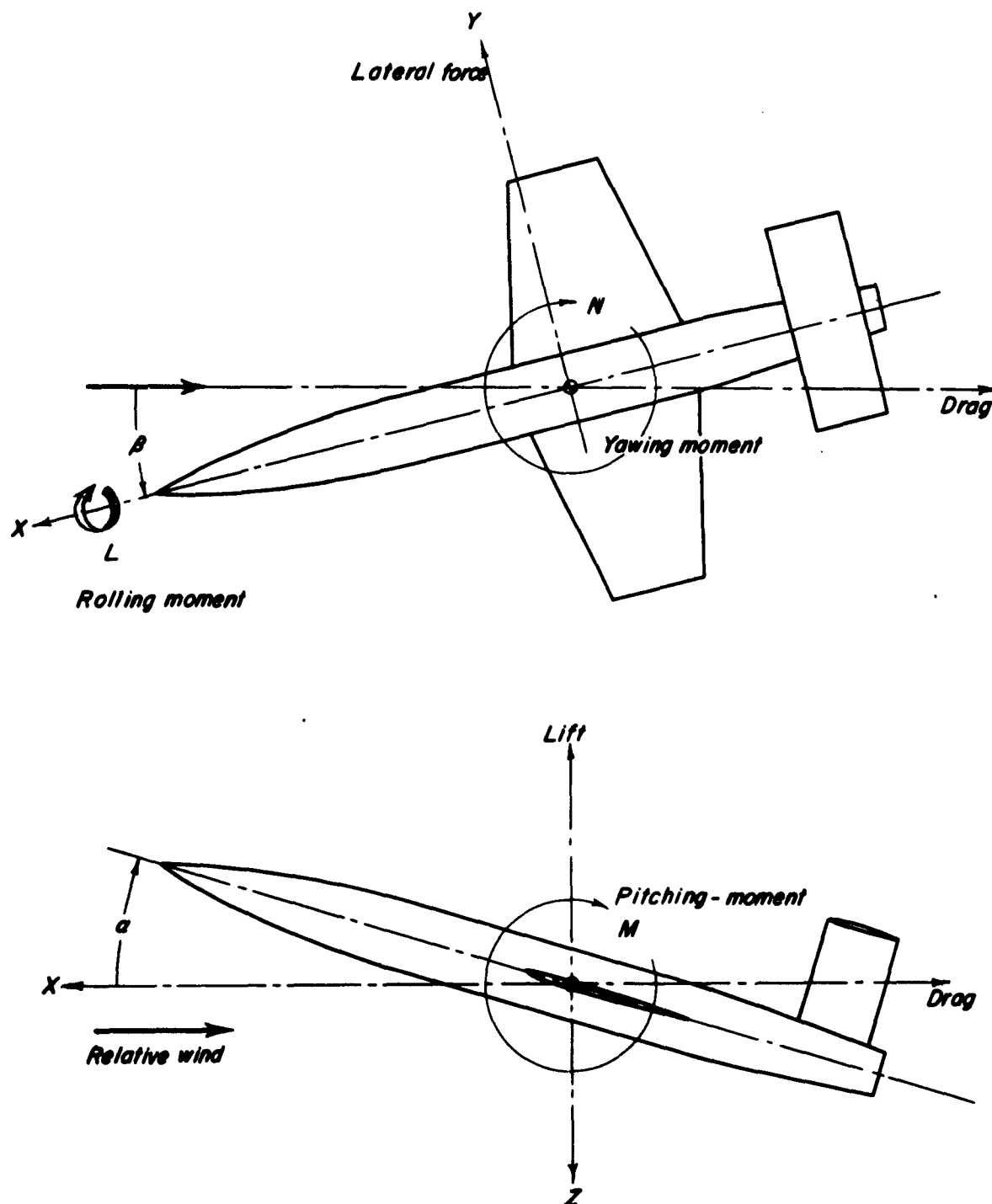


Figure 1.- Stability system of reference axes showing positive directions of forces, moments, and angular deflections.

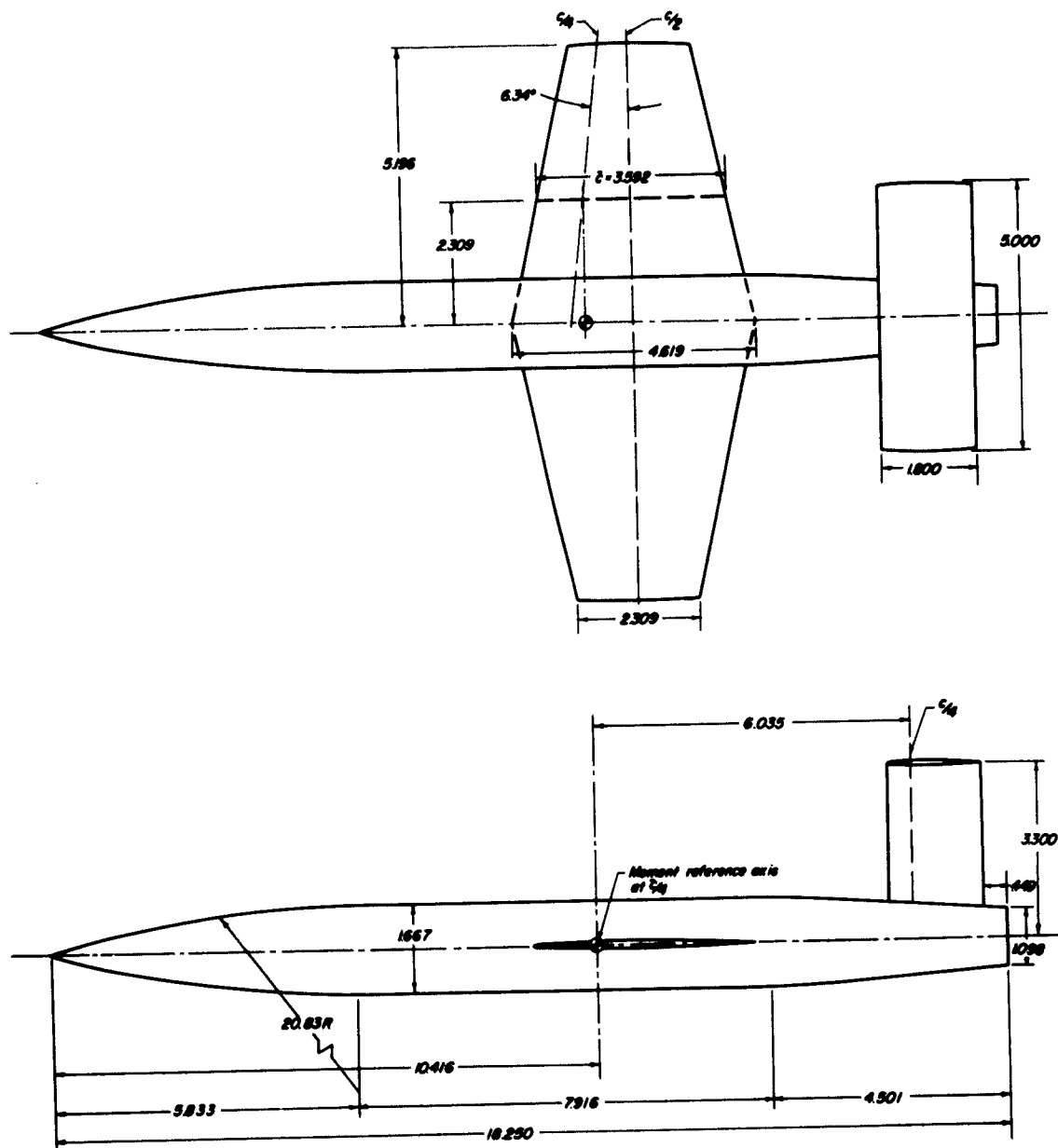


Figure 2.- General arrangement of the test configuration with tail 1 installed. Linear dimensions are in inches.

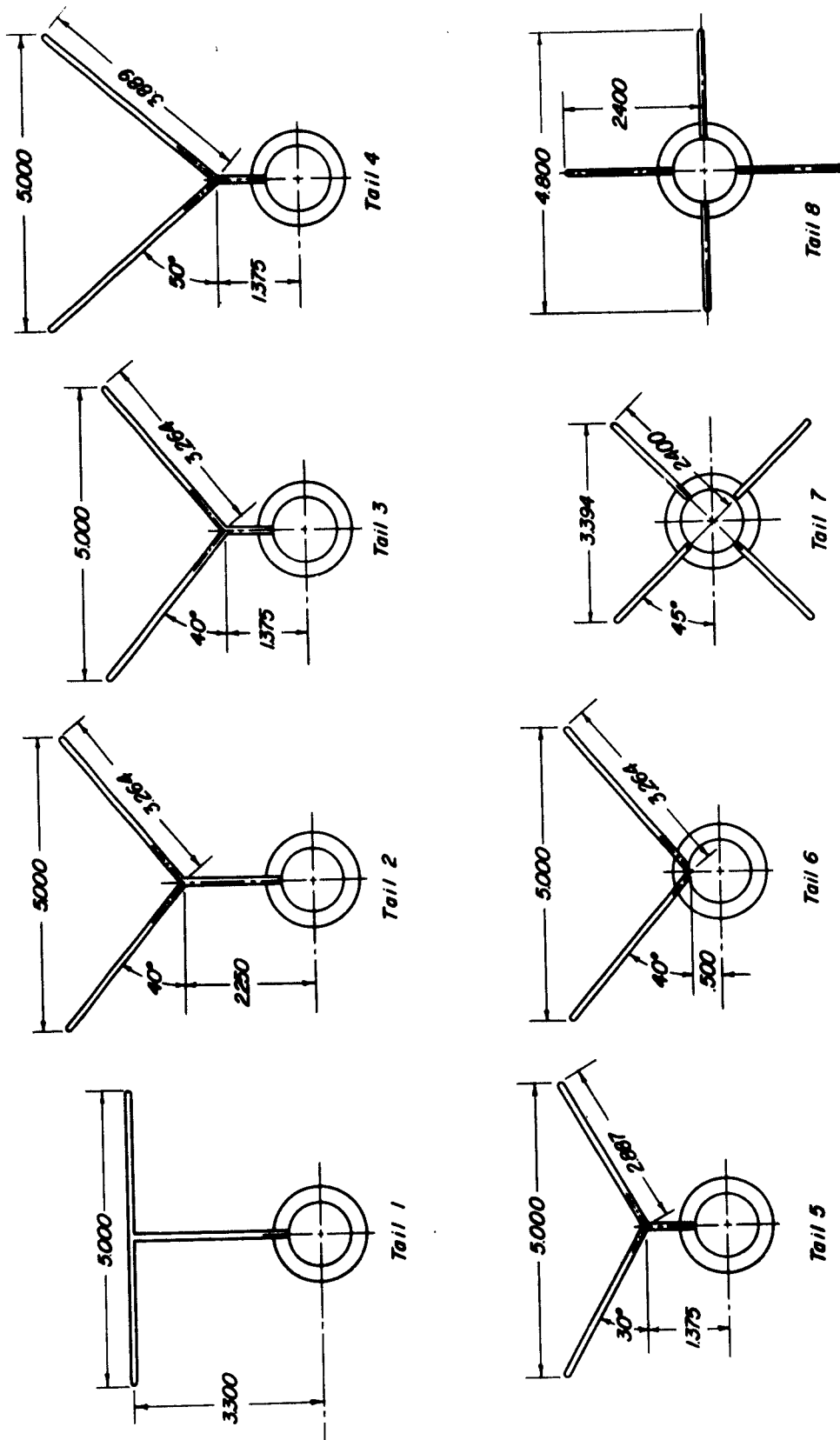
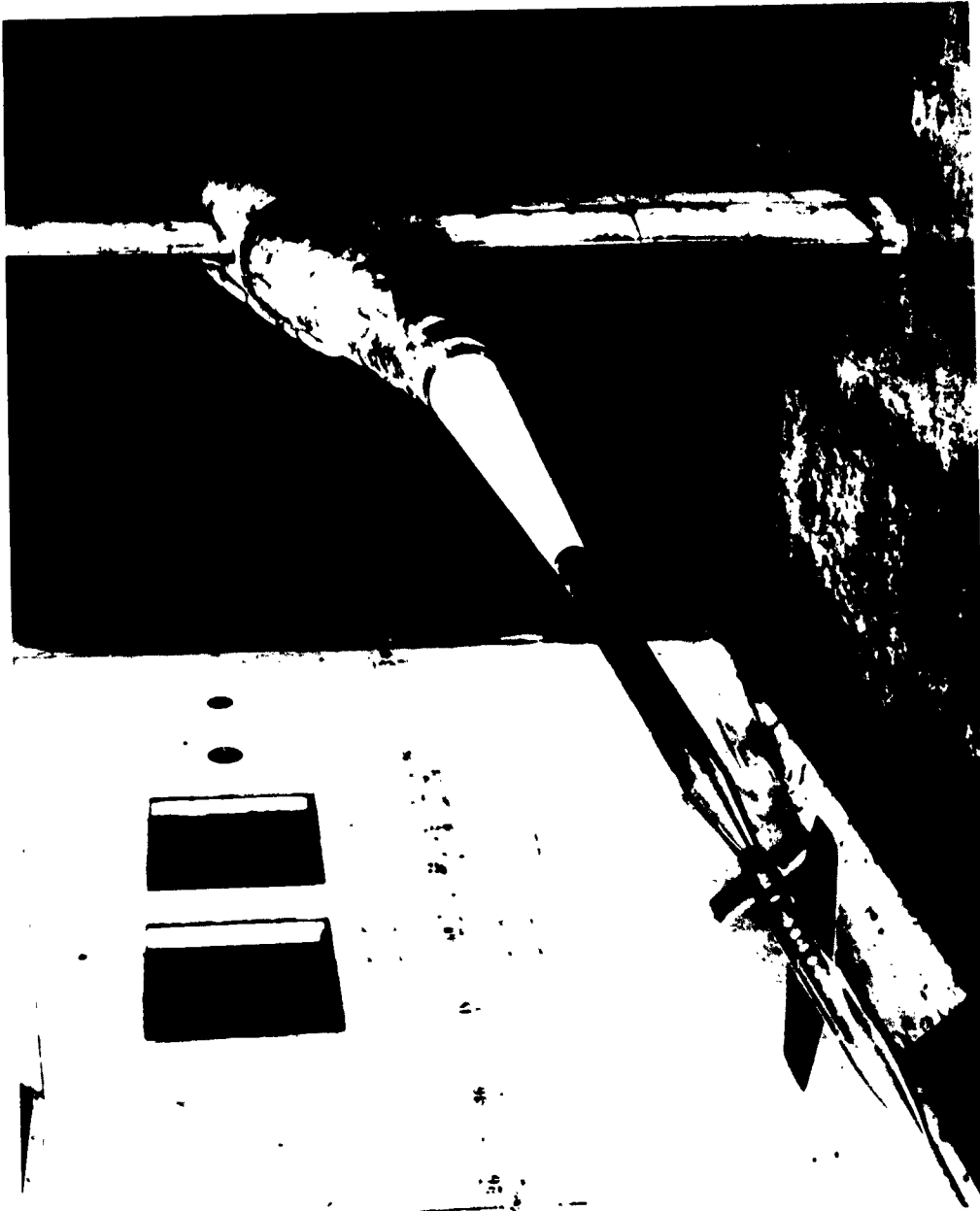


Figure 3.- Rear view of the various tail configurations mounted on the fuselage. Linear dimensions are in inches.



L-85555
Figure 4.- Photograph of the test model and various tail arrangements.



L-85853
Figure 5.- View of the model with the X-tail mounted on the sting support
in the Langley high-speed 7- by 10-foot tunnel.

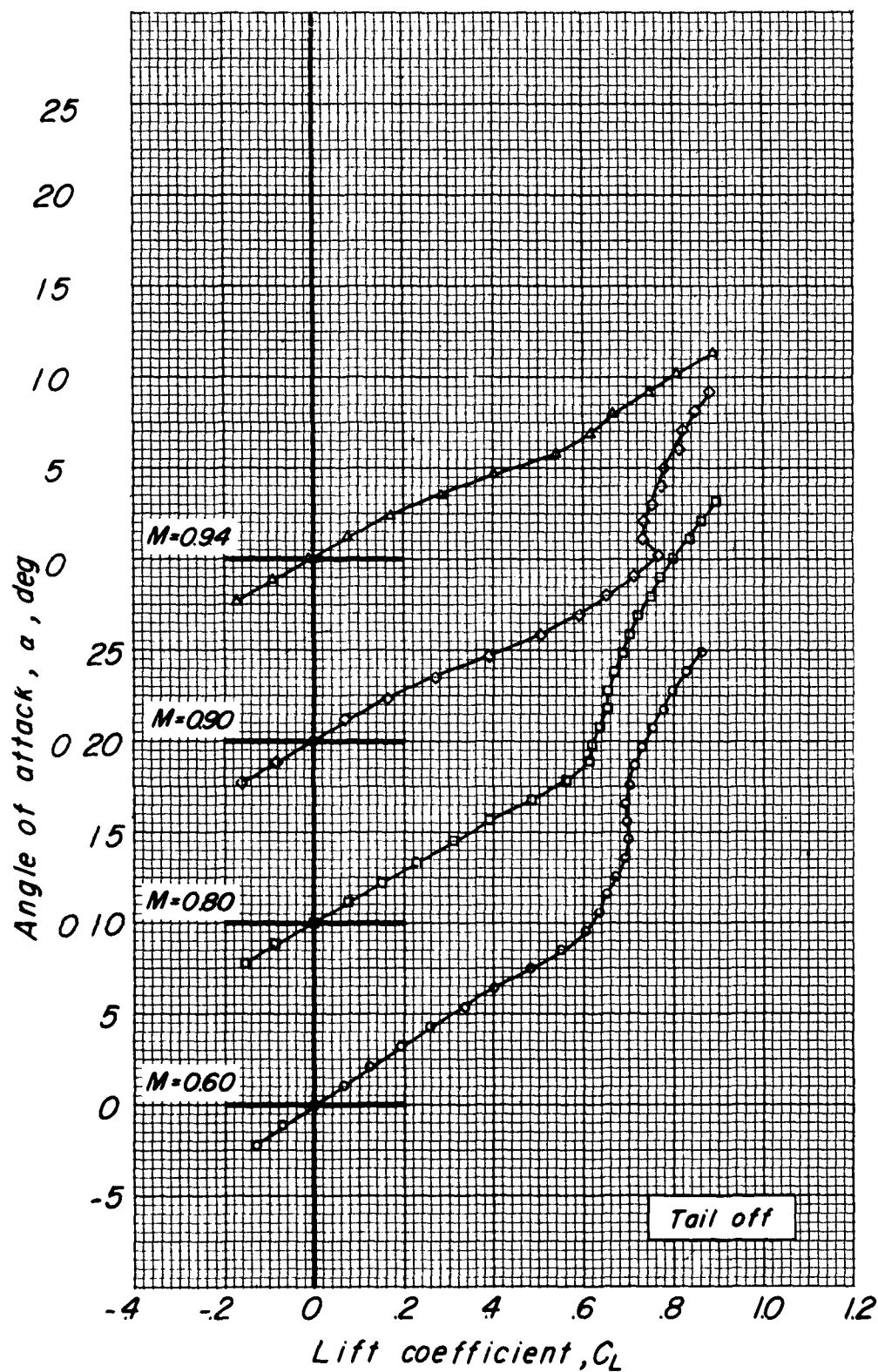


Figure 6.- Aerodynamic characteristics in pitch of the wing-fuselage configuration.

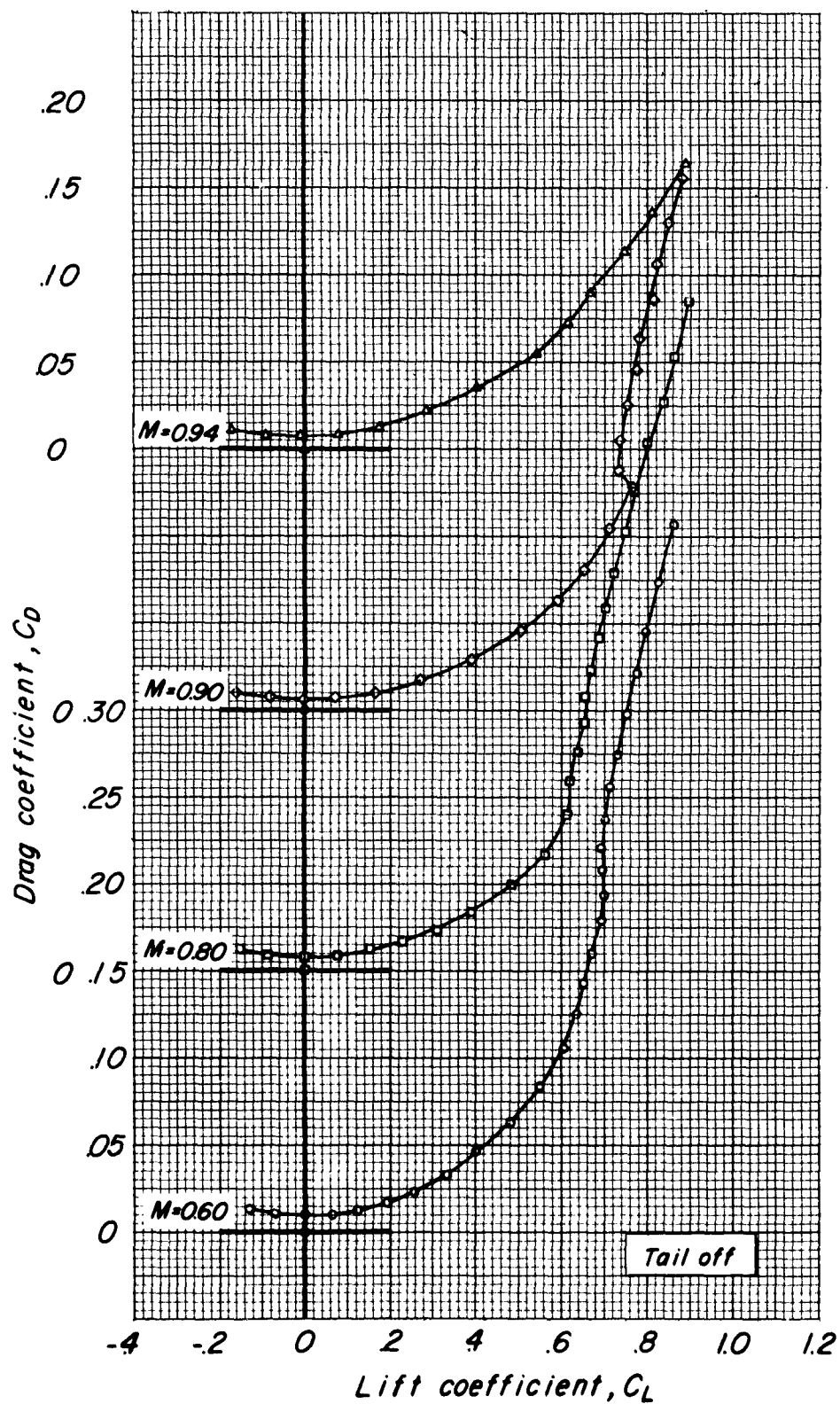


Figure 6.- Continued.

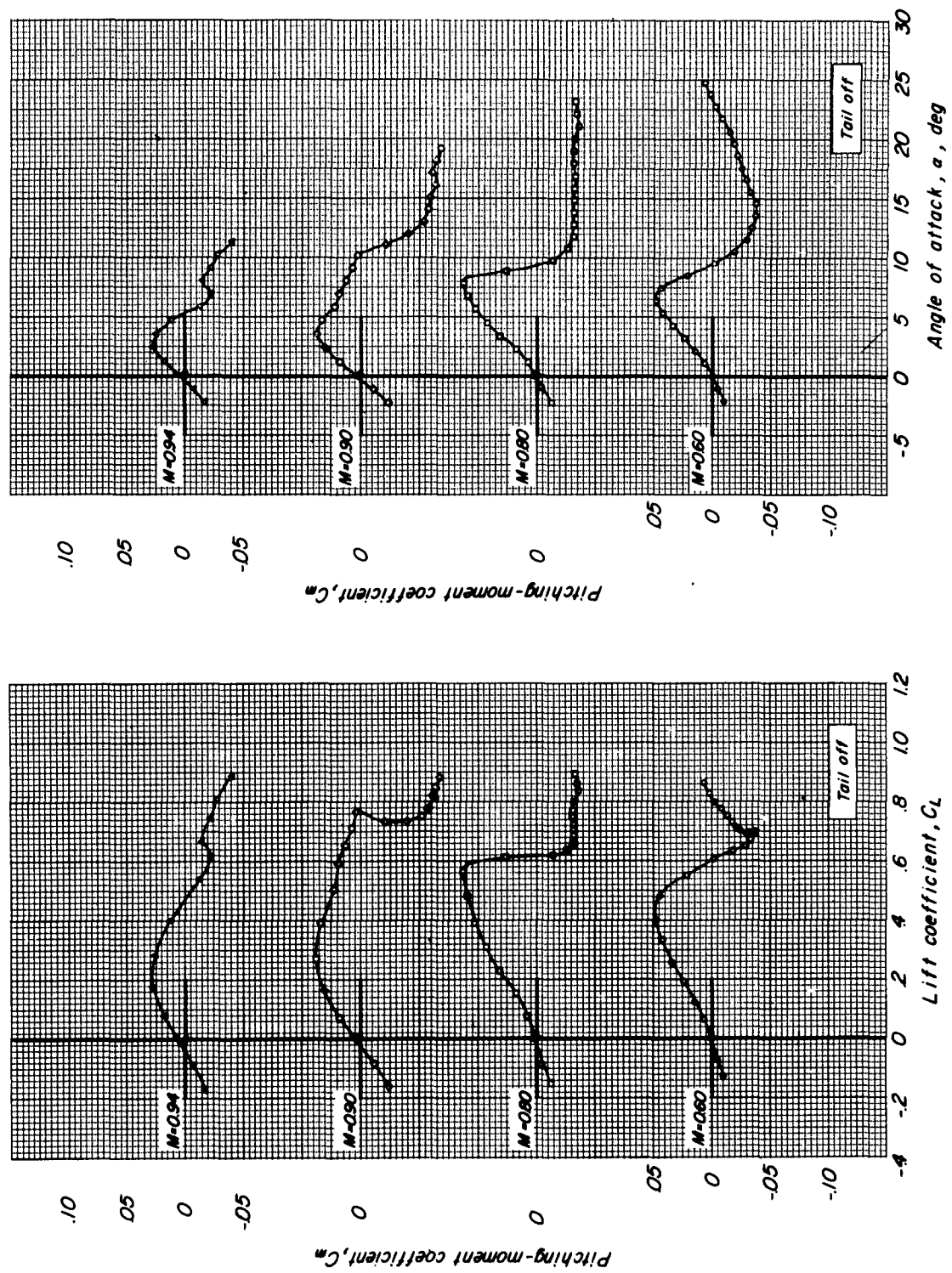


Figure 6.- Concluded.

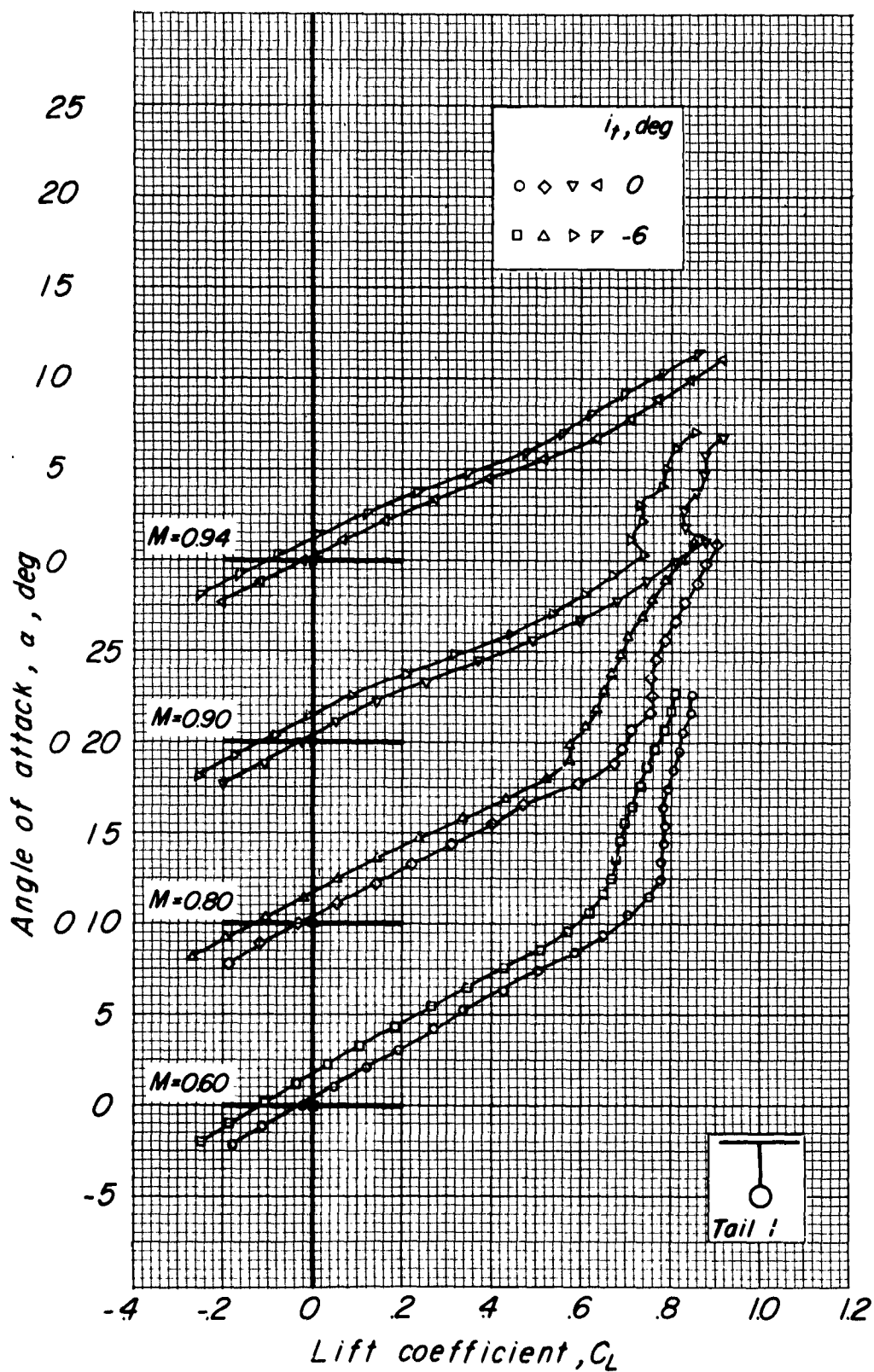


Figure 7.- Aerodynamic characteristics in pitch of the model with tail 1.

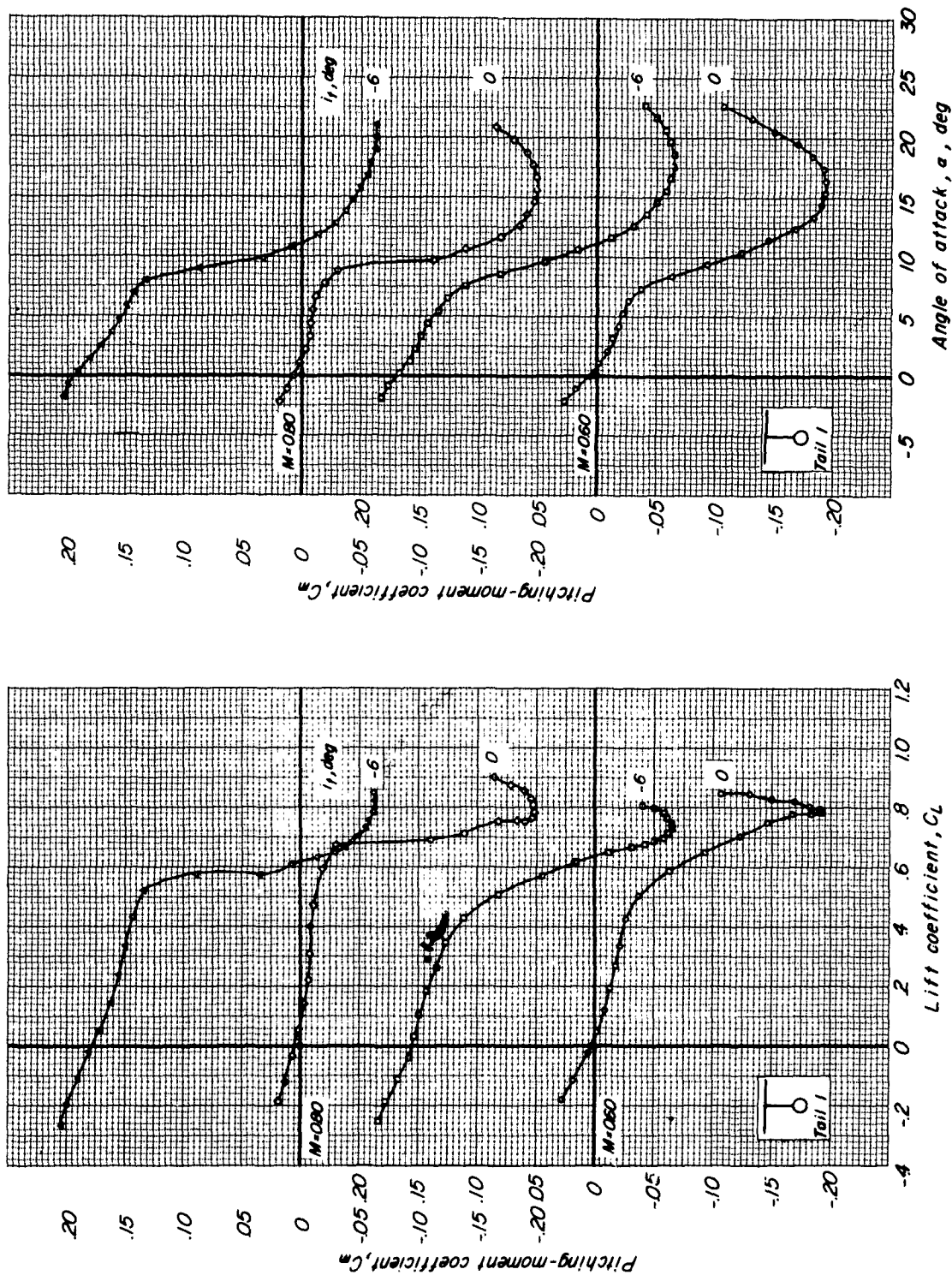


Figure 7.- Continued.

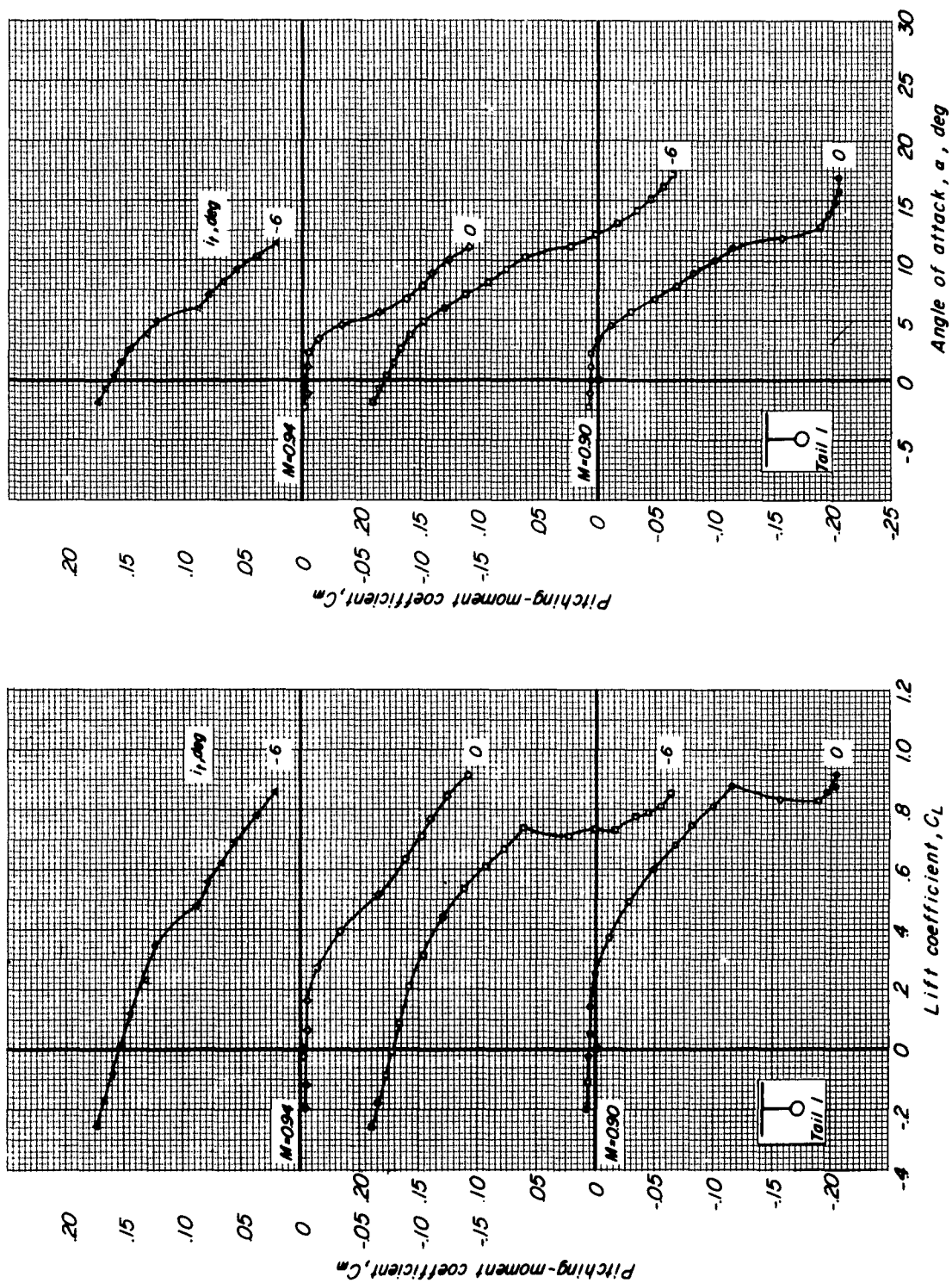


Figure 7.- Concluded.

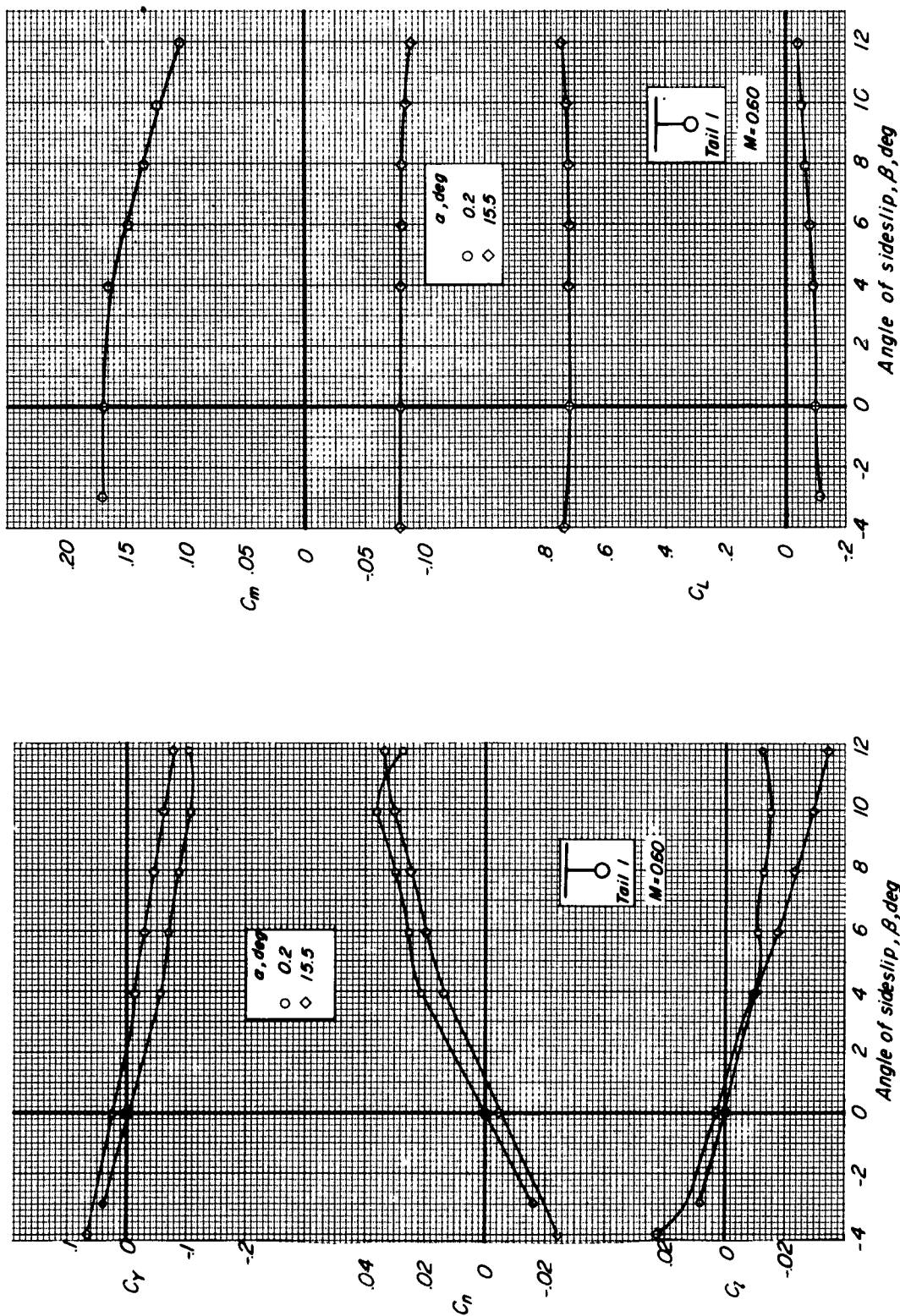


Figure 8.- Aerodynamic characteristics in sideslip of the model with tail 1. $\alpha_t = -6^\circ$.

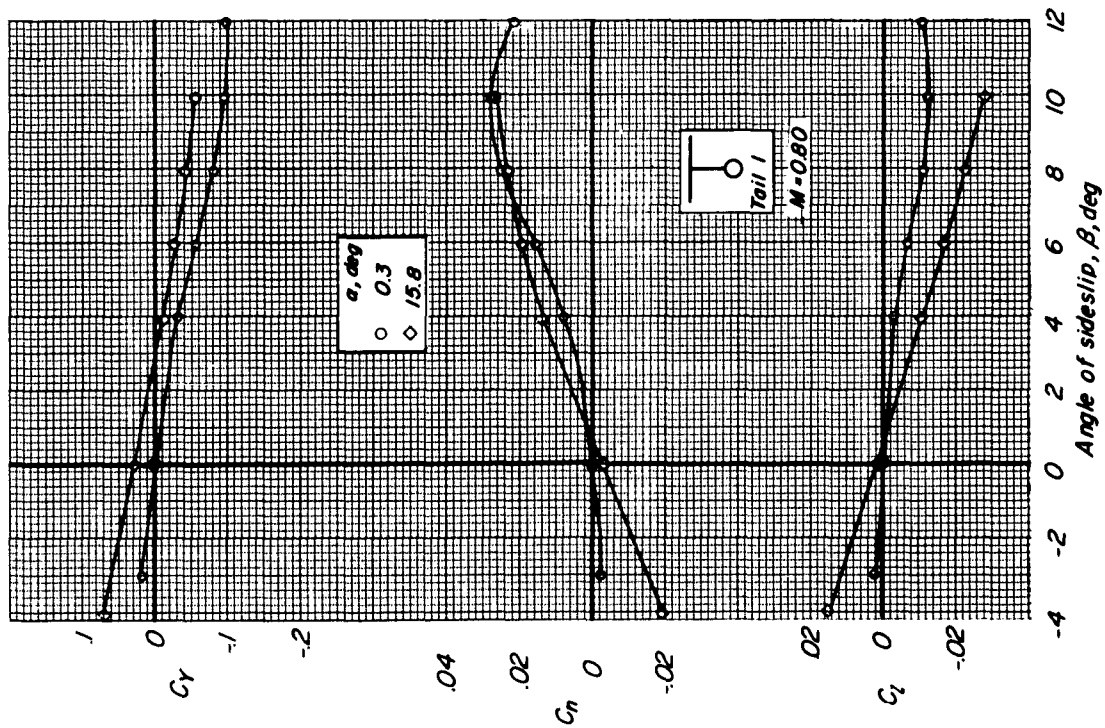
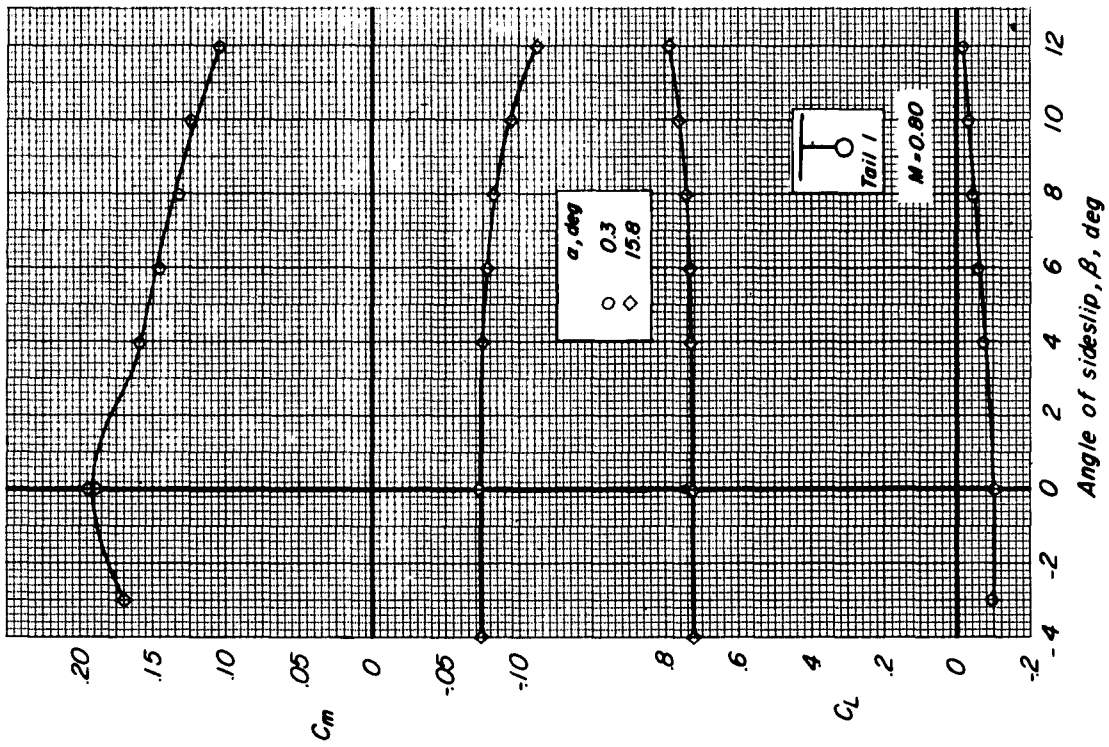


Figure 8.- Continued.

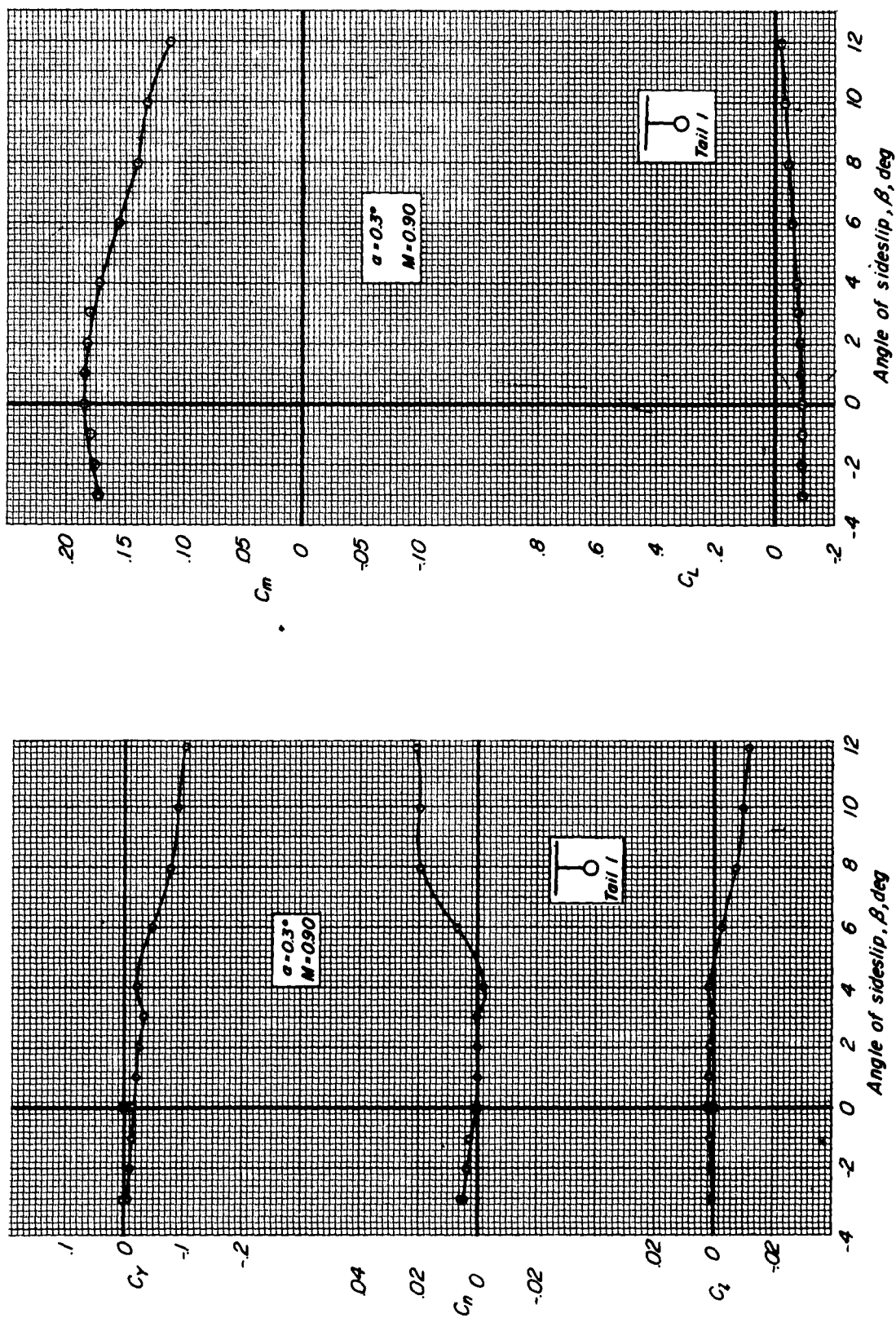


Figure 8.- Continued.

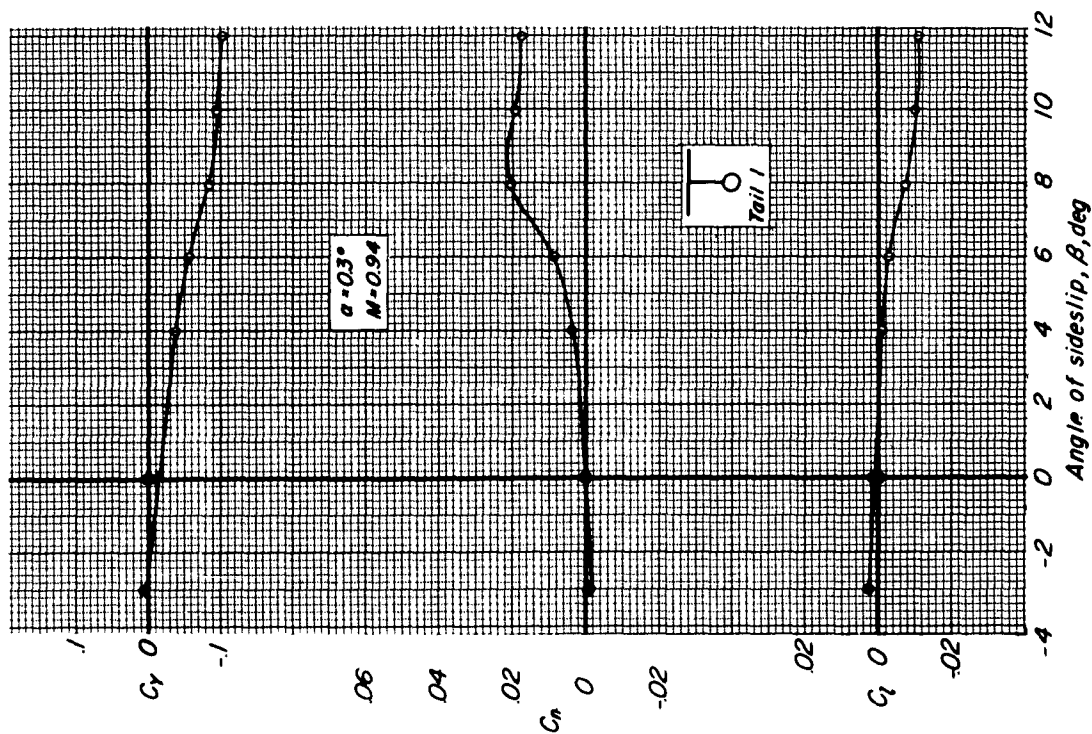
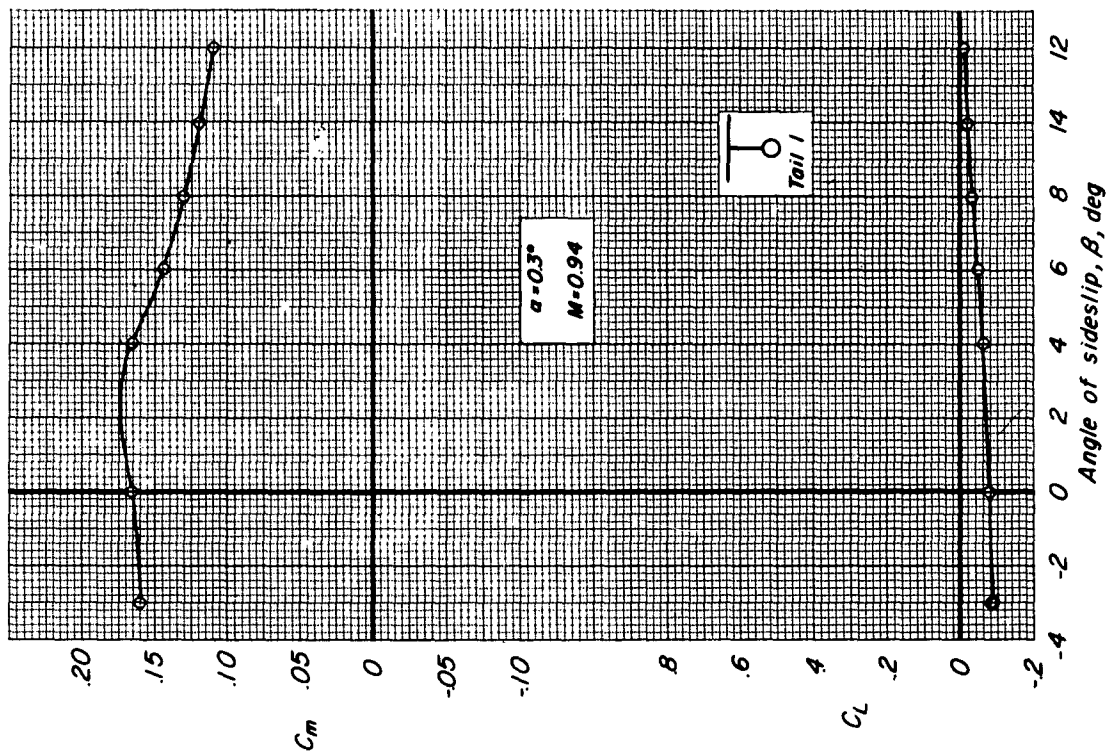


Figure 8.- Concluded.

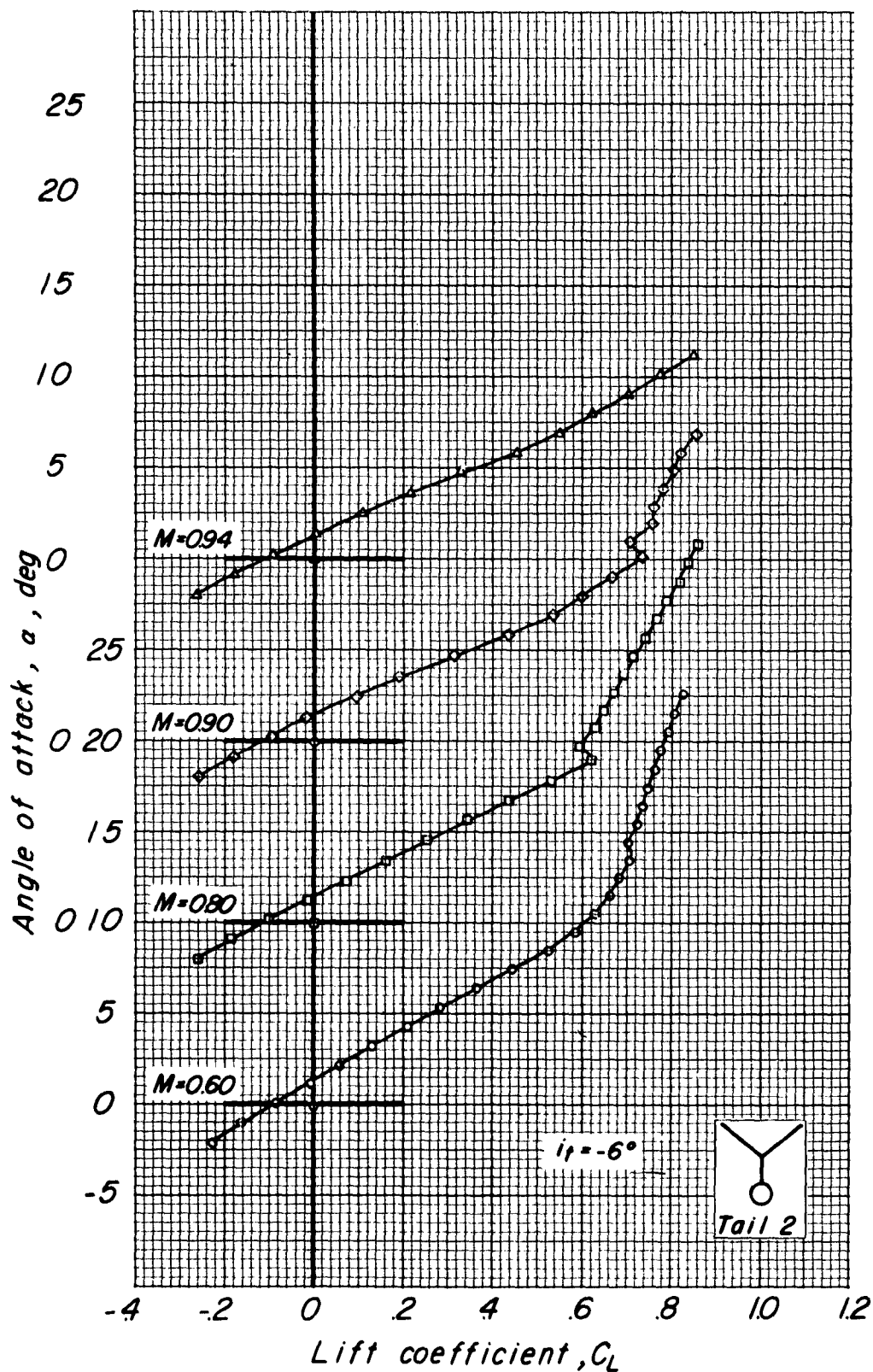


Figure 9.- Aerodynamic characteristics in pitch of the model with tail 2.

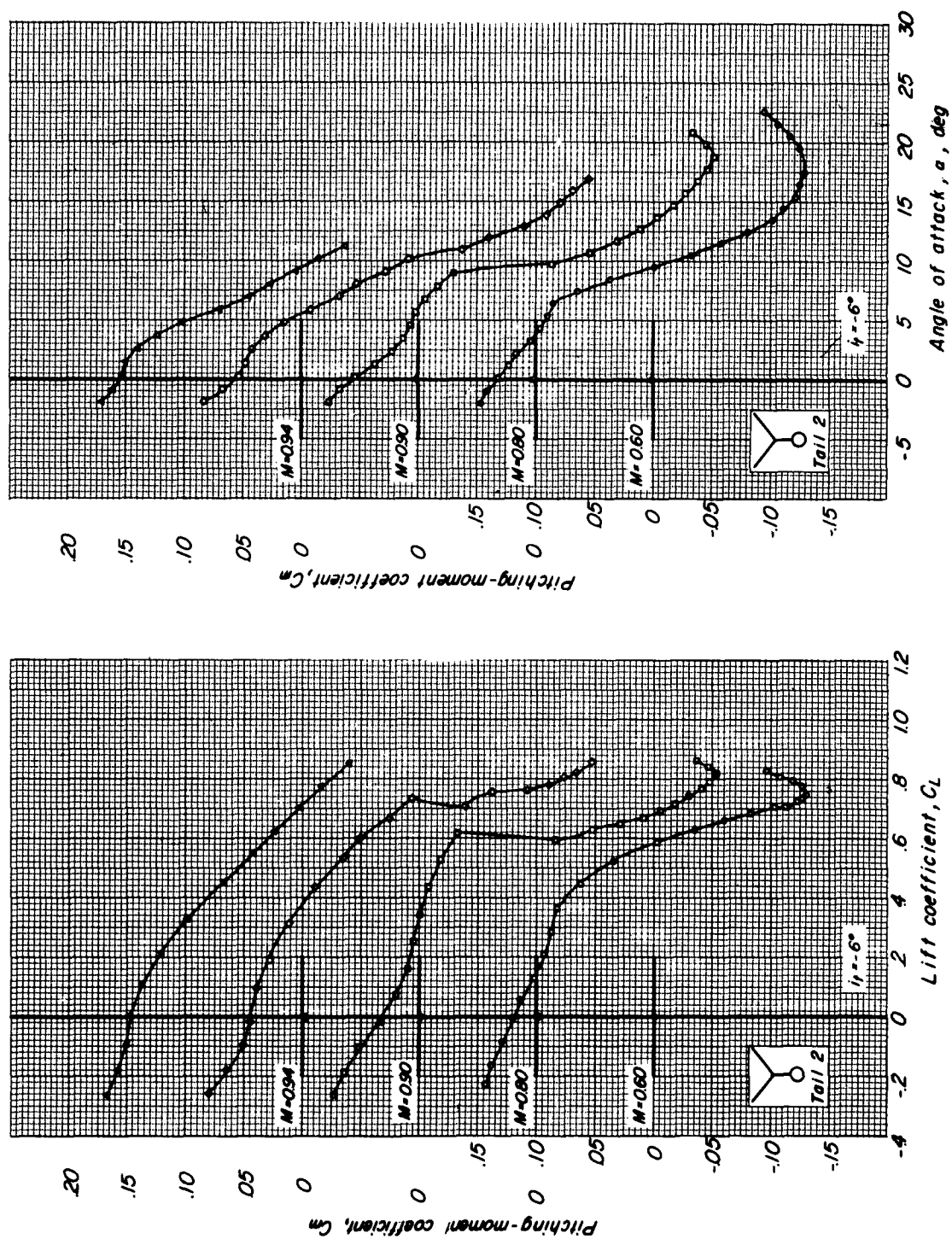


Figure 9.- Concluded.

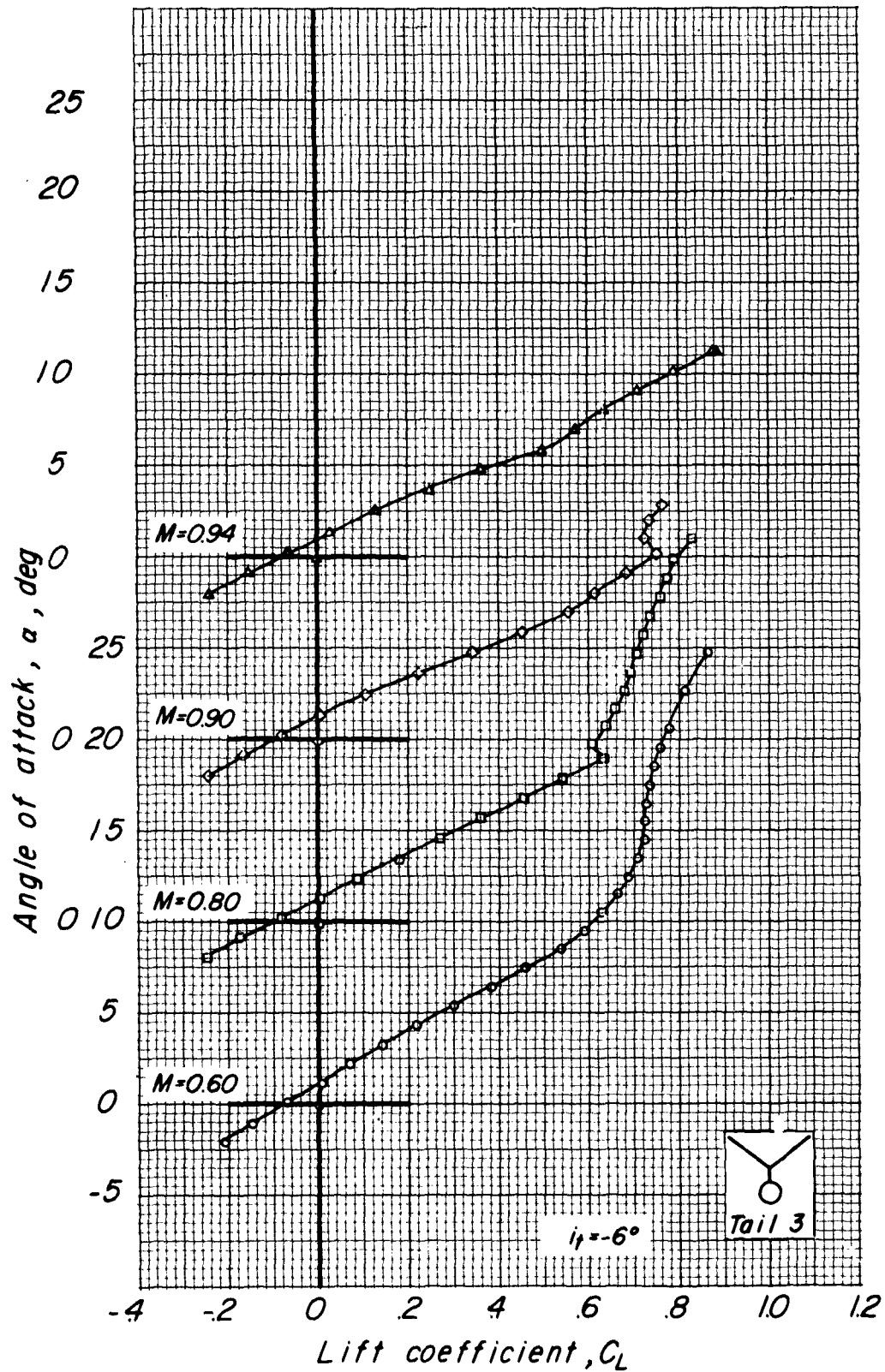


Figure 10.- Aerodynamic characteristics in pitch of the model with tail 3.

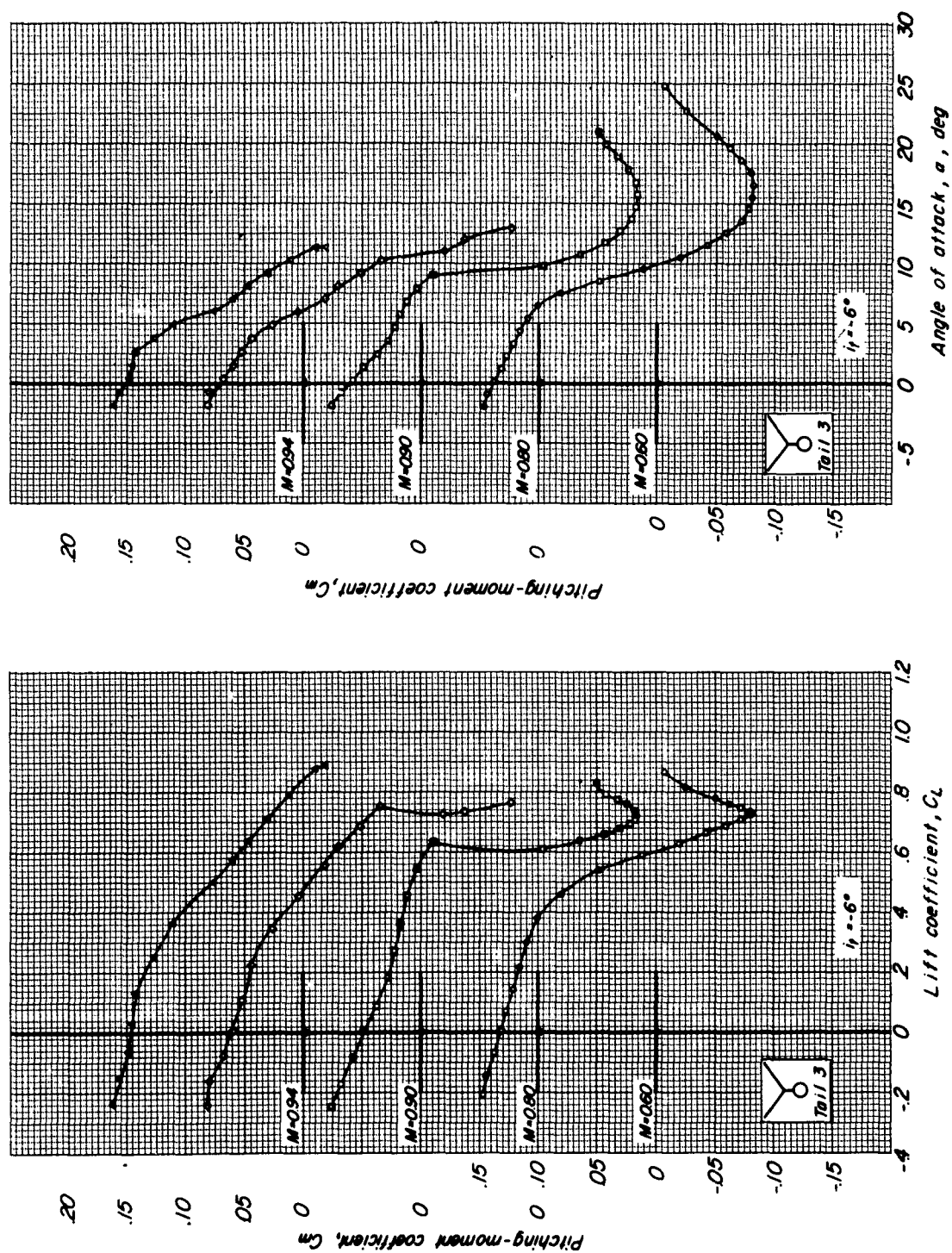


Figure 10.- Concluded.

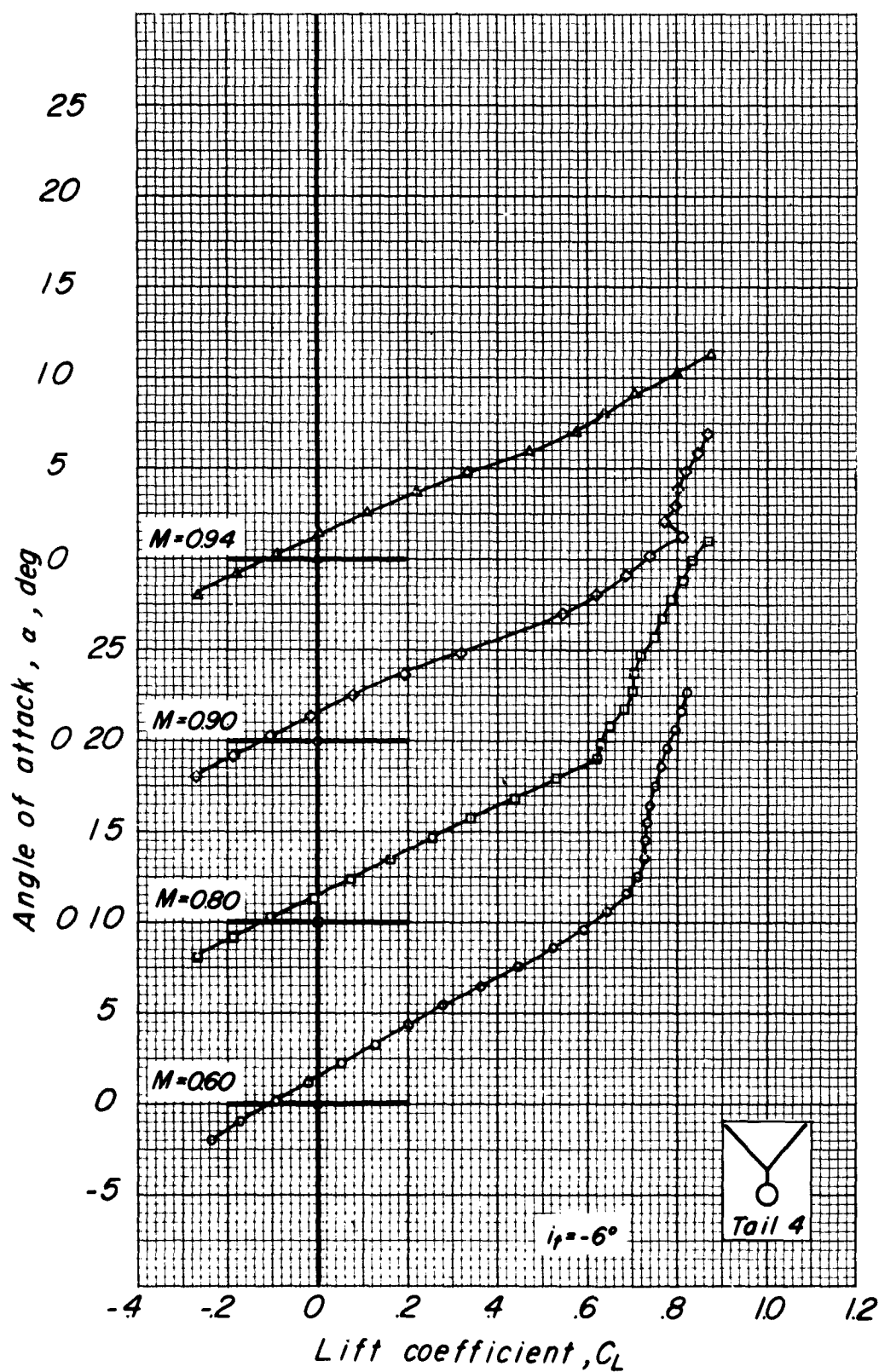


Figure 11.- Aerodynamic characteristics in pitch of the model with tail 4.

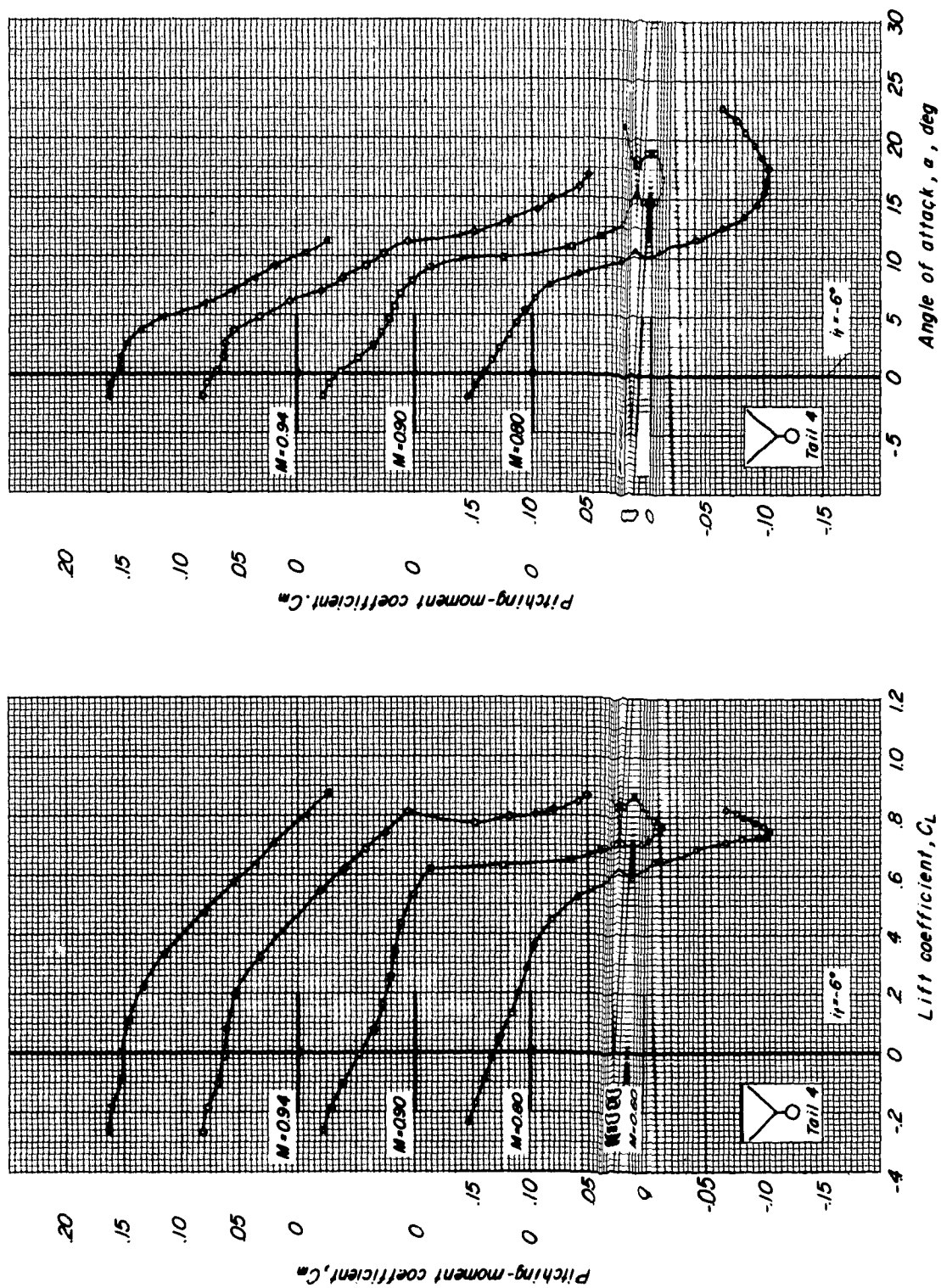


Figure 11.- Concluded.

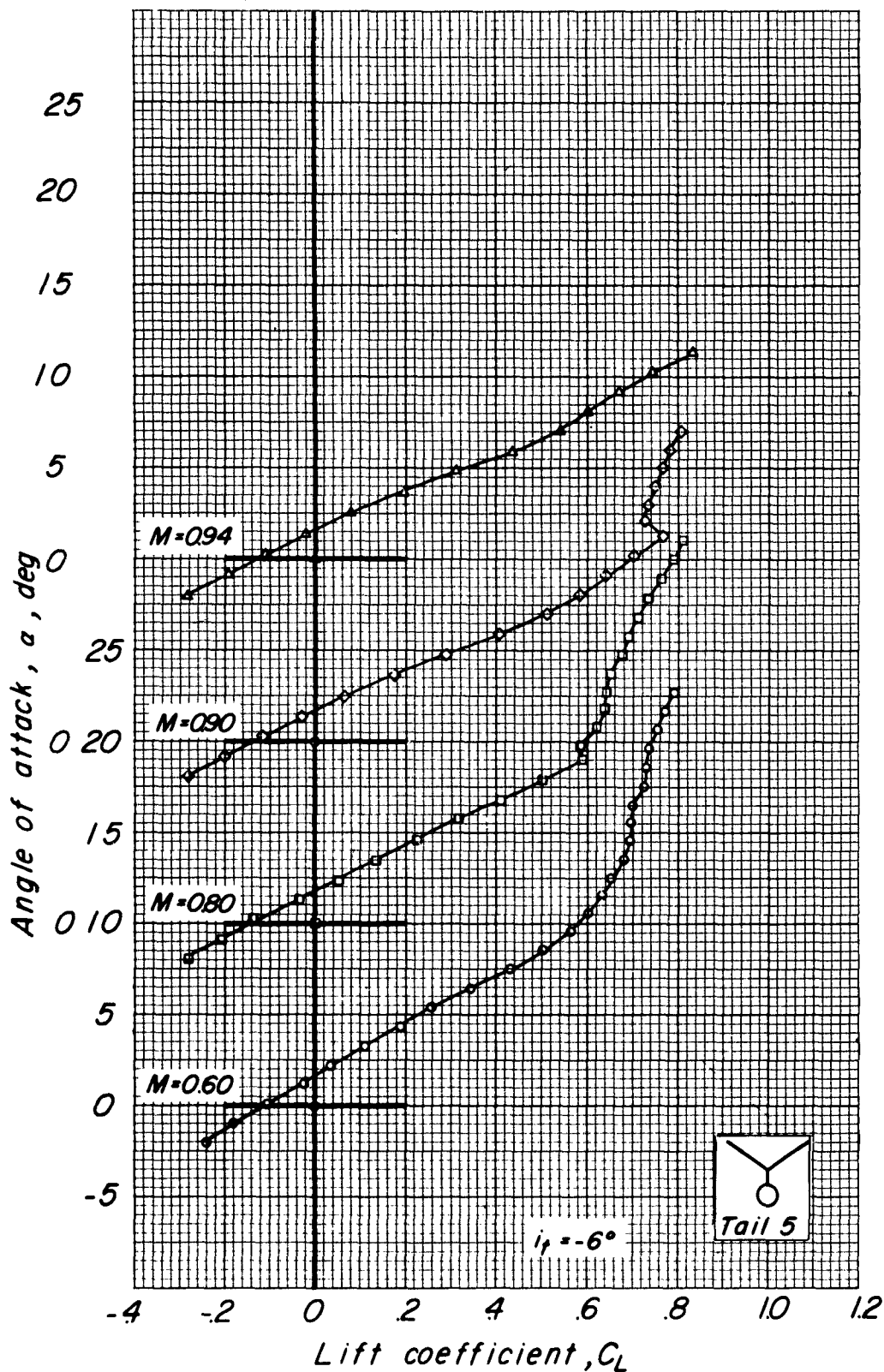


Figure 12.- Aerodynamic characteristics in pitch of the model with tail 5.

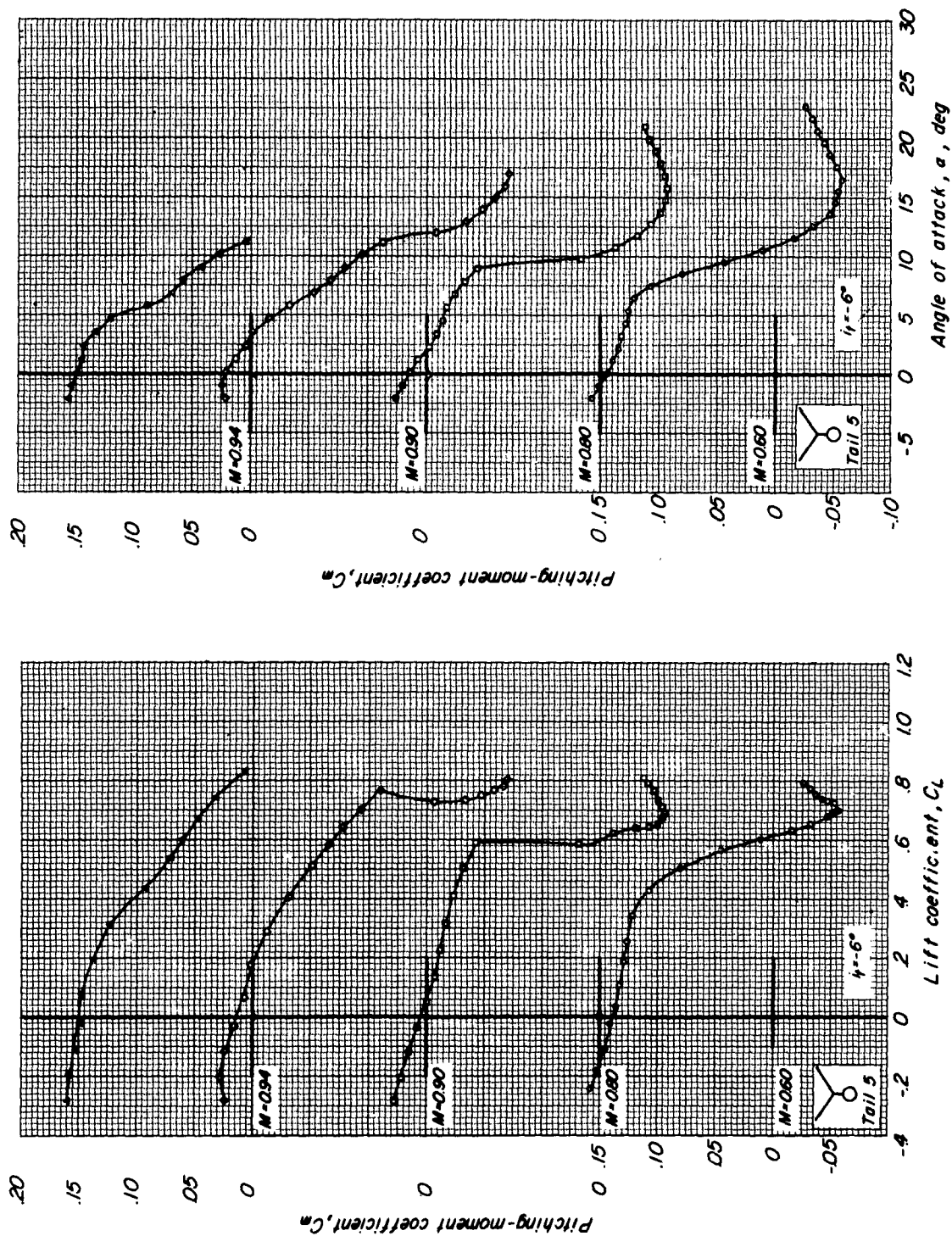


Figure 12.- Concluded.

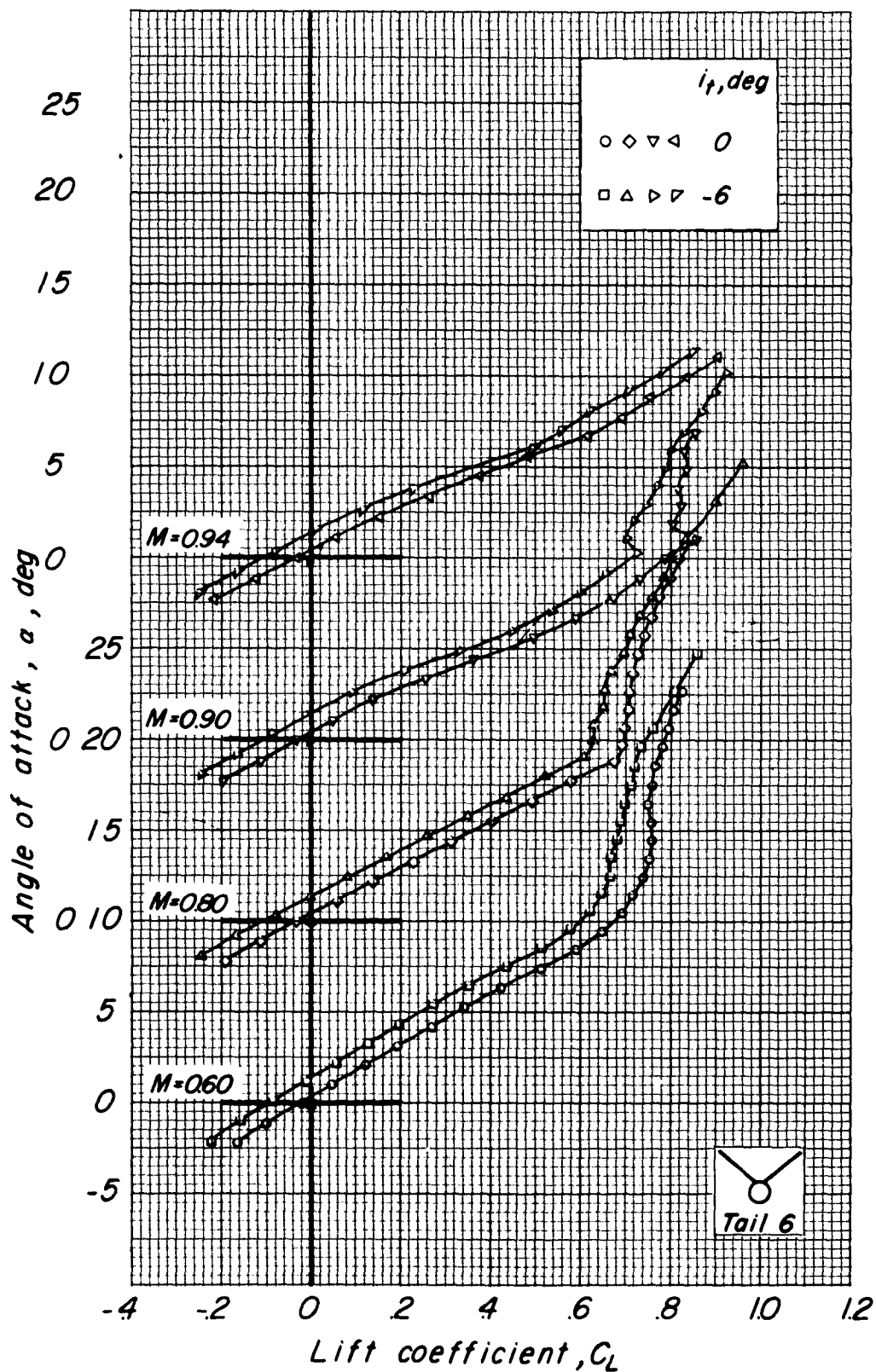


Figure 13.- Aerodynamic characteristics in pitch of the model with tail 6.

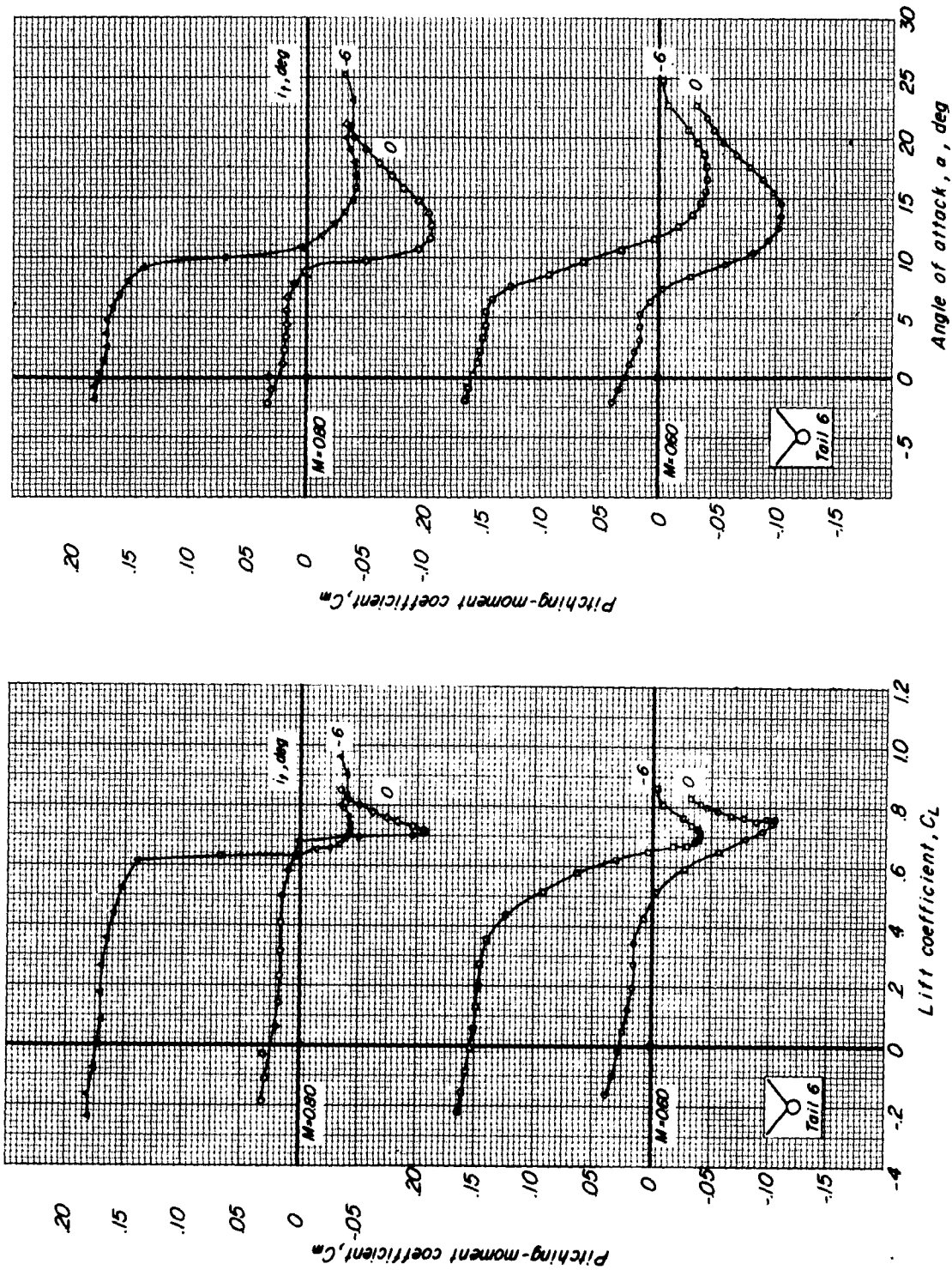


Figure 13.- Continued.

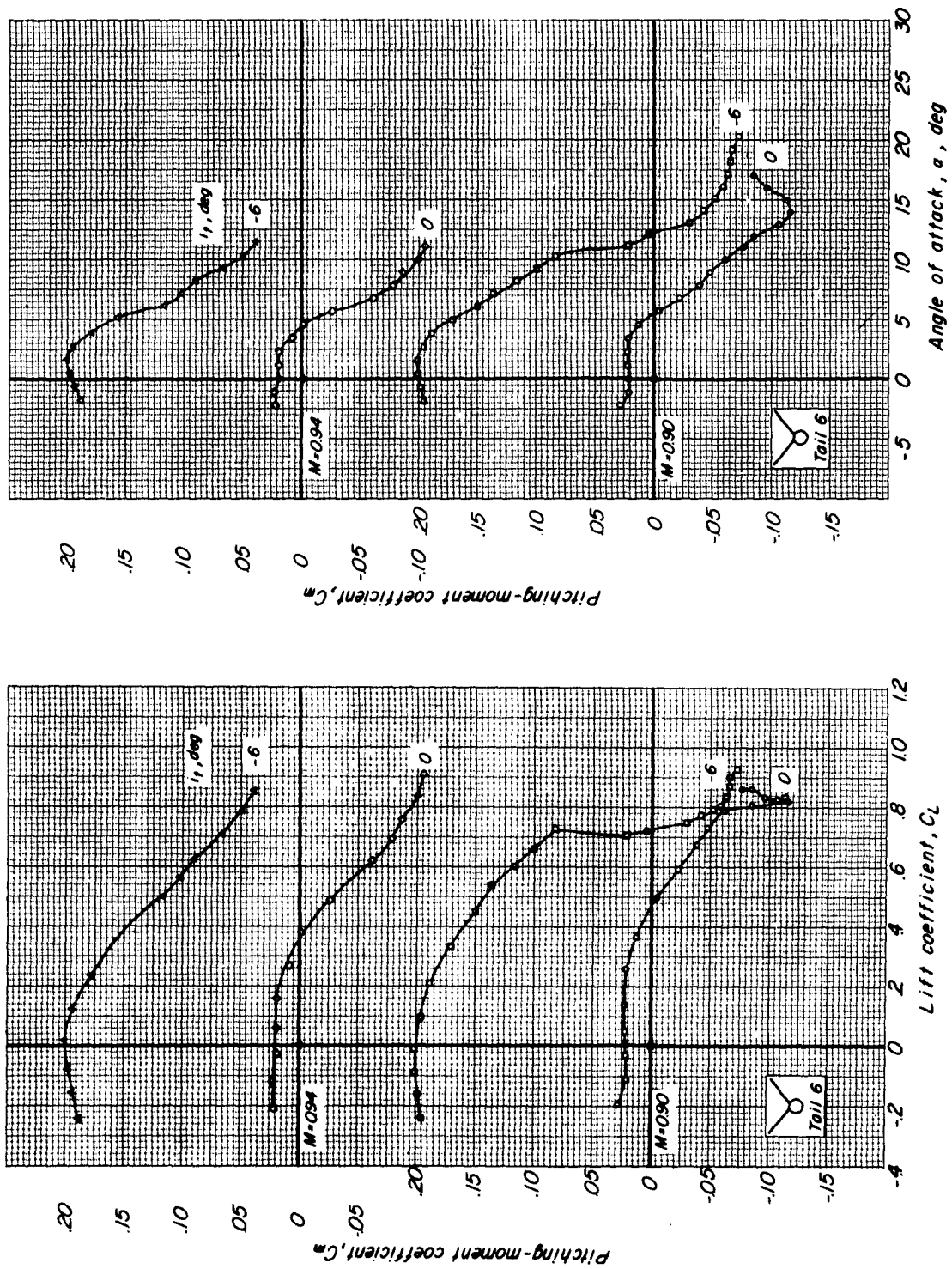


Figure 13.- Concluded.

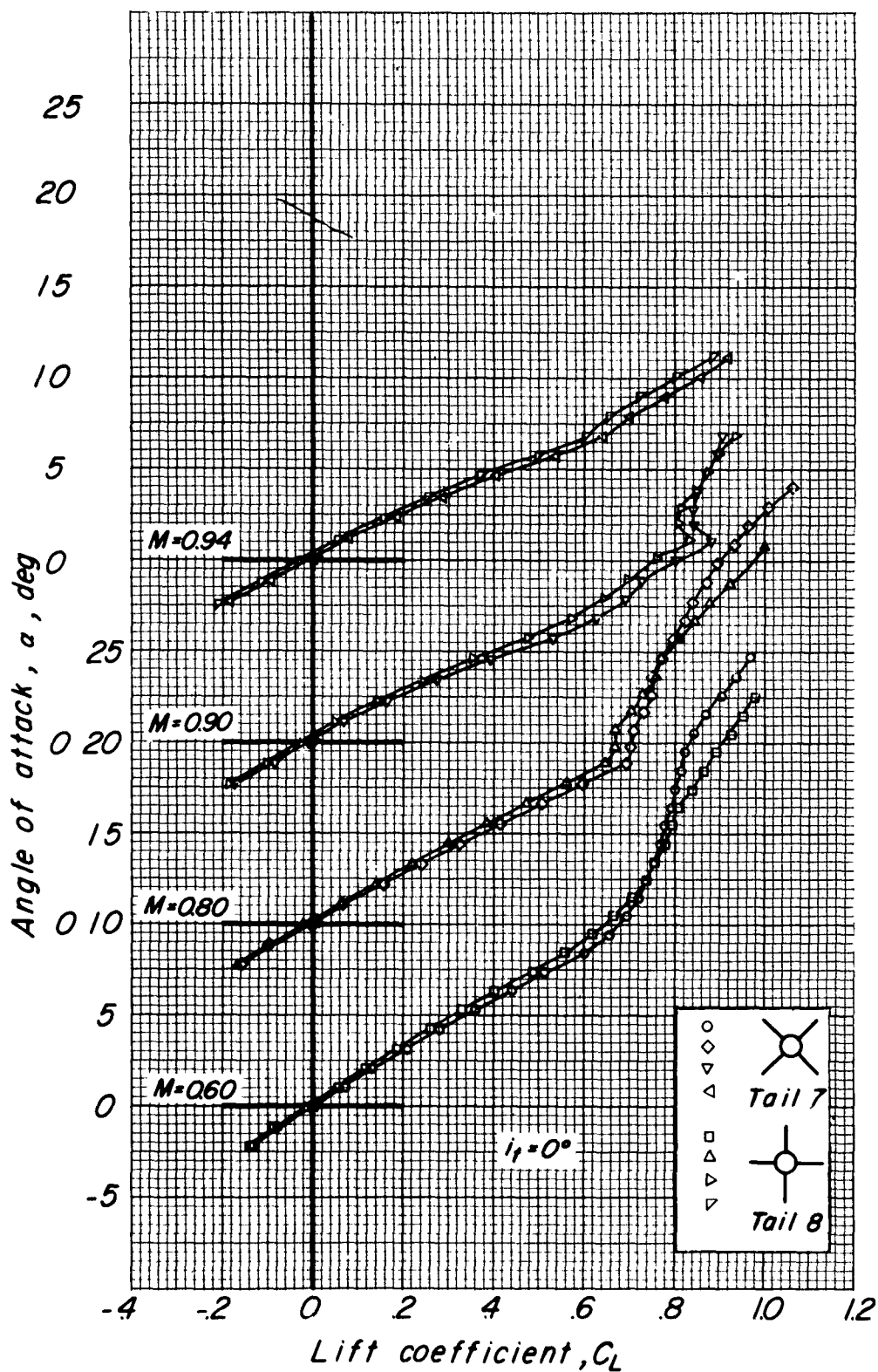


Figure 14.- Aerodynamic characteristics in pitch of the model with tail 7 and tail 8.

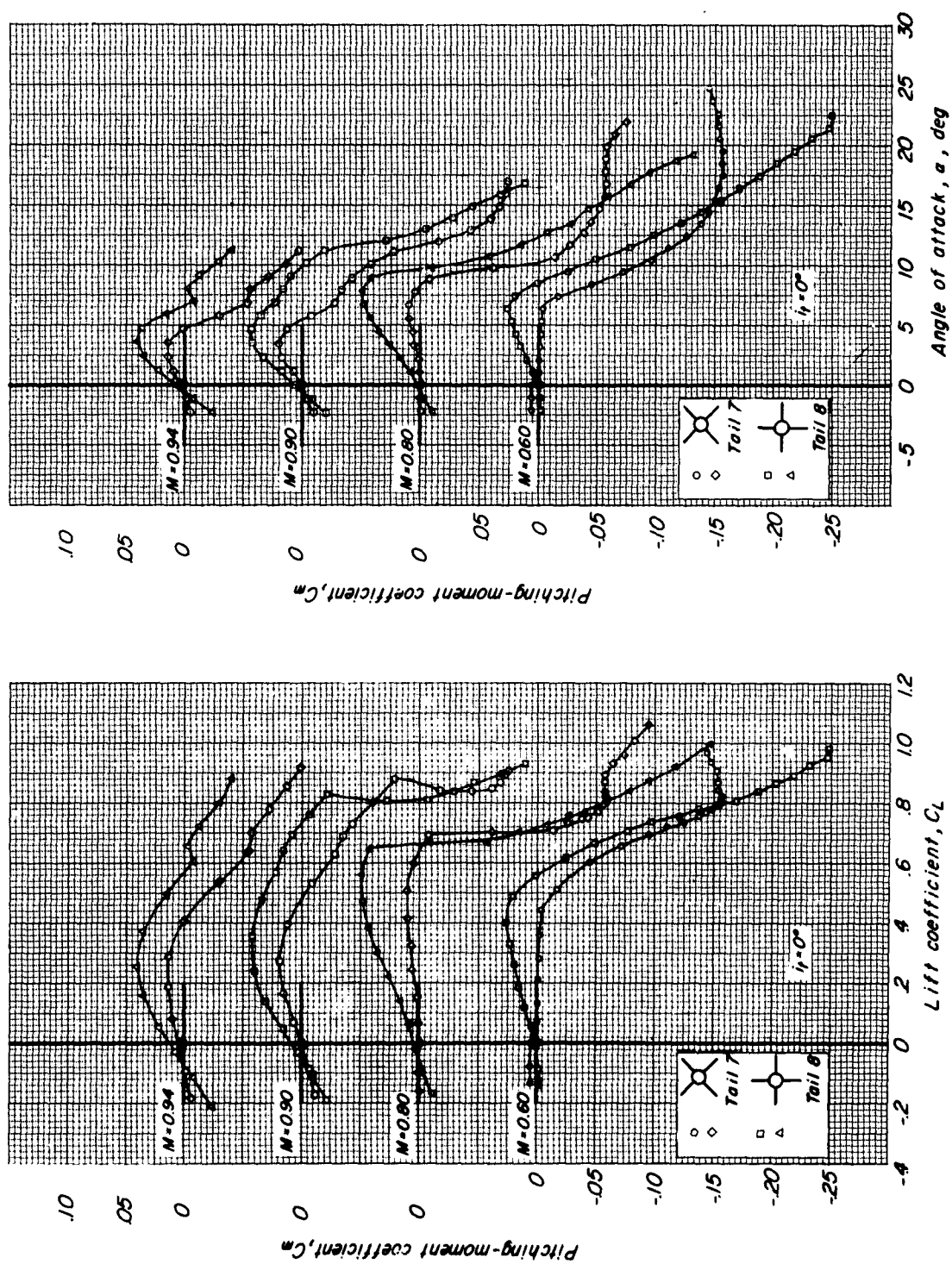


Figure 14.- Concluded.

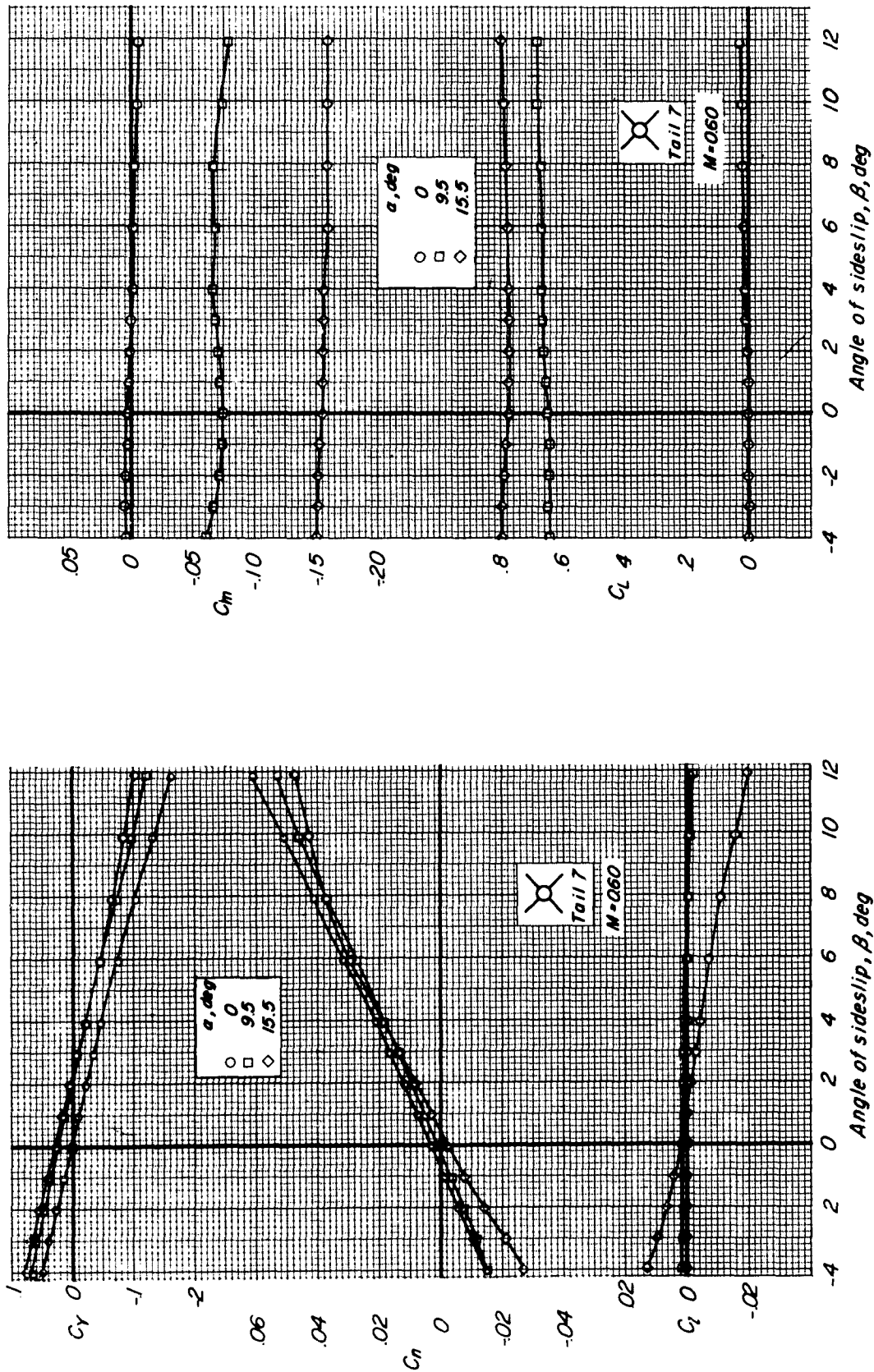


Figure 15.- Aerodynamic characteristics in sideslip of the model with tail 7. $i_t = 0^\circ$.

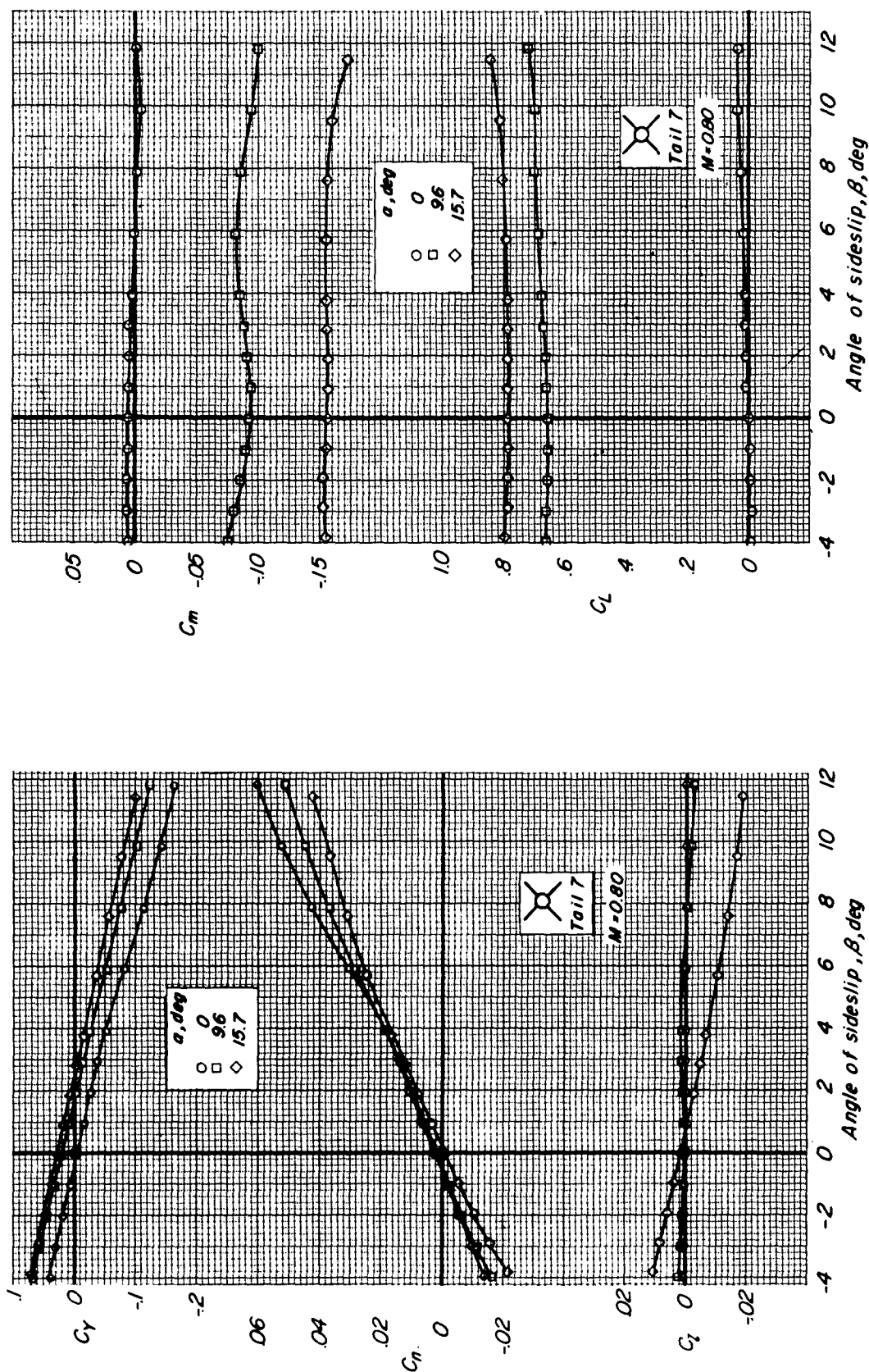


Figure 15.- Continued.

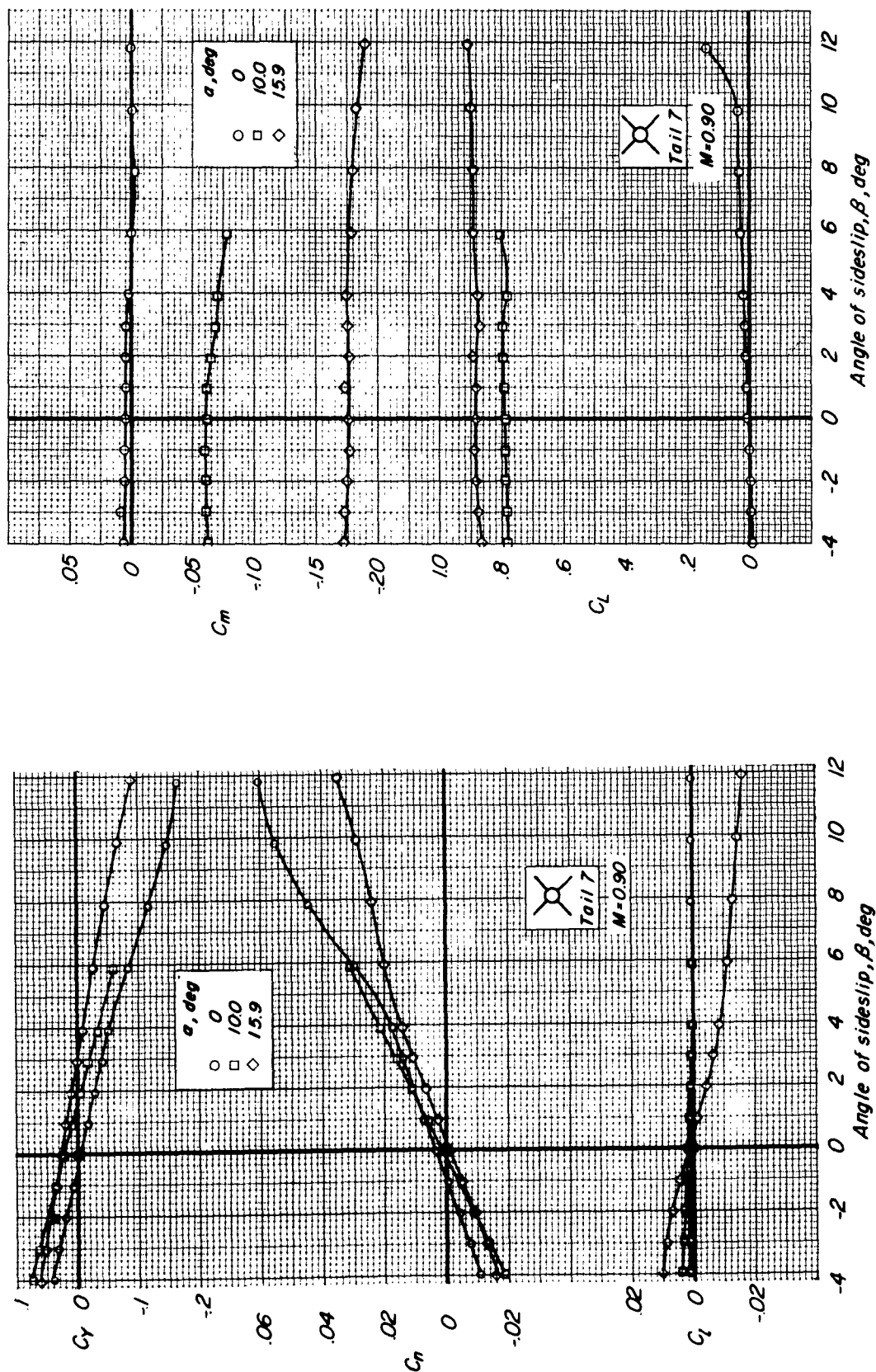


Figure 15.- Continued.

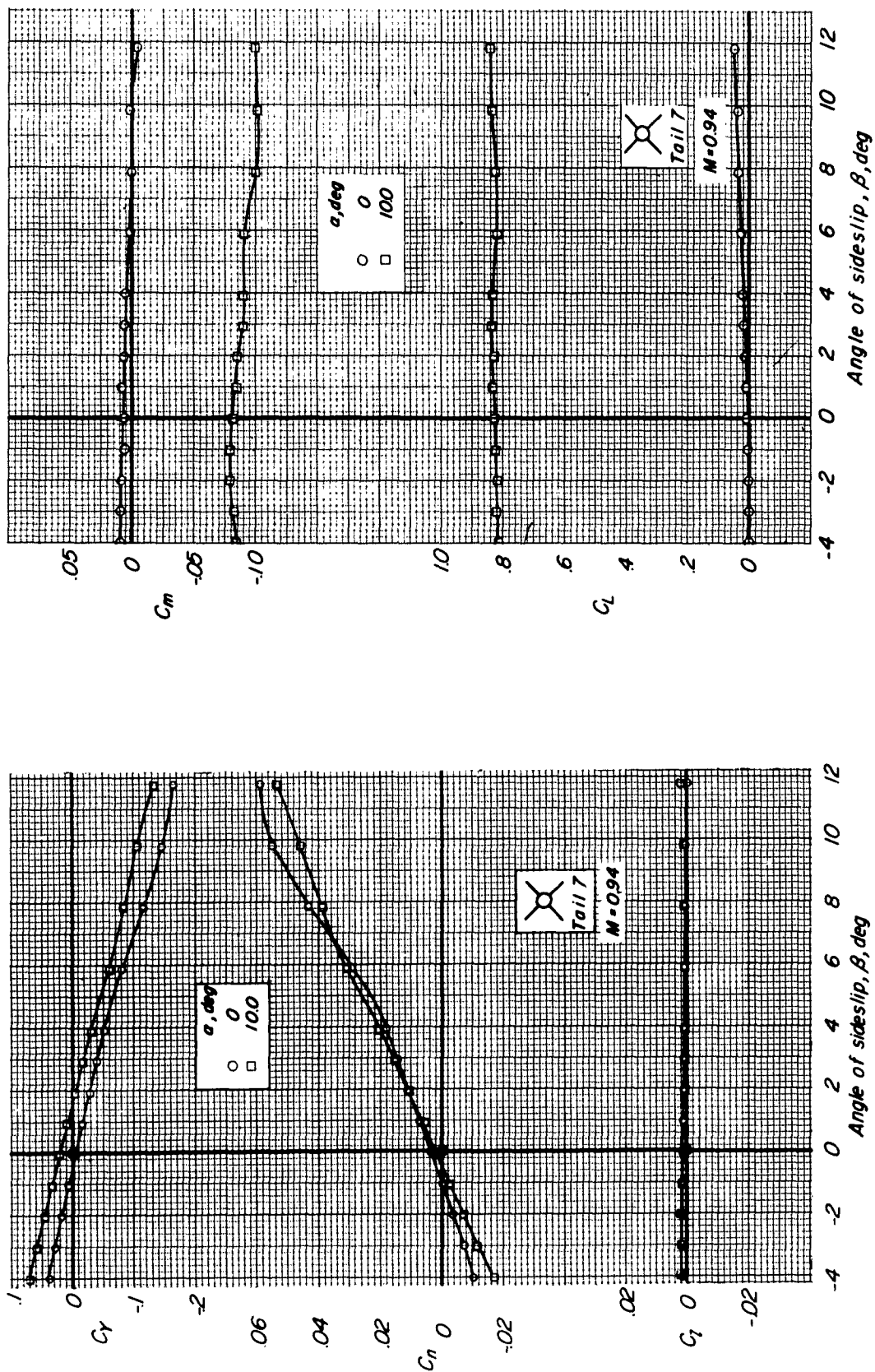


Figure 15.- Concluded.

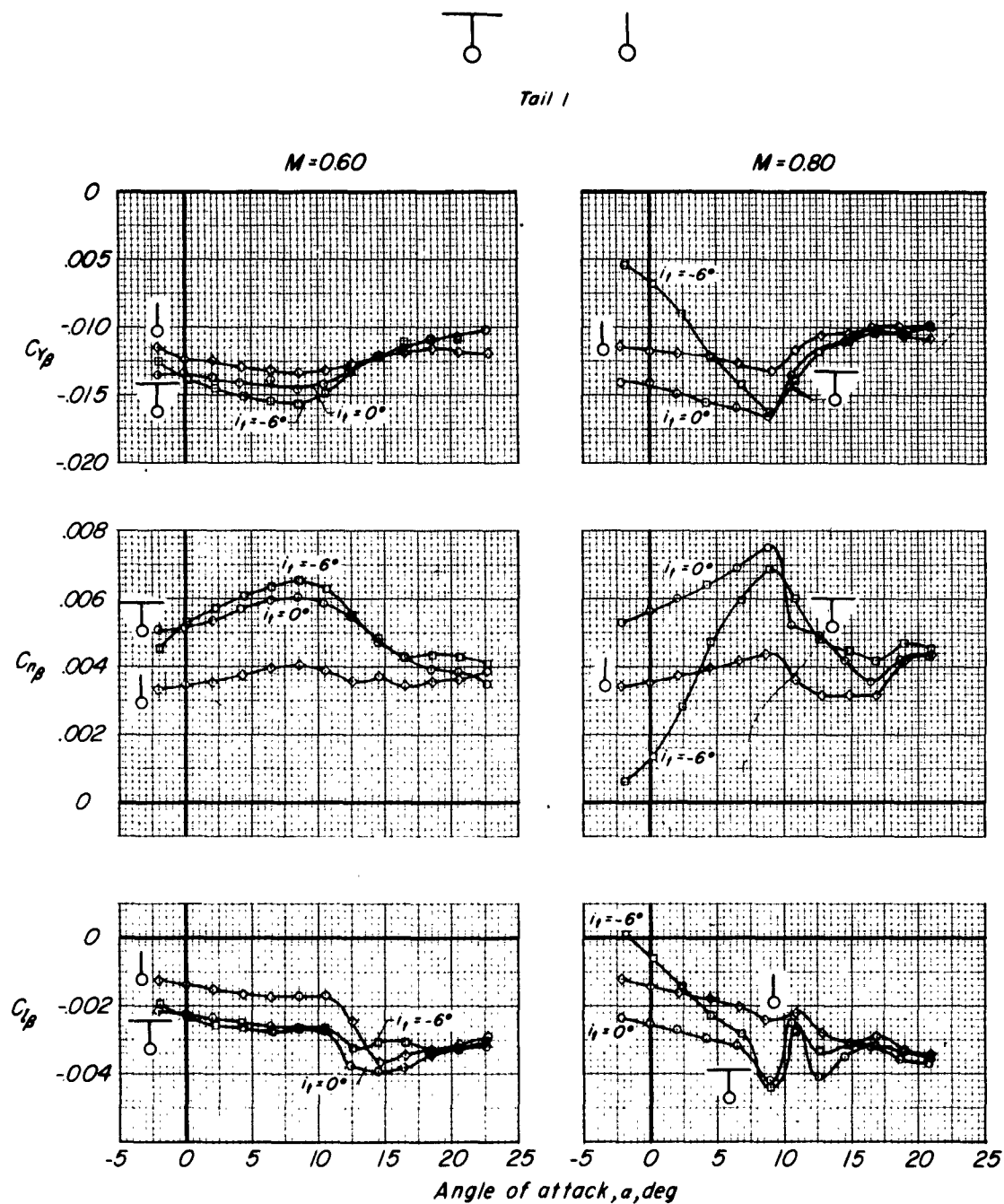
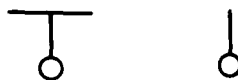


Figure 16.- Lateral-stability derivatives for the model with tail 1, showing effects of the horizontal tail and stabilizer incidence.



Tail I

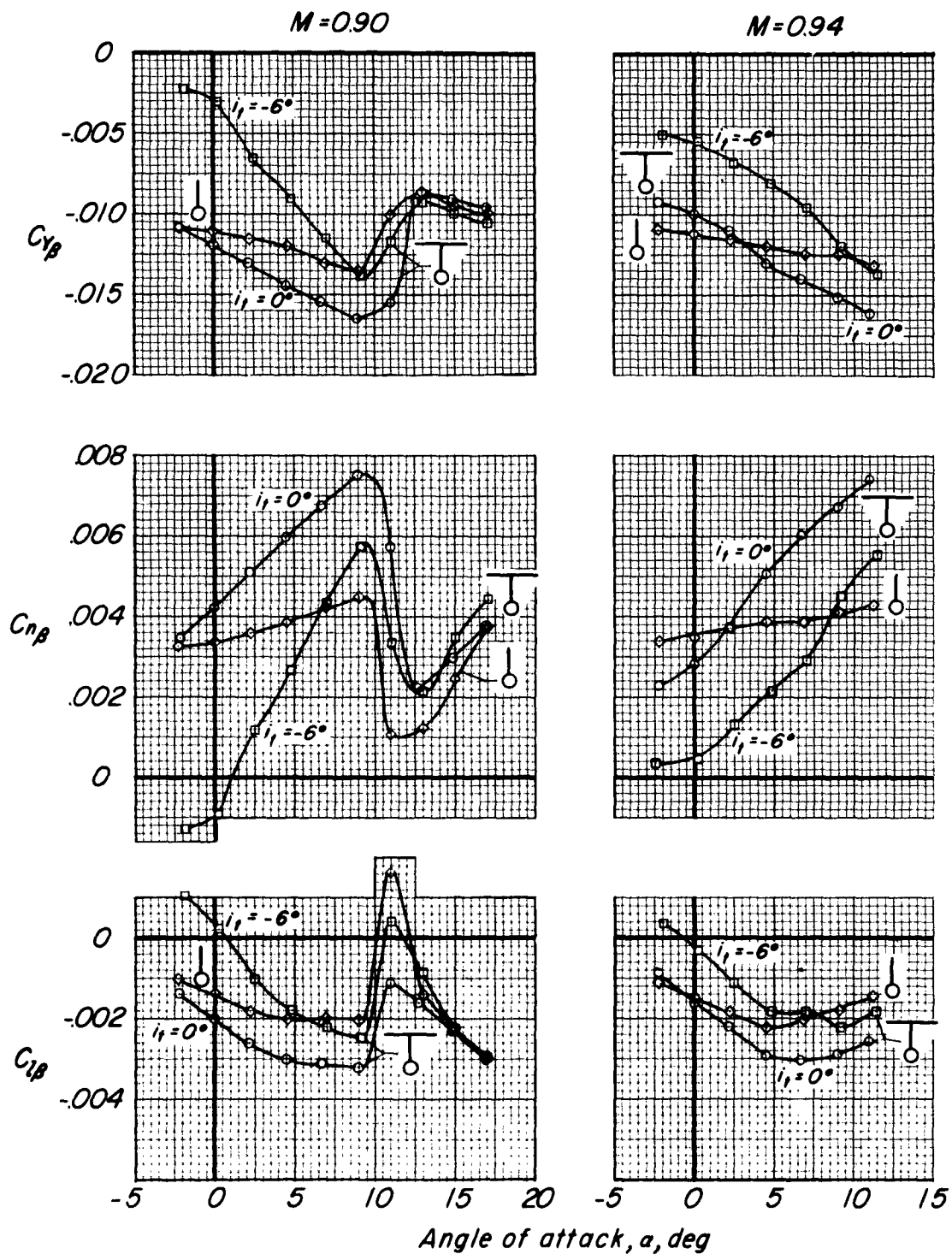


Figure 16.- Concluded.

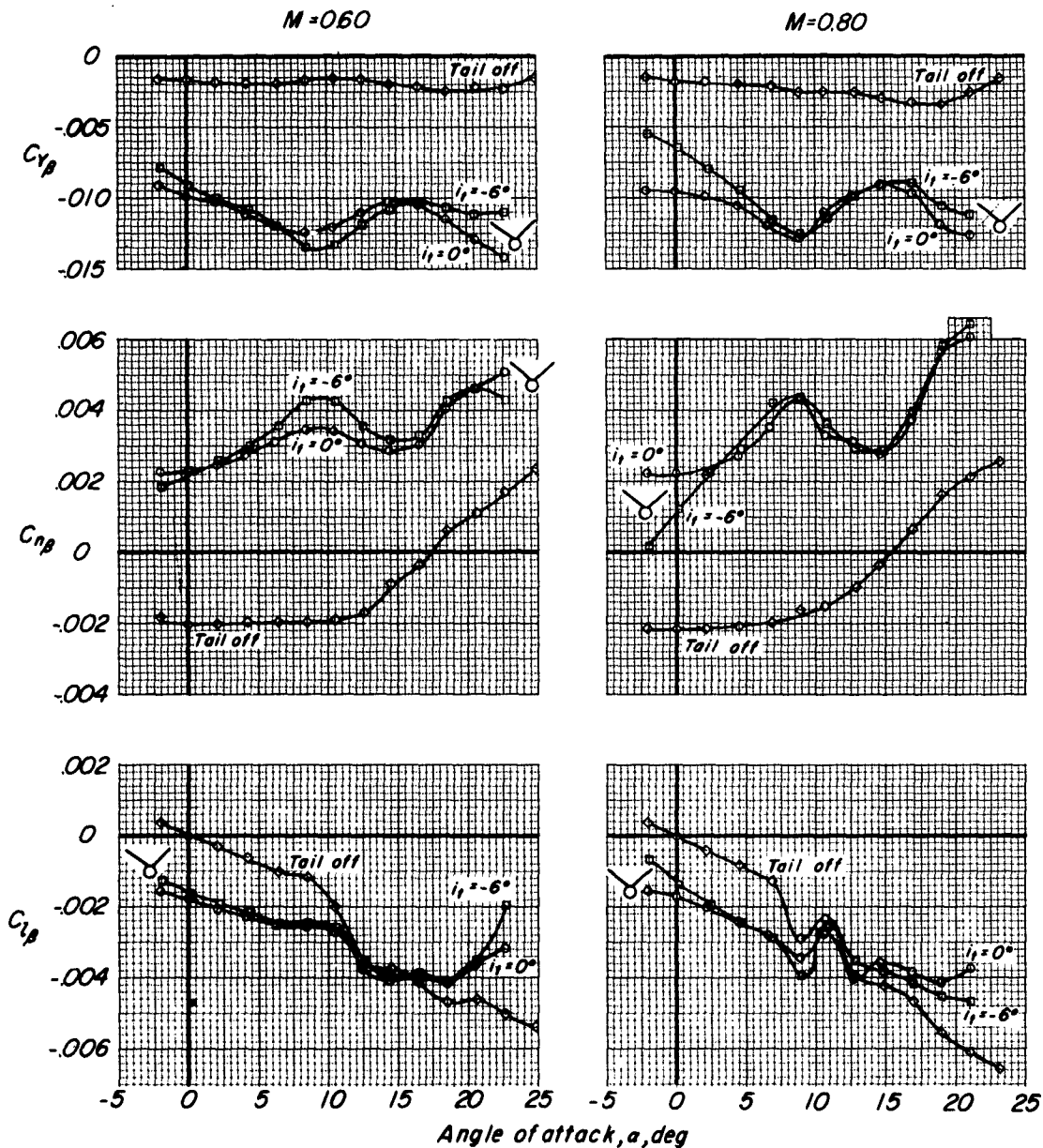


Figure 17.- Lateral-stability derivatives of wing-fuselage configuration and with tail 6, showing effects of stabilizer setting.

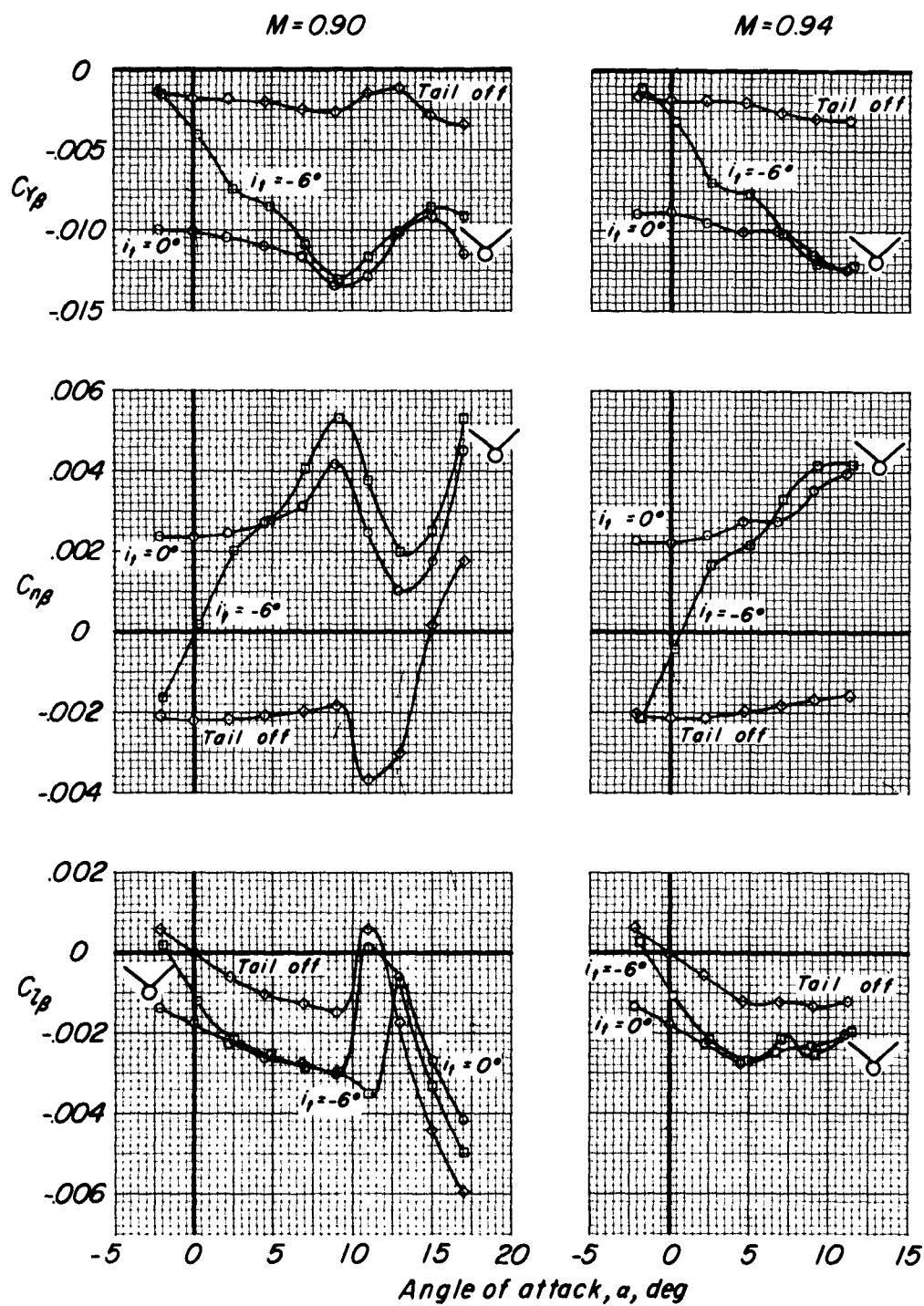


Figure 17.- Concluded.

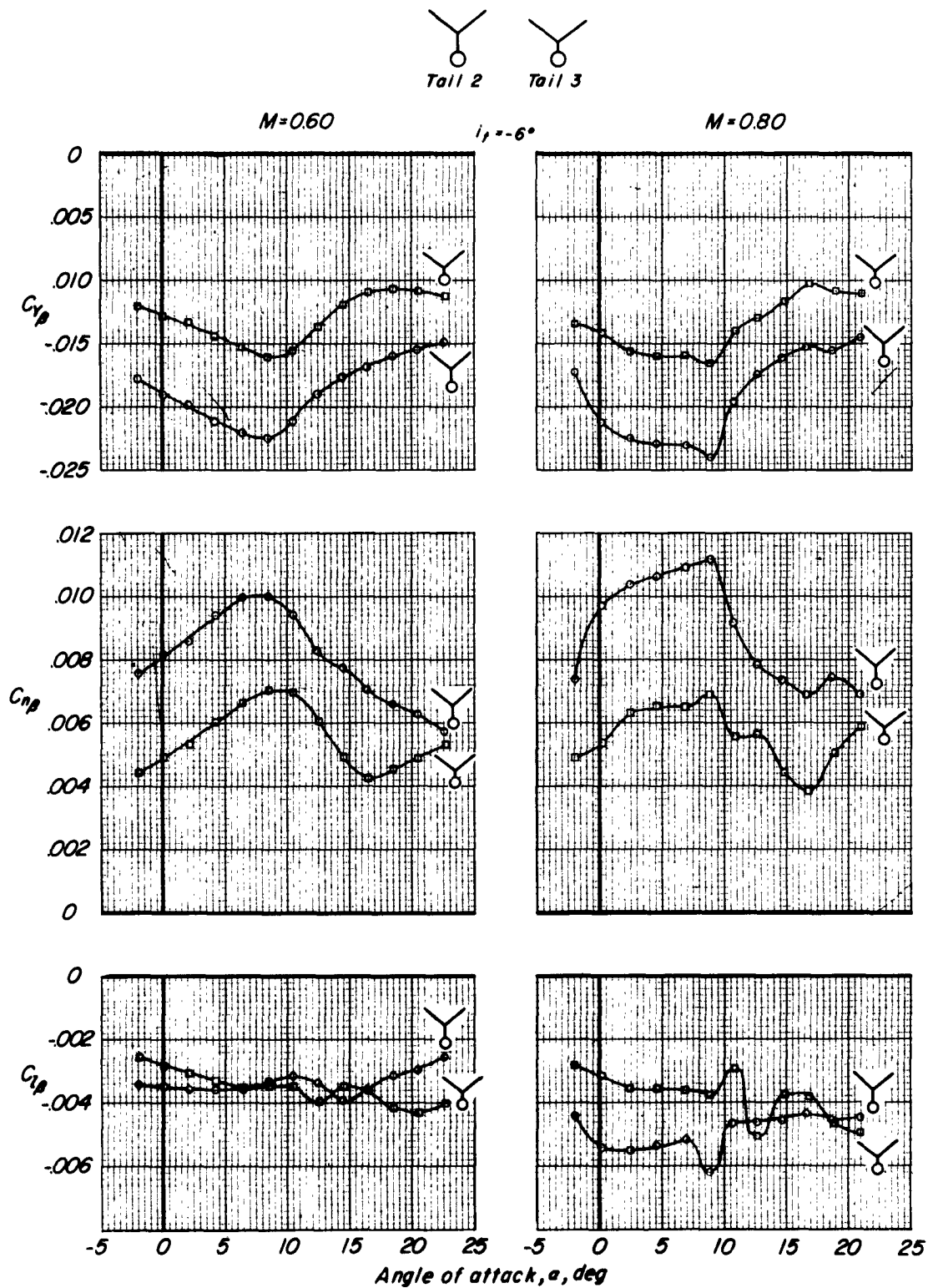


Figure 18.- Lateral-stability derivatives for the model with tail 2 and tail 3, showing effects of stub height. $i_t = -6^\circ$.

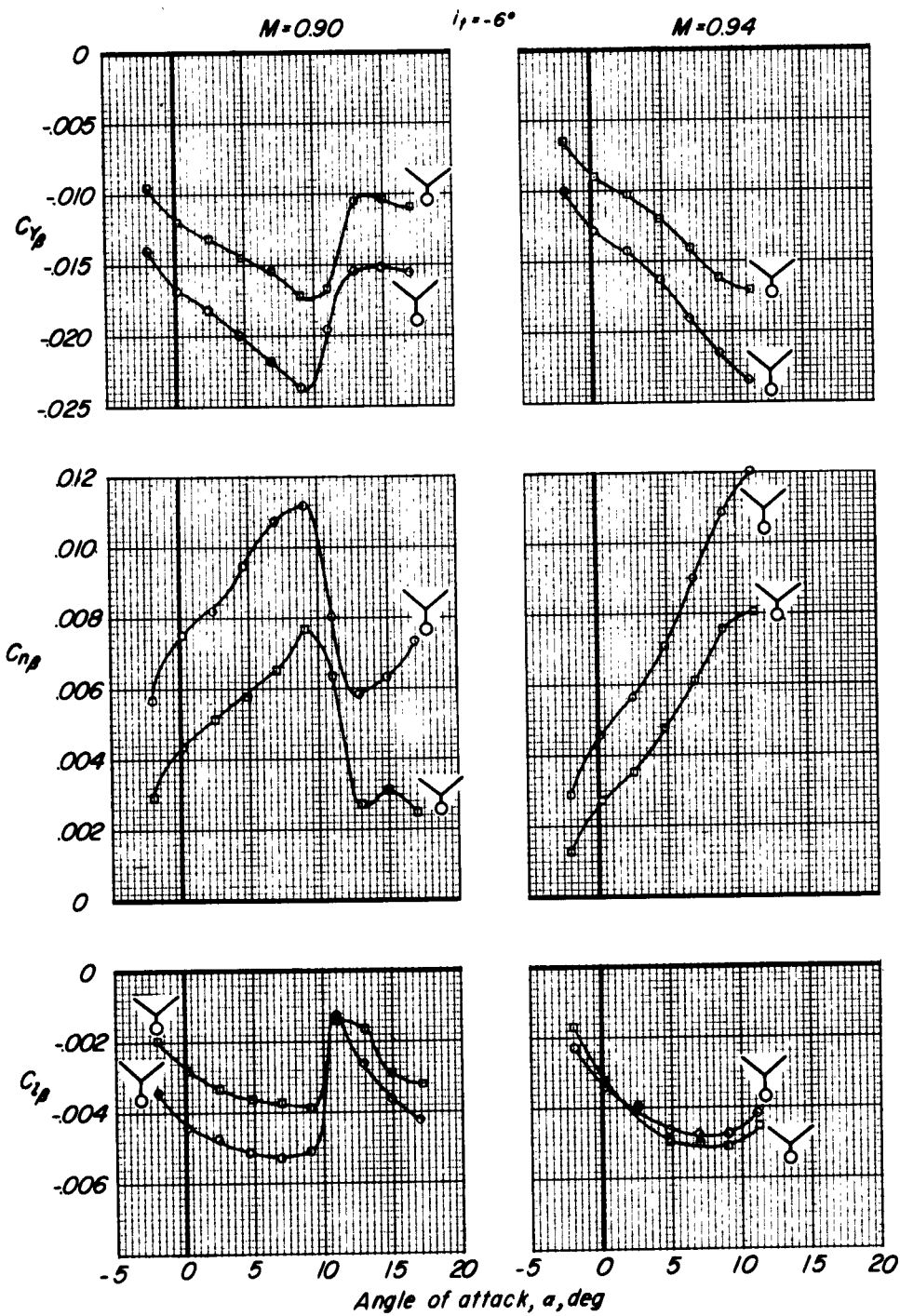
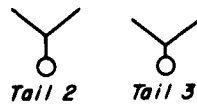


Figure 18.- Concluded.

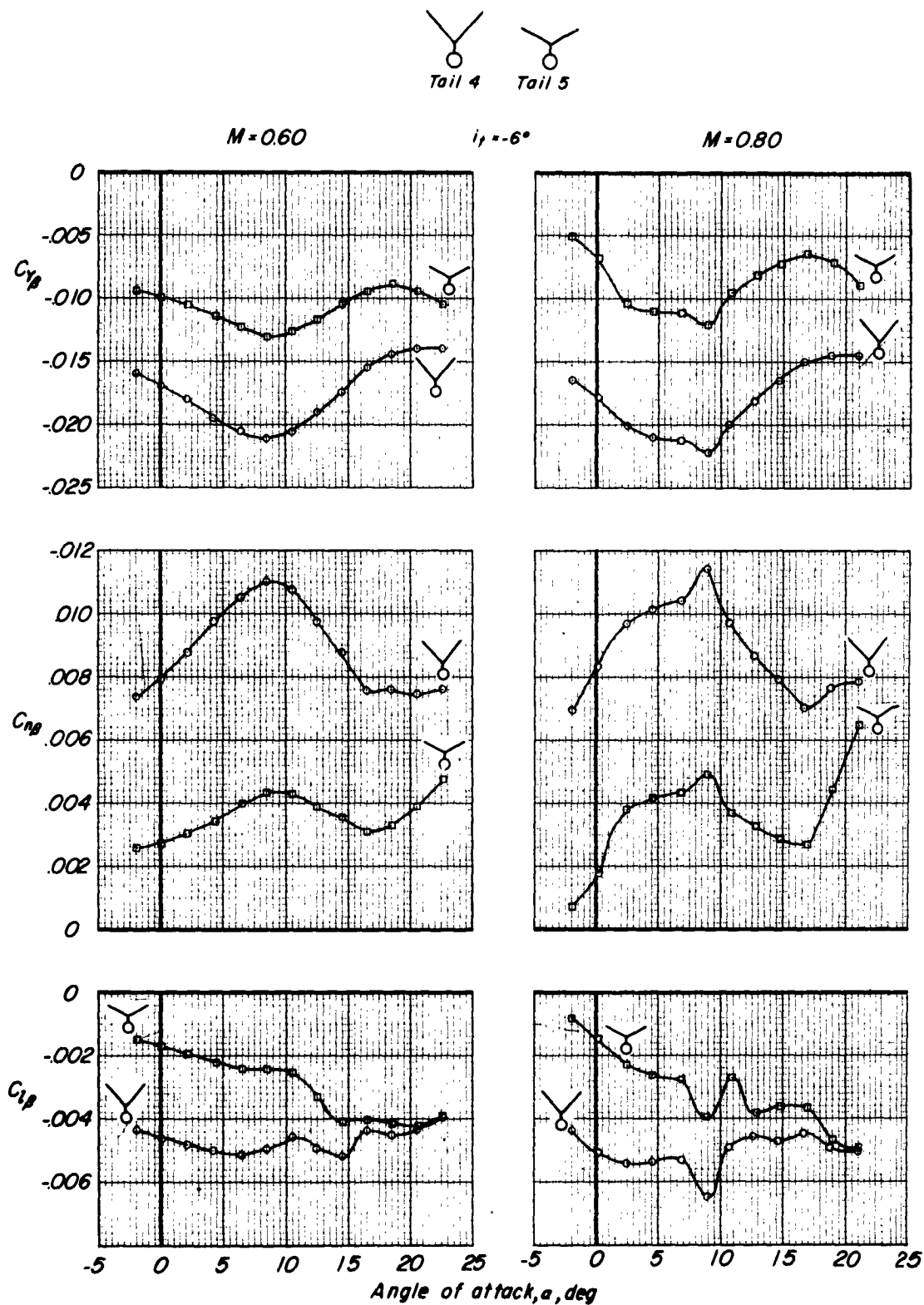


Figure 19.- Lateral stability derivatives for the model with tail 4 and tail 5, showing effects of dihedral angle. $i_t = -6^\circ$.

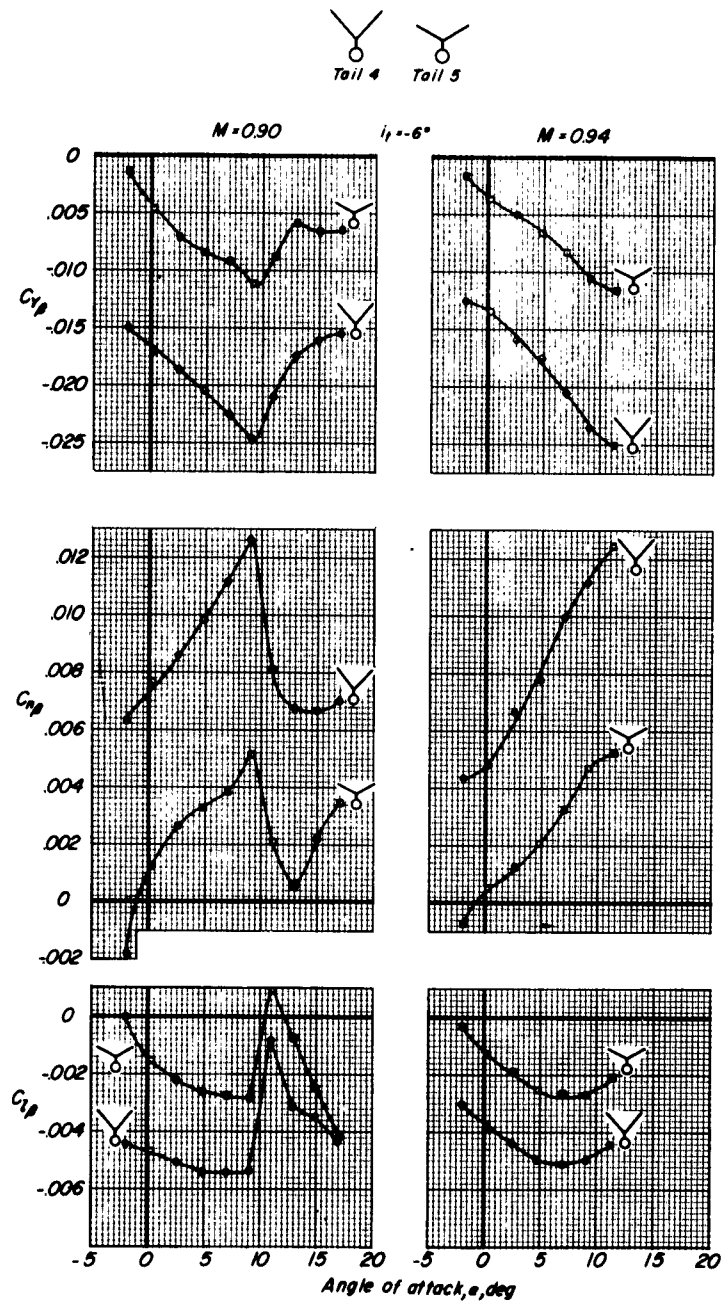


Figure 19.- Concluded.

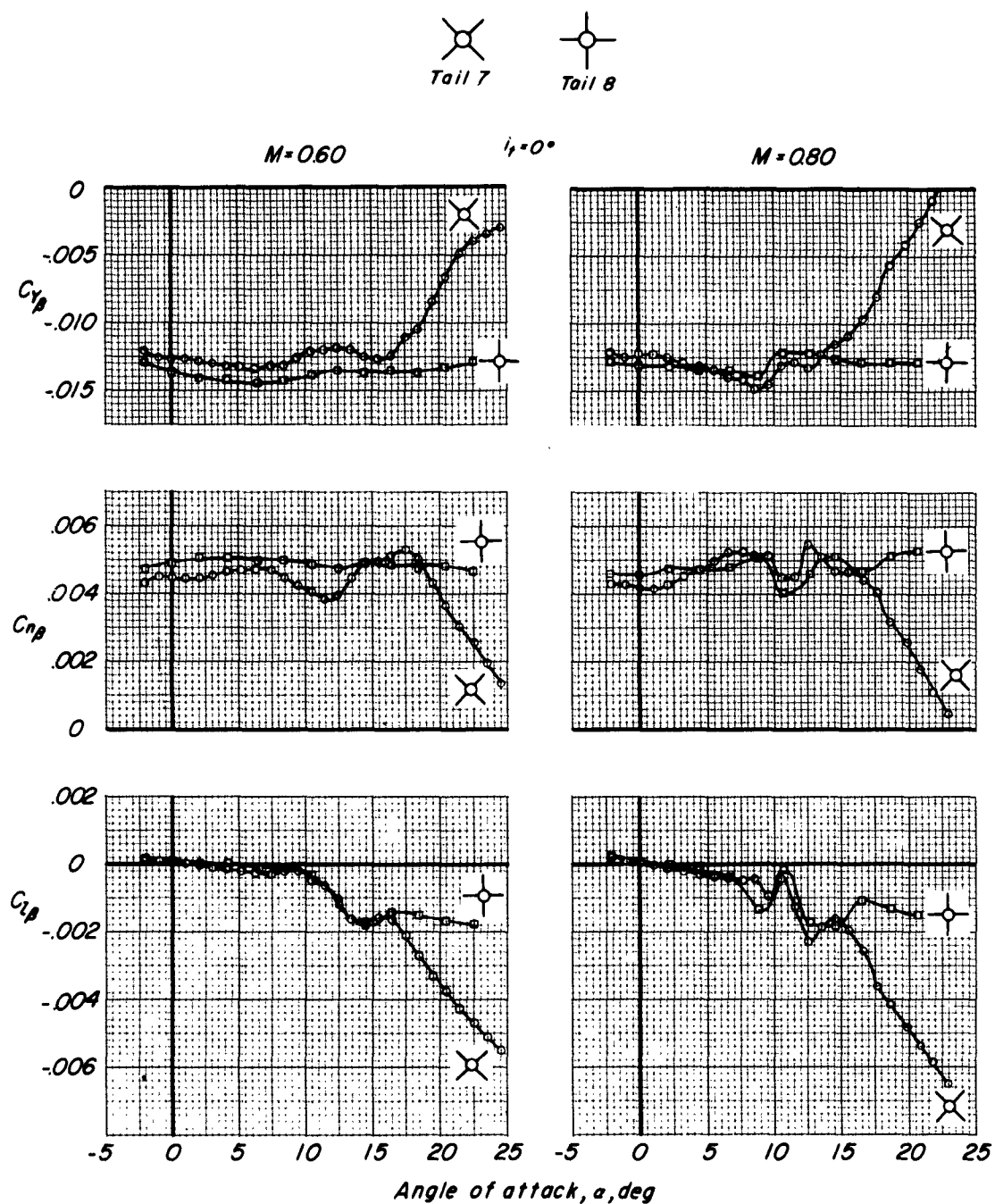


Figure 20.- Lateral stability derivatives of the model with tail 7 and tail 8. $i_t = 0^\circ$.

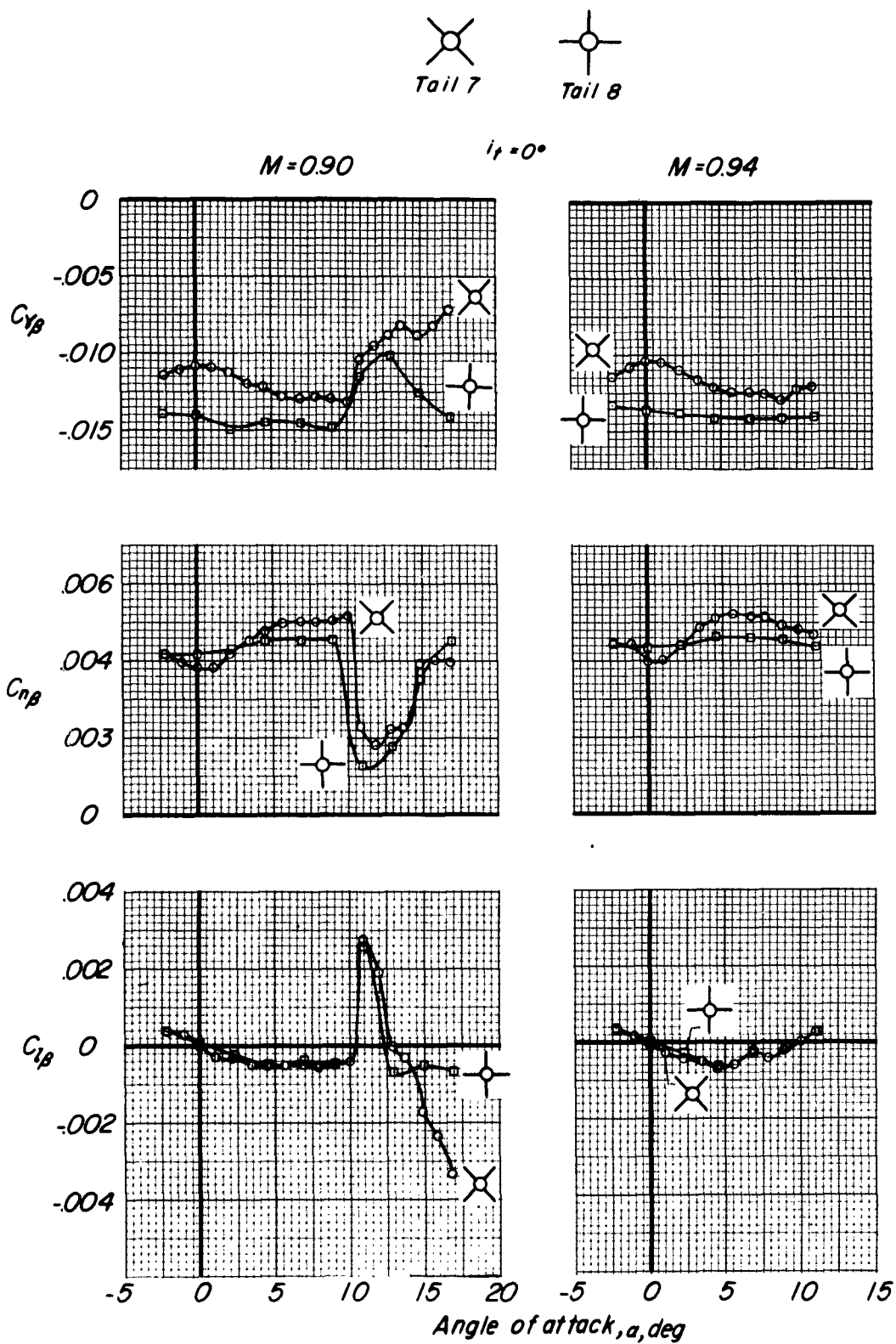
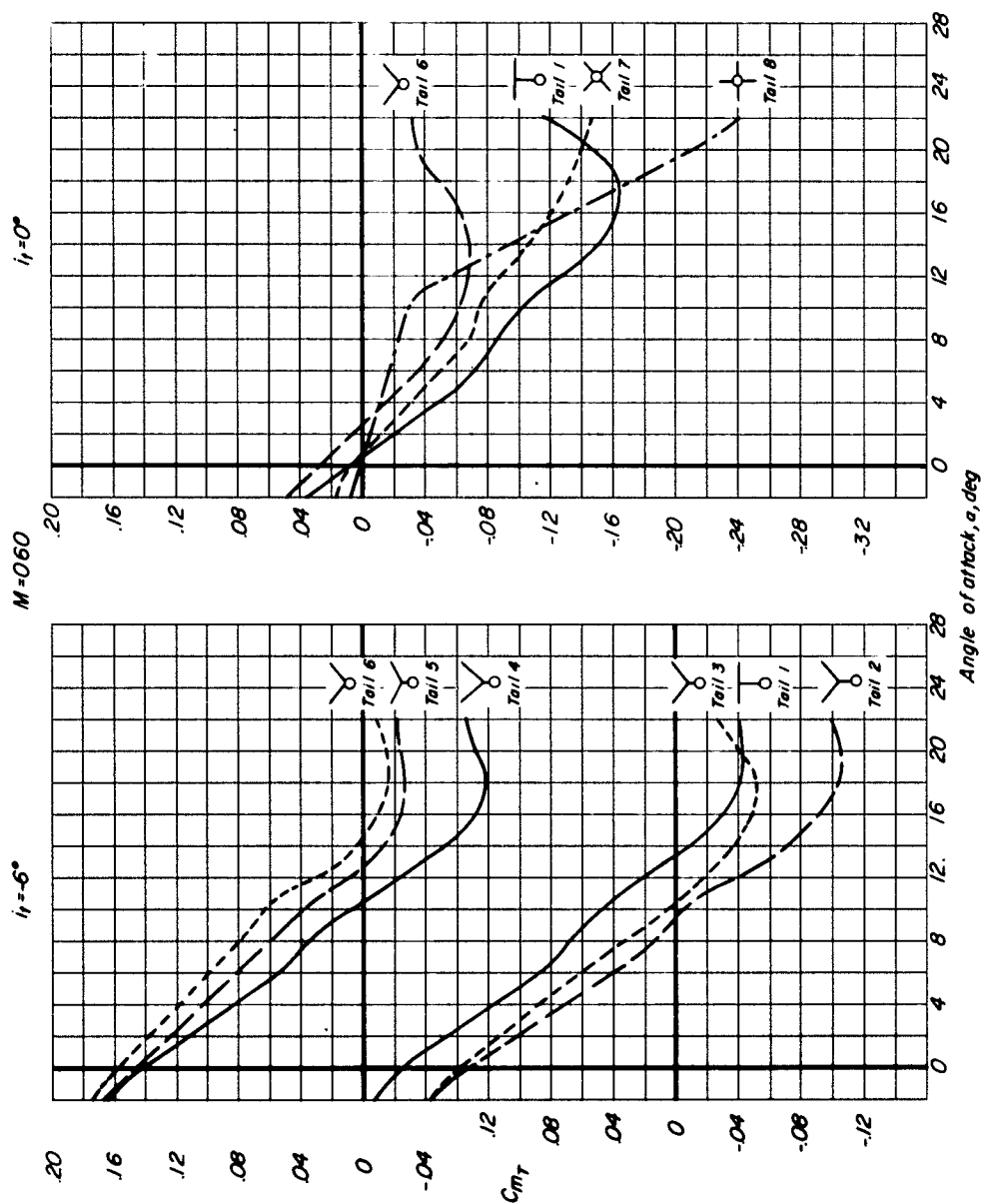
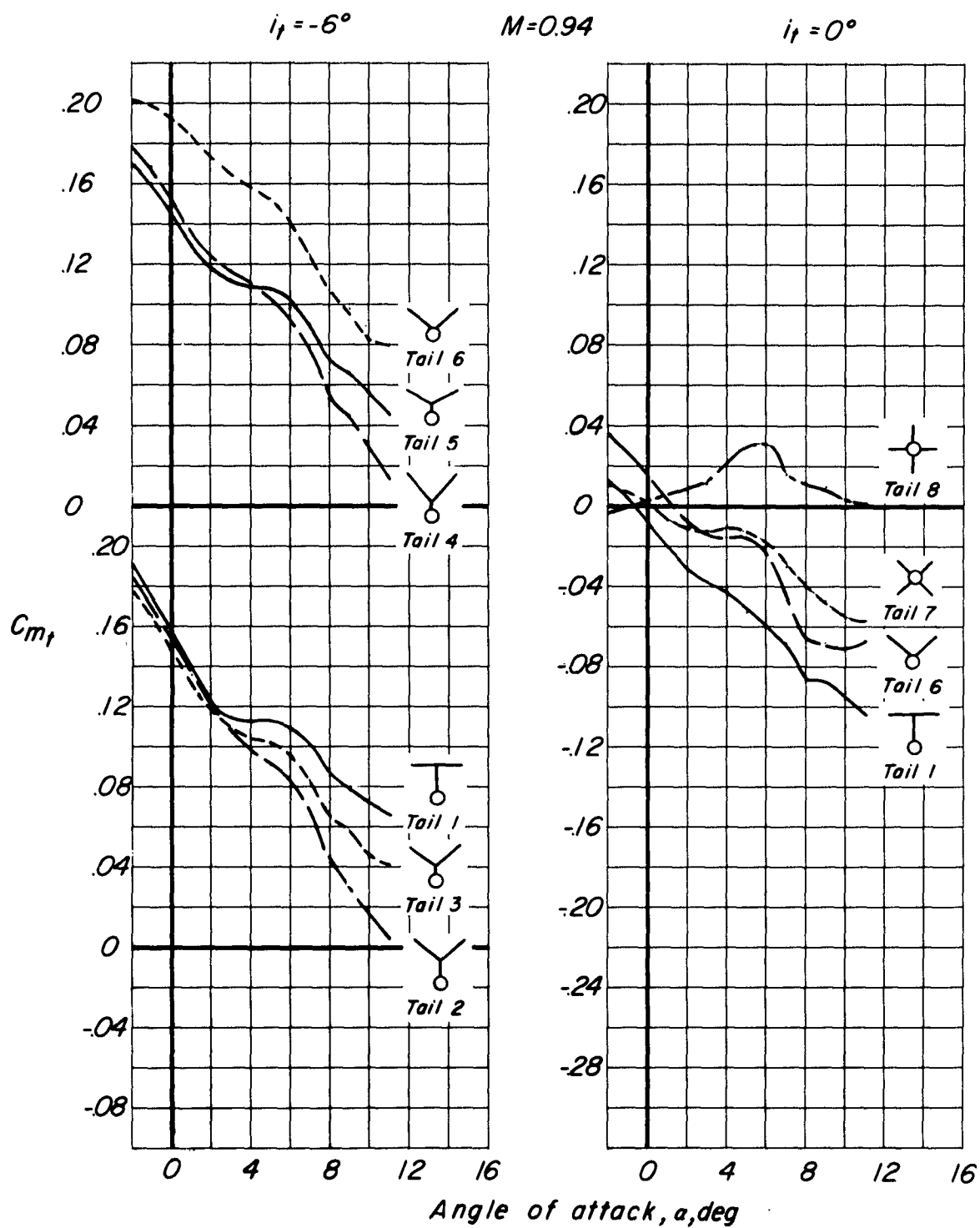


Figure 20.- Concluded.



(a) $M = 0.60$.

Figure 21.- Effects of tail configuration on the tail pitching-moment contribution.



(b) $M = 0.94$.

Figure 21.- Concluded.

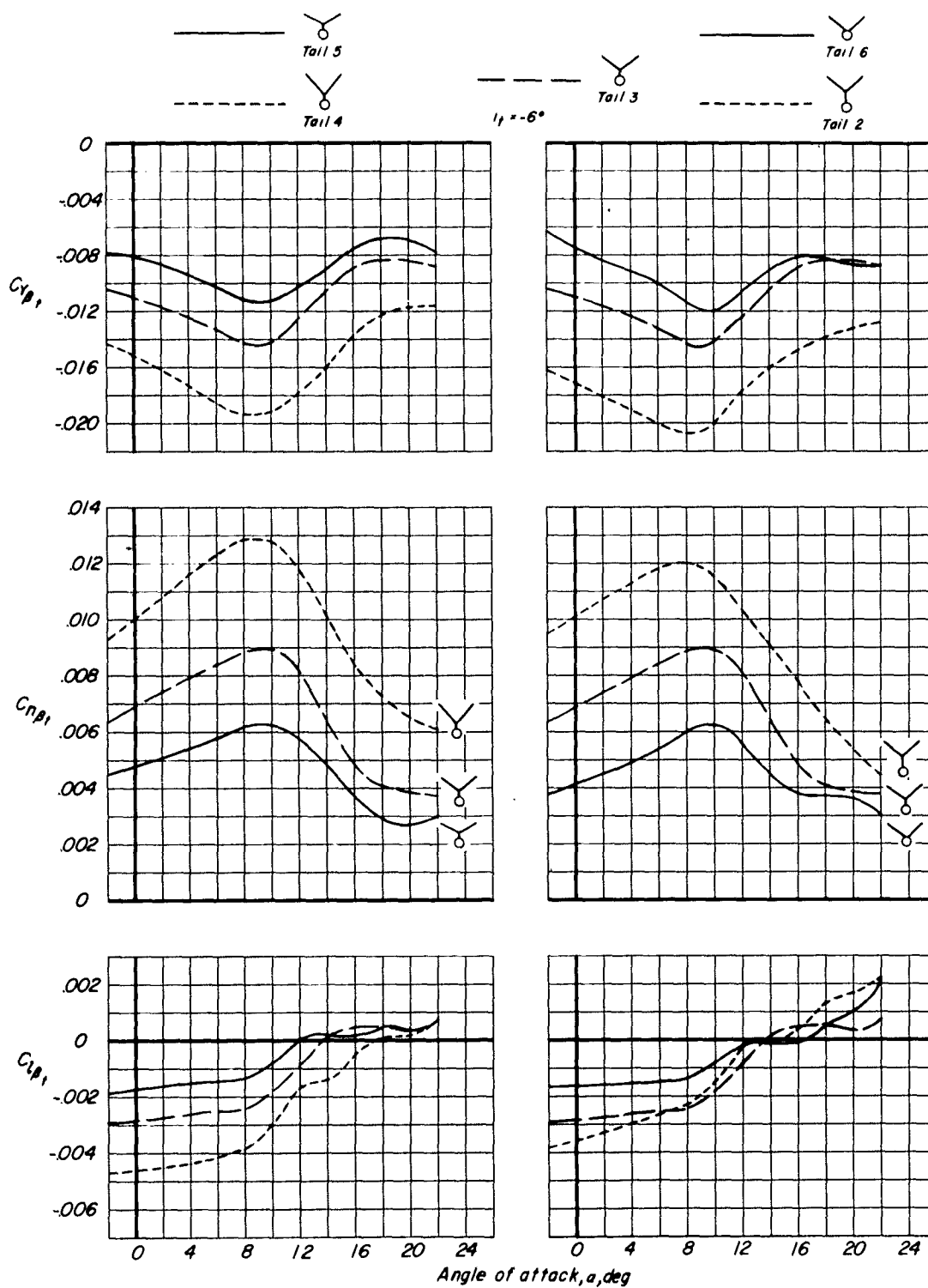
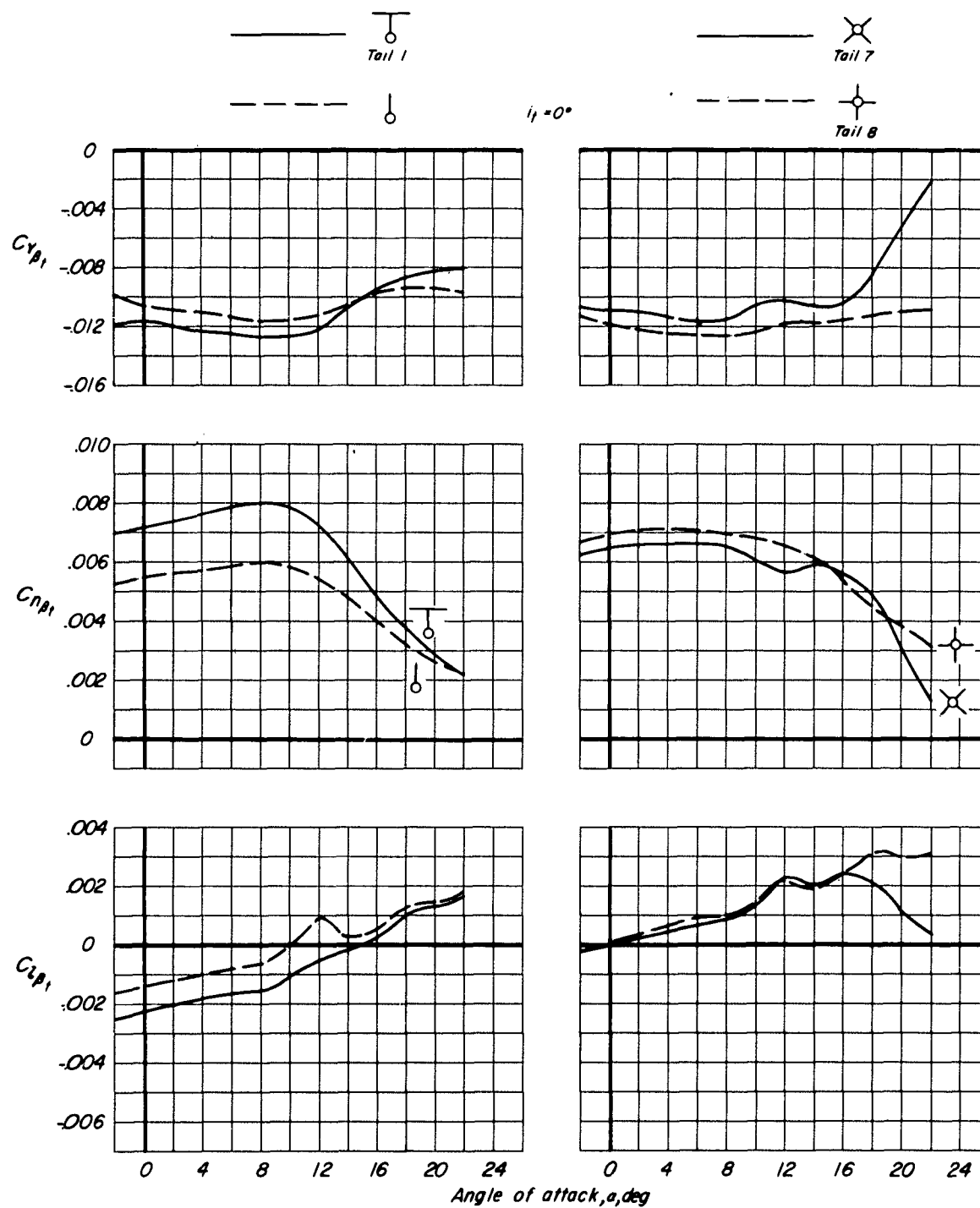
(a) $M = 0.60$.

Figure 22.- Effects of tail configuration on the tail contribution to lateral-stability derivatives.



(a) Concluded.

Figure 22.- Continued.

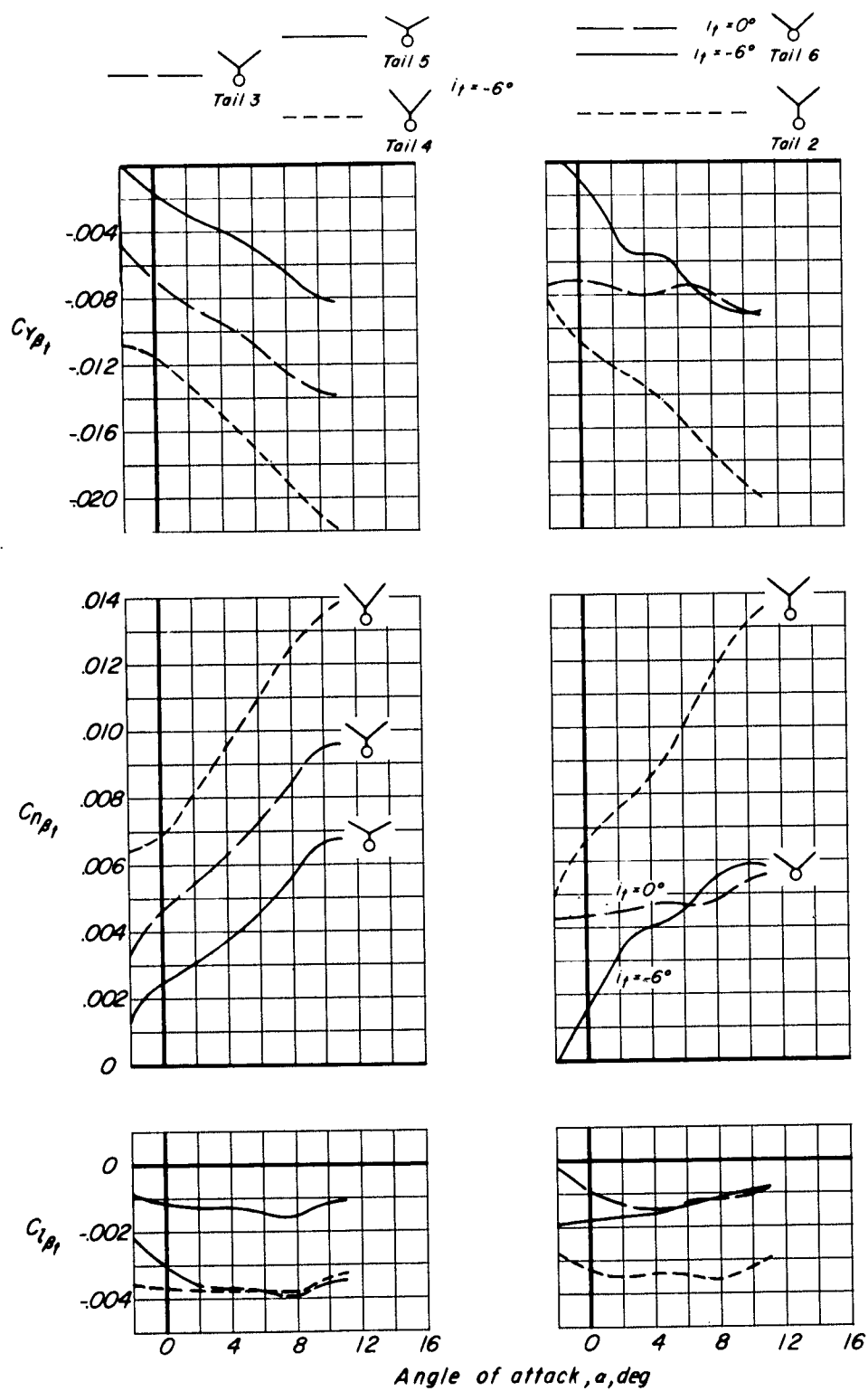
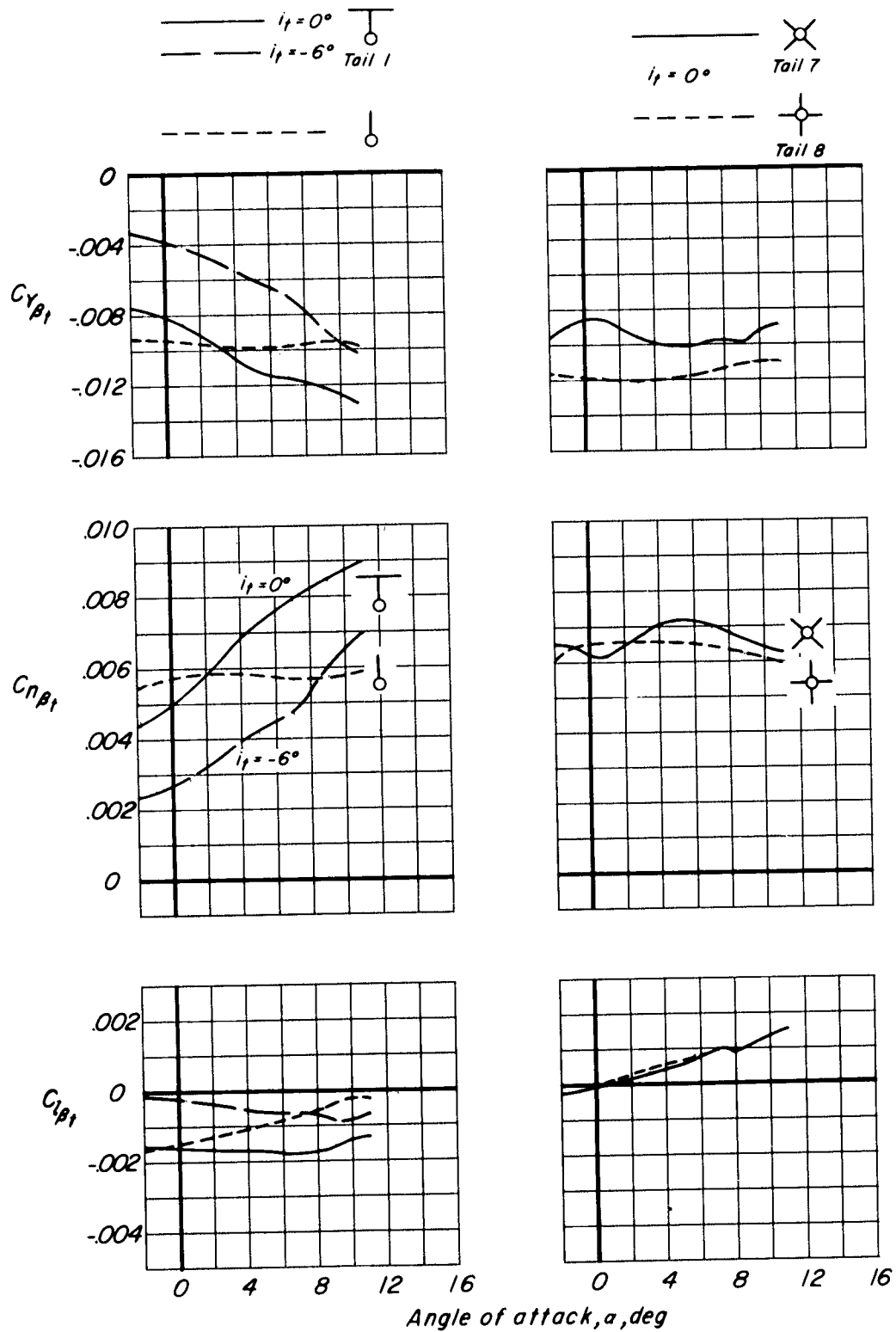
(b) $M = 0.94$.

Figure 22.- Continued.



(b) Concluded.

Figure 22.- Concluded.

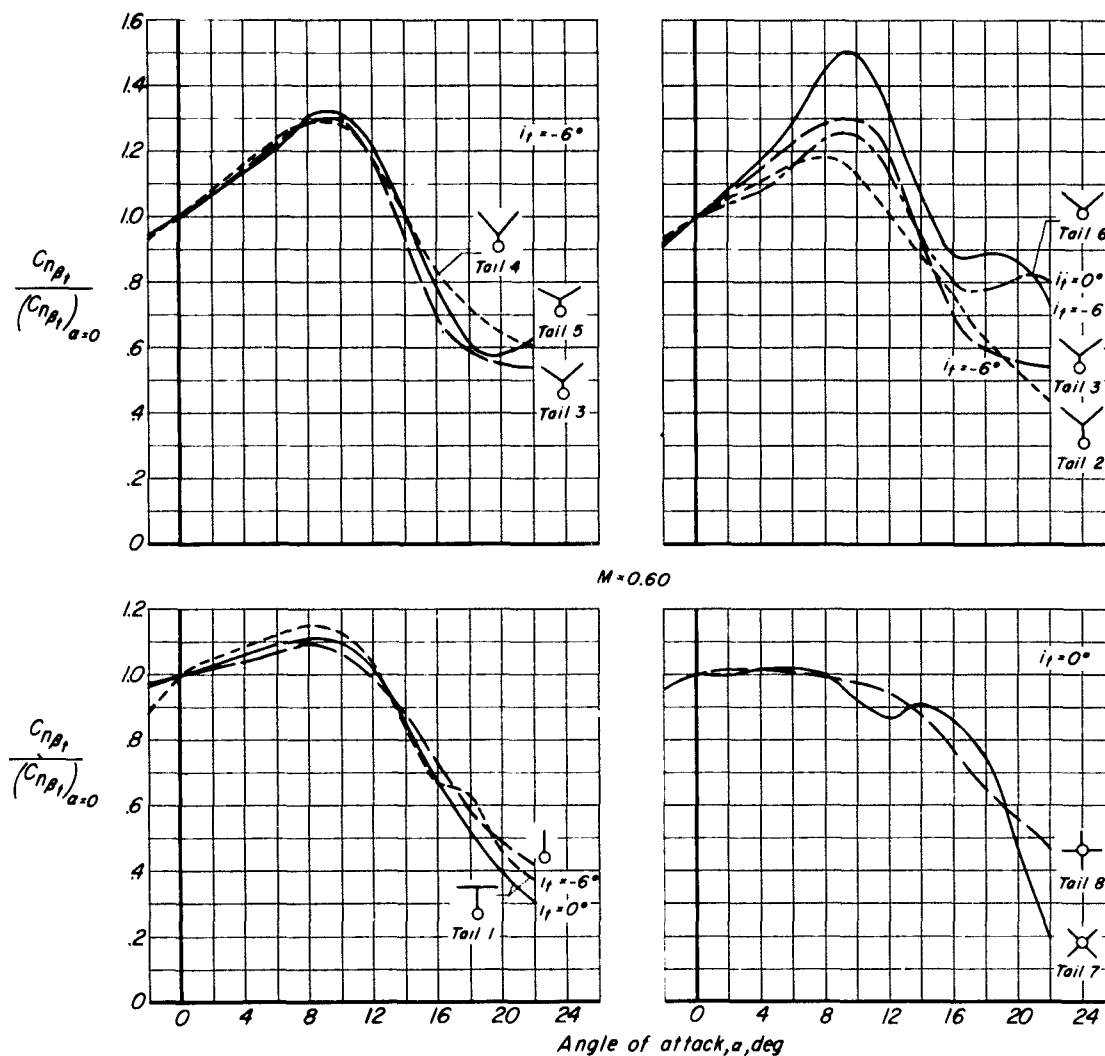


Figure 23.- Effects of angle of attack on the tail contribution to directional stability of the various tail configurations at Mach number of 0.60.

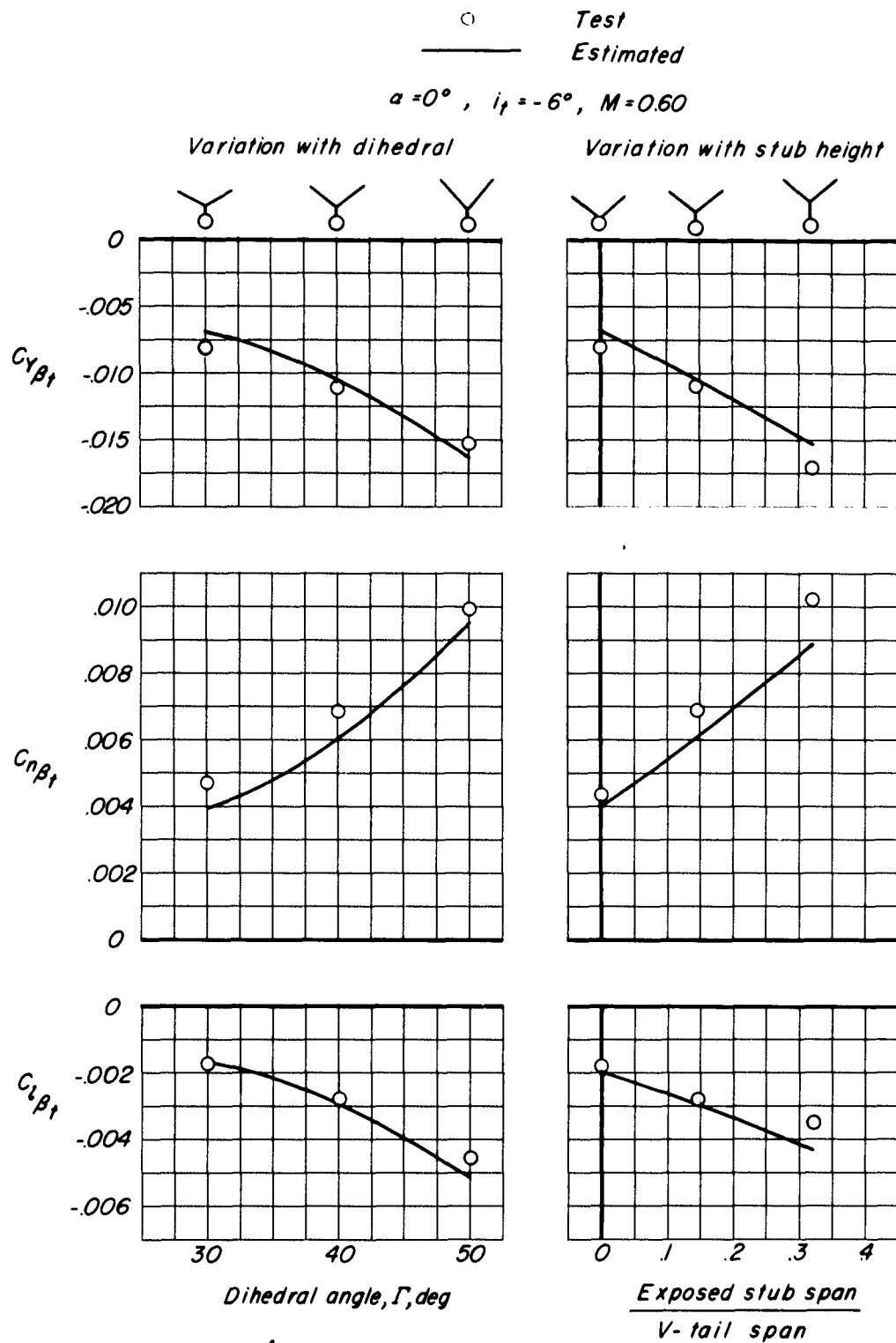


Figure 24.- Comparison of experimental and estimated tail contribution to lateral stability derivatives at an angle of attack of 0° and a Mach number of 0.60. $i_t = -6^\circ$.

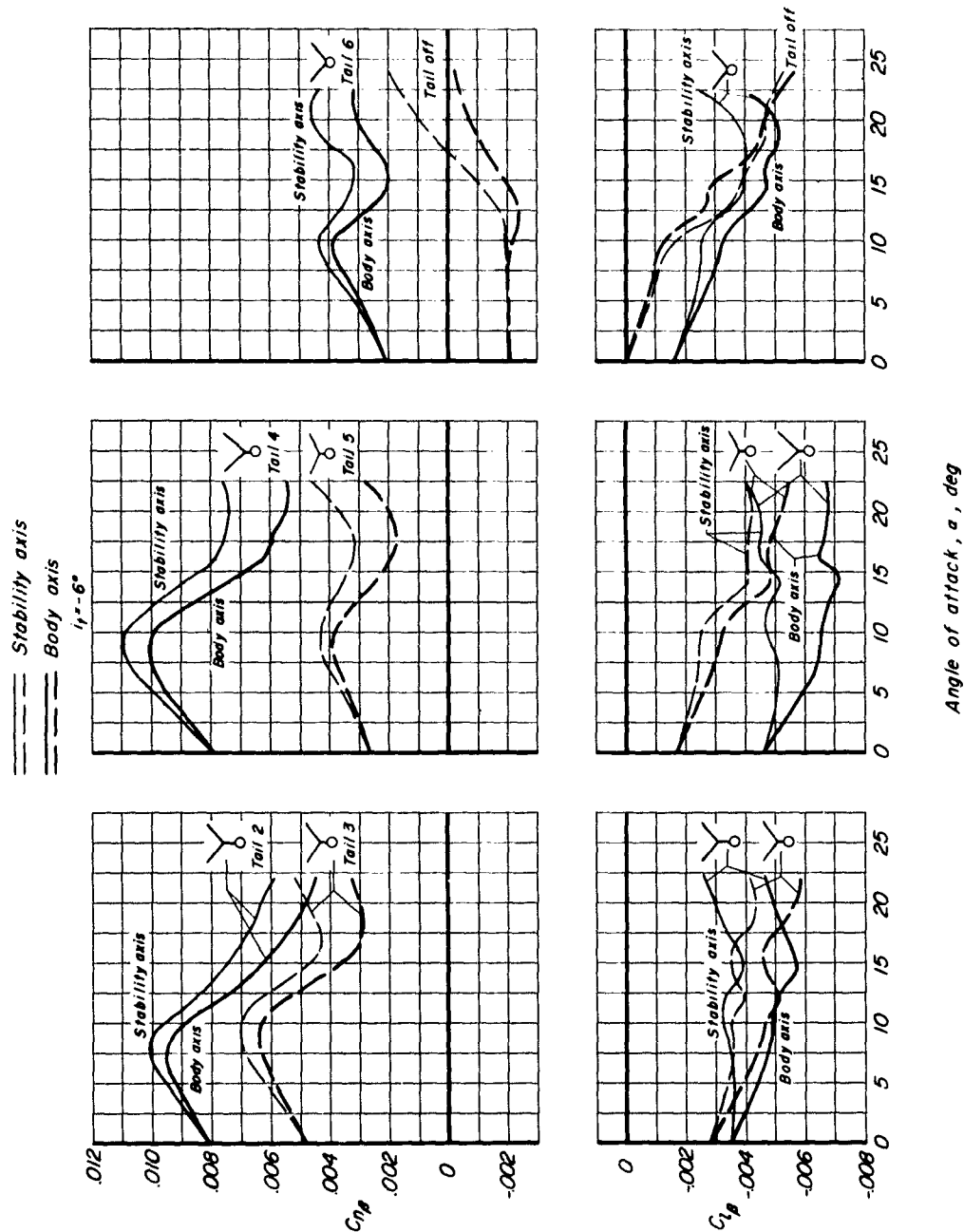


Figure 25.- Effect of reference axis system on the lateral derivatives, yawing moment and rolling moment due to sideslip at Mach number of 0.60.

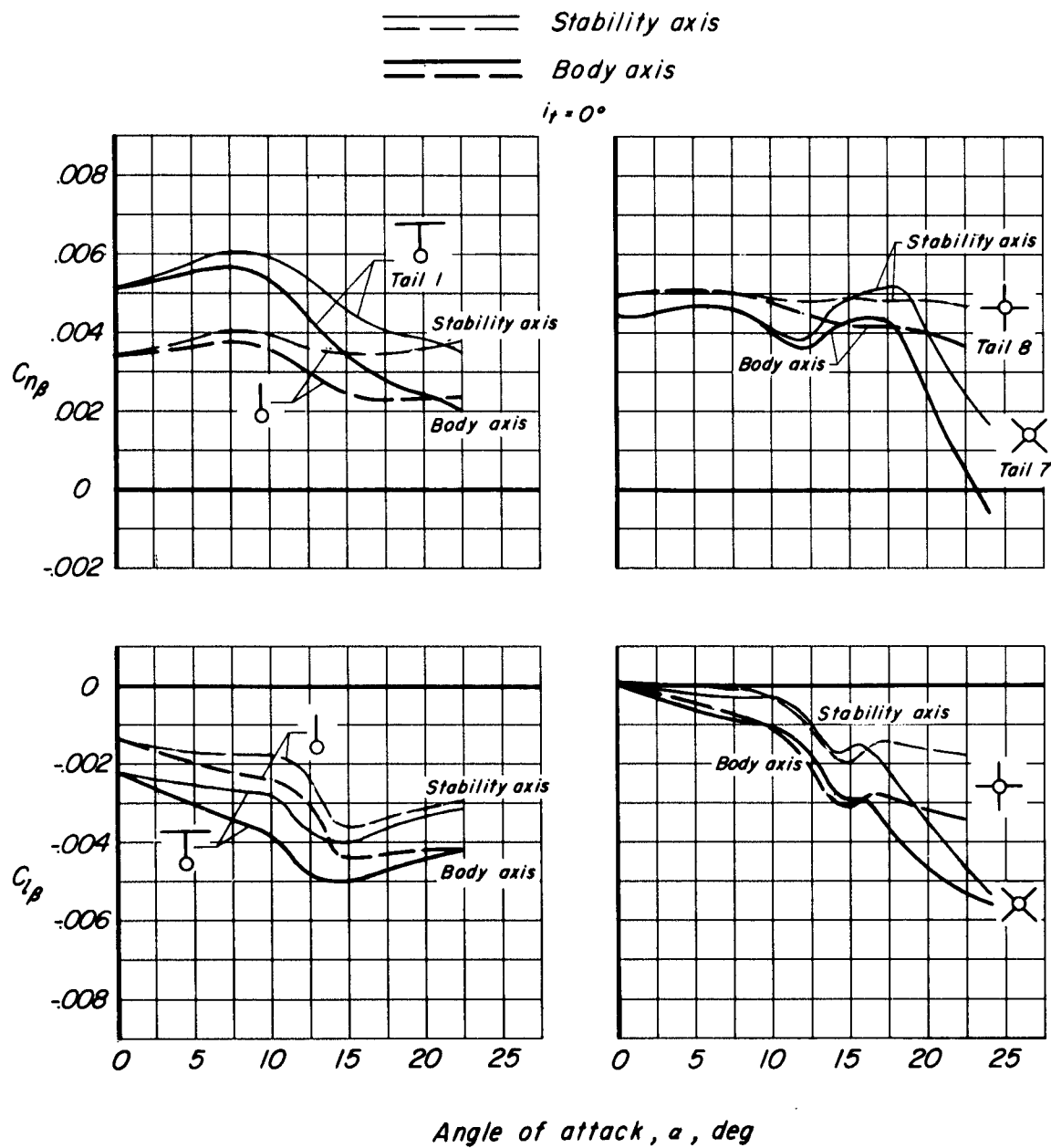


Figure 25.- Concluded.